Design and Implementation of a Redundantly Actuated Reconfigurable Planar Parallel Manipulator

by

Ryan Fisher
B. Eng., University of Victoria, 2000

A Thesis Submitted in Partial Fulfillment of the
Requirements for the Degree of

MASTER OF APPLIED SCIENCE

in the Department of Mechanical Engineering.

We accept this thesis as conforming
to the required standard

[redacted]

Dr. R. P. Podhorodeski, Supervisor (Department of Mechanical Engineering)

[redacted]

Dr. A. Suleman, Departmental Member (Department of Mechanical Engineering)

[redacted]

Dr. W.S. Lu, Outside Member (Department of Electrical Engineering)

[redacted]

David Lokhorst, M.A.Sc., External Examiner (Tactex Controls, Inc.)

Supervisor: Dr. R. P. Podhorodeski

Abstract

This work presents the design and implementation of the Reconfigurable Planar Parallel Manipulator (RPPM). The RPPM was designed to act as a testbed manipulator for theories on redundant actuation in parallel manipulators. The RPPM is capable of forming three planar mechanism types, a 3-DOF (degree of freedom) 8-Bar mechanism, a 3-DOF 6-Bar mechanism, and a 2-DOF 5-Bar Mechanism. The reconfigurable device is designed to allow multiple actuation configurations. Implementation of the non-redundantly actuated RPPM is done with PID control. Hybrid position/force control is used to implement redundantly-actuated configurations. The kinematics of the RPPM is formulated with screw coordinates representing the joints, and by using associated-reciprocal screw coordinates to represent the forces that each joint can apply to the platform. When redundantly actuated, there are an infinite number of solutions for the joint torques required to supply an output force of the end effector. A concept of force scaling is introduced to allow force capability optimization.

Examiners:

Dr. R. P. Podhorodeski, Supervisor (Department of Mechanical Engineering)

Dr. A. Suleman, Departmental Member (Department of Mechanical Engineering)

Dr. W.S. Lu, Outside Member (Department of Electrical Engineering)

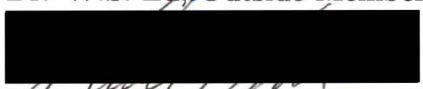

David Lokhorst, M.A.Sc., External Examiner (Tactex Controls, Inc.)

Table of Contents

List of Figures

List of Tables

Acknowledgements

First, I would like to thank my supervisor, Dr. Ron P. Podhorodeski, for his continued support and assistance throughout the tenure of my time in graduate studies.

I would also like to thank all the other RAM members for their input, especially Scott Nokleby and Paul Sobejko for their work in the never ending task of developing the hardware basis required for the RPPM.

Finally, I would like to extend my gratitude to all of my other friends and my familly, who have had to deal with my pleasant personality while I was finishing my thesis.

To those who have not had their story told. . .

Chapter 1

Introduction

1.1 Overview

This chapter presents a brief introduction to the research presented in the thesis. Section 1.2 discusses the initial motivation and also outlines the objectives of the research. Section 1.3 gives an introduction into manipulators, leading up to planar parallel manipulators, the basis of the Reconfigurable Planar Parallel Manipulator (RPPM). Section 1.4 introduces the implementation issues surrounding application of the RPPM. Section 1.5 introduces the kinematics associated with parallel manipulators. Section 1.6 discusses the concept of force capabilities for a manipulator, and the concept of a force capability plot. Section 1.7 provides a sample of previous work done related to the research of the thesis. Section 1.8 provides a brief summary of the chapters, and Section 1.9 outlines the major contributions of the research.

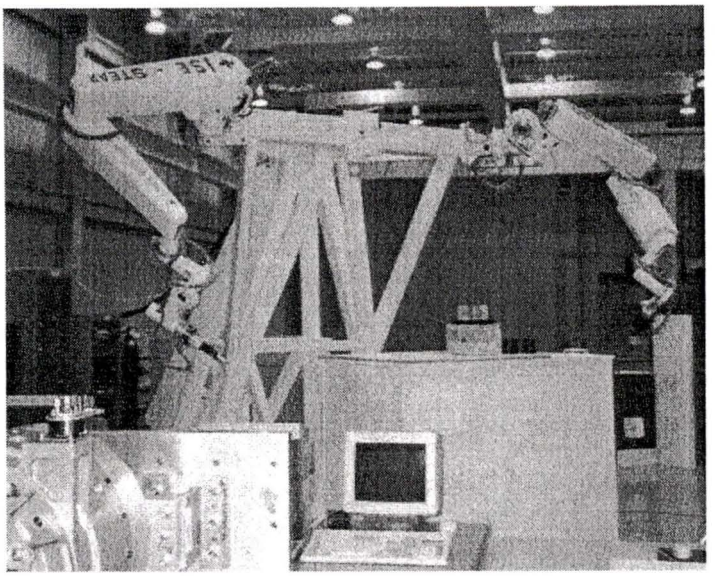

Figure 1.1: The STEAR Testbed Manipulator (STM).

1.2 Motivation and Objectives of Research

Motivation for the thesis was initiated with the need of the Robotics and Mechanisms Laboratory (RAM Lab) at the University of Victoria to test theories on redundant actuation in parallel manipulators. When multiple serial manipulators are cooperating, they effectively become a parallel manipulator with redundant actuation. For example, the Canadian Space Agency has in its possession the STEAR (Strategic Technologies for Automation and Robotics) Testbed Manipulator (STM), shown in Figure 1.1. The STM consists of two serial manipulators that work in cooperation. When cooperating, the manipulators form a closed system, and become a two branched parallel manipulator. Some of the research currently under way in the RAM Lab deal with use of redundant actuation in parallel manipulators to accomplish goals such as elimination of force unconstrained (singular) configurations.

The main objective of the research is to design a planar parallel testbed manipulator, which is capable of reconfiguration in actuation and in mechanism type. The Reconfigurable Planar Parallel Manipulator (RPPM) is designed to allow for testing on theories of redundant actuation on a variety of planar mechanisms. The three desired planar mechanisms are the 2-DOF (degree of freedom) 5-Bar mechanism, the 3-DOF 6-Bar mechanism, and a 3-DOF three branch 8-Bar mechanism. Not only was it desired to have reconfigurability in mechanism type, but in actuation configurations as well. It was desired to have all possible main-arm joints, both the elbow joint and the shoulder joint for each branch, actuated or passive.

The implementation of basic control schemes for the RPPM to facilitate operation when either non-redundantly actuated or when redundantly actuated was desired. The control schemes need to be simple but effective. They need to prove the abilities of the RPPM for later use as a testbed manipulator.

It was also desired to present a theory which would be an excellent candidate for future testing on the RPPM. One such theory that may be tested on the RPPM is the force capabilities work presented. The maximization of the sustainable or applicable force of an end effector of a parallel manipulator is something that can be of great use. Redundant actuation in a parallel manipulator creates an overconstrained system. These extra actuators can be utilized to increase the sustainable force load of the manipulator by creating an internal force on the platform. The ability to maximize an output load can also be seen as minimizing the joint torques required to sustain a constant load, and therefore, smaller actuators can be used with an optimal force solution, over what would otherwise be required.

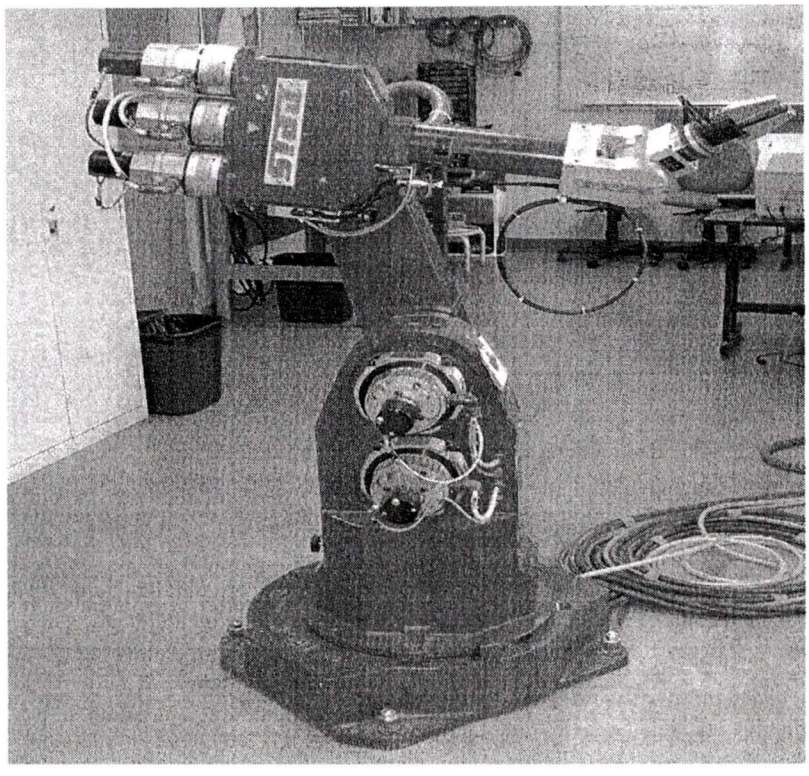

Figure 1.2: The REIS robot, a 6-DOF serial manipulator. (Photo courtesy of Scott Nokleby)

1.3 Manipulators

1.3.1 Serial Manipulator

There are two main types of manipulators, serial manipulators and parallel manipulators. Serial manipulators are manipulators in which the joints are located consecutively in the manipulator arm. The number of joints typically equals the DOF of the manipulator. An example of a serial manipulator is the REIS Robot shown in Figure 1.2. The REIS has six joints, and 6-DOF. All joints are actuated and sensed allowing for the end effector to be positioned and oriented in space.

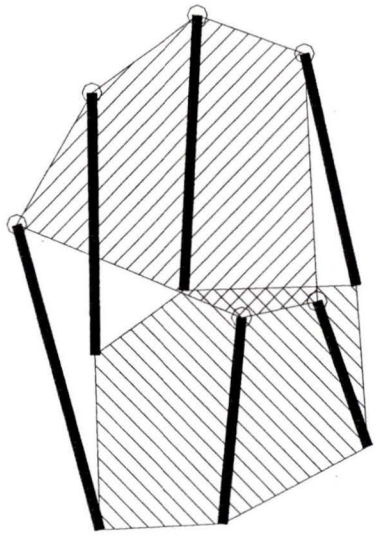

Figure 1.3: A general Stewart-Gough Manipulator.

1.3.2 Parallel Manipulators

Parallel manipulators are defined as manipulators with multiple branches acting on a common payload. A fully-parallel manipulator is a parallel manipulator where the number of branches is equal to the DOF of the manipulator, with each branch having one actuated and/or sensed joint. Figure 1.3 shows a schematic of a general Stewart-Gough Manipulator. The Stewart-Gough Manipulator has six branches acting on the payload. Each branch has only one actuated and/or sensed joint, in this case the prismatic cylinders that vary the lengths of the branches. The other five joints in each branch are passive.

A planar parallel manipulator is a parallel manipulator which only has motion in a plane. This limits the manipulator to 3-DOF, linear motion in the $\hat{\mathbf{x}}$ and $\hat{\mathbf{y}}$ directions, and orientation about $\hat{\mathbf{z}}$. To make the manipulator fully-parallel requires three branches, each with one actuated joint.

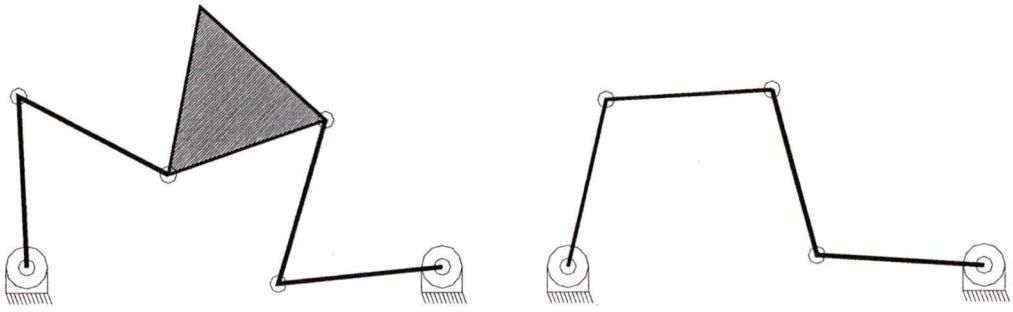

Figure 1.4: Schematics of a 6-Bar and a 5-Bar planar mechanisms.

There are also other mechanisms of interest. They are a 2-DOF 5-Bar and a 3-DOF 6-Bar. Schematics of these manipulators are shown in Figure 1.4 The 5-bar device could be classed as a fully parallel 2-DOF manipulator, as it has two branches acting on the common payload (in this case, the "point" of intersection of the two branches) and it has only 2-DOF. The 6-Bar can be classed as a parallel manipulator, but is not considered to be fully-parallel because it has 2 branches yet 3-DOF. It therefore requires two actuated joints in one of the branches and one actuated joint in the other branch.

1.3.3 Redundancy in Parallel Manipulators

A parallel manipulator is redundantly actuated when there are more actuators than the device DOF. The DOR (degree of redundancy) of a manipulator is equal to the number of actuators minus the DOF. If all four branch joints on the 6-Bar mechanism of Figure 1.4 are actuated, then the system would have 1-DOR. This DOR can be used for such tasks as singularity elimination and force optimization.

Similarly, a parallel manipulator can have redundant sensing as well. If both

joints in the universal at the base of each branch of a Stewart-Gough Manipulator were sensed as well as the length of the prismatic cylinders, this would give a known location for the spherical joint (wrist) on the payload. Since the general Stewart-Gough Manipulator with only the displacements of the cylinders known, can have up to 40 solutions to the FDP (forward displacement problem) [1], redundancy in sensing can save much time as it can be used to provide a unique FD solution [2]. Also, known geometry of the payload and device can be used with redundant sensing for multiple benefits such as sensor calibration and fault detection algorithms [3].

1.4 Control of the RPPM

1.4.1 PD and PID Control

PD and PID control is based on the theory that a mass has a desired position and velocity. The actual position and velocity of the mass is in error from the desired. The errors can be used to create a force which will correct the position and velocity of the mass. The same can be true for a rotational system. PD (proportional derivative) and PID (proportional integral derivative) control can vary in complexity, however. The choices of the control constants will depend on the type of desired output of the controller. A great deal of work has already been done in the field of PD and PID control for DC motors. This work presents the application of a simple yet effective PID controller.

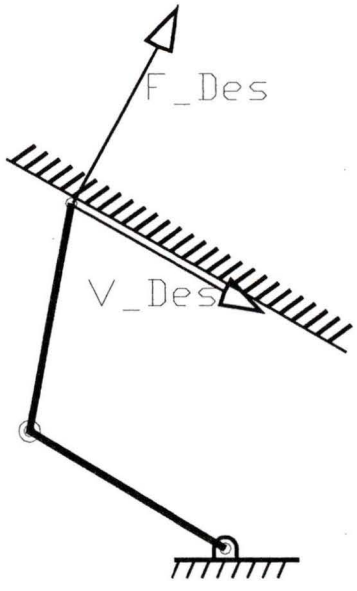

Figure 1.5: A 2-R planar manipulator, moving while pushing on a barrier.

1.4.2 Classical Hybrid Position/Force Control

J.J. Craig [4] explains Hybrid Force Control with a manipulator in contact with its surroundings. He creates a set of constraints, natural and artificial to the manipulator which must be satisfied. Shown in Figure 1.5 is a 2-R manipulator. This manipulator has a desired velocity V_Des of the end effector and a desired load, F_Des, to be applied to the wall. Craig shows that the manipulator can be controlled by a summation of what is required to move the manipulator and what is required to apply the force. The constraints of the system would be in the location of the barrier, which the manipulators cannot go through. If the contact is considered to be frictionless, that the direction of the force must be perpendicular to the barrier at the point of contact, defining another constraint on the manipulation system.

Shown in Figure 1.5 is a manipulator that is desired to push on the barrier while

at the same time moving along the barrier. This is similar to many real manipulator tasks such as grinding or scraping of a surface. It is also similar to moving a branch of a redundantly actuated parallel manipulator. Each branch of the manipulator can be considered to be a single manipulator, constrained with a desired motion and a desired force to be applied to the payload. A typical position-based controller would only be able to create the desired trajectory, not the desired loading. A small error in known position would cause large errors in force, anywhere from not quite touching the surface to the manipulator trying to push right through the barrier.

The main reason for investigating a controller which uses force in its algorithms is for the case of the redundantly-actuated RPPM. When non-redundantly actuated, and using a PID controller, a difference in the actual position of a motor from the sensed position will not cause any problems other than the unknown position error. With the redundantly-actuated RPPM, an error in actual position from the sensed position will yield problems as with the barrier in the above example.

For example, imagine when redundantly actuated, each actuator encoder is calibrated incorrectly by a small angle. Using PID control, as each joint tries to reach their proper position, they will not be able to do so because the system is overconstrained. This will cause, for each joint, a steady state error. Since position control is based on correcting errors in position, this error will cause a voltage to be applied to the motors. This will cause undesired forces at the wrists. With PID control the steady state error will be integrated, and the undesired forces will increase over time. Hence, it is proposed to not only control the position of each motor, but also the torques. If the torques are also being controlled in conjunction with the position, the torques from the position errors will cause forces which the force controller will balance. The balance will be a weight between the desired forces and the desired po-

sition. This is expected to leave steady state position errors which are greater than the PID controller would leave, but this is preferable to the alternative of having increasingly uncontrolled forces.

1.5 Kinematics of Parallel Manipulators

1.5.1 Displacement Solutions

The FDS (forward displacement solution) of a parallel manipulator solves for the position and orientation of the end effector for known joint displacements. With the minimum number of sensed joints, there is typically multiple solutions to the FDS. It was shown by M. Raghavan in 1993 that for known lengths of prismatic cylinders, the general Stewart-Gough manipulator can have up to 40 solutions for the location of the platform [1]. The use of redundant sensing, as mentioned, can reduce the problem to a unique solution.

The IDS (inverse displacement solution) of a parallel manipulator solves for the joint displacements for a known position and orientation of the end effector (common payload). The IDS typically involves finding the location of each of the branch wrists on the payload, then solving for the required joint displacements of each branch. There can be multiple solutions to the IDS for each branch, depending on the branch layouts.

1.5.2 Screw Coordinates

To kinematically analyze parallel manipulators, screw coordinates and associated-reciprocal screws coordinates are used. Screw coordinates can be described as a line

in space with a pitch and an associated amplitude. Screw coordinates can be used to model joints of manipulators. With the joints of manipulators modelled as screw coordinates, the force that can be exerted by each actuated joint can be modelled with associated-reciprocal screw coordinates. This allows for the total output force of a parallel manipulator to be found.

1.6 Force Capabilities

The force capabilities of a manipulator are defined as the maximum force and moment a manipulator is capable of sustaining or applying. Force capabilities are an instantaneous quantity, i.e., they are dependant on the position and orientation of the end effector. They are also dependant on the joint torque limits. In many robotics applications, the desired direction of the applied force and moment are known. The maximum available torques of each actuator can be used to determine the sustainable loads.

A force capability plot (force polygon) shows all the force capabilities of a manipulator in all directions. For example, the force capability plot of the simple 2-DOF serial manipulator is shown in Figure 1.6. The force polygon is drawn around the loading point to which it is calculated (for this case the end of the manipulator). The polygon is a scaled plot of the magnitude of the force the manipulator can sustain in any given direction. For example if it was desired for this manipulator to sustain a load at approximately 125 degrees from the $\hat{\mathbf{x}}$ axis, the maximum force would be equivalent to the magnitude of the line from the loading point to the polygon in the same direction of the force being applied, shown as $\mathbf{F}$. Here, the point the load is being applied to the manipulator is at (0,0). These plots will be used to show the

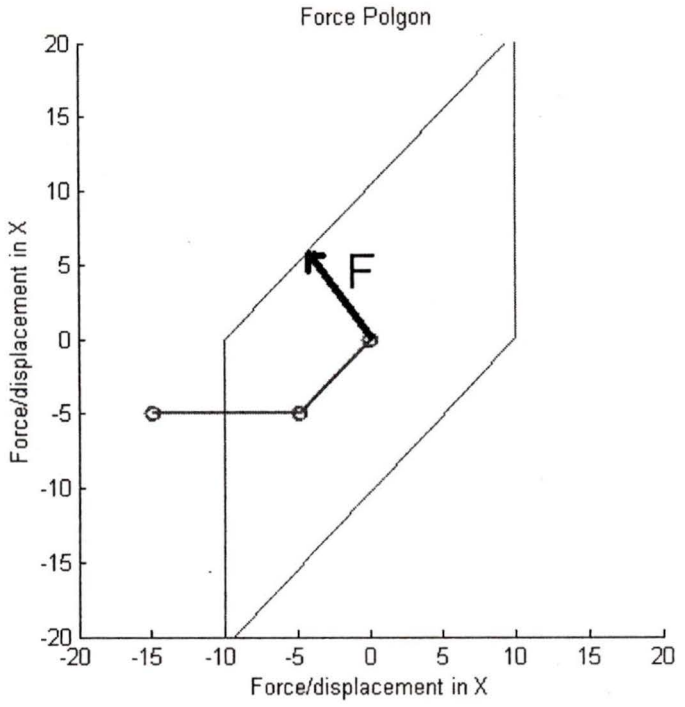

Figure 1.6: An arbitrary force polygon, drawn for a planar serial manipulator

force capabilities of the RPPM.

1.7 Previous Work and Literature

1.7.1 Devices Similar to the RPPM

Modular or reconfigurable manipulators have been previously designed. A great deal of research has been done on self-reconfigurable robots, though that is not the focus of this research. Redundantly-actuated parallel manipulators have also been designed. No device identical to the RPPM has been found. The following is a sample of some of the reconfigurable and of redundantly-actuated manipulators that possess at least

some similarities to the RPPM:

Podhorodeski and Nokleby [5] (2000), presented the Reconfigurable serial-layout Main-Arm (RMA), which can assemble into all of the kinematically-simple main-arm configurations presented by Podhorodeski and Pittens [6] (1994).

Yang, Chen, Lim, and Yeo [7] (2001), discuss issues surrounding the kinematic design of three-legged modular parallel manipulators. They use an example modular parallel manipulator which is reconfigurable in branch structure, based mainly on the kinematically simple branch structure of Podhorodeski and Pittens [6] (1994). Their manipulator however, avoids actuation redundancy.

Cheng, Liu, Yiu, Xiong and Li [8] (2001), present research mainly on the dynamic equations of redundantly-actuated parallel manipulators, but as an example they utilize a 2-DOF three-branch planar manipulator with one actuator in each branch. This is the testbed manipulator they utilize in much of the controls and dynamics research they are involved in.

Hamlin and Sanderson [9] (1996), presented work on the TETROBOT. The tetrobot is a highly-redundant reconfigurable modular parallel manipulator with up to 18 nodes, 48 links, and 15 actuators.

Schonlau [10] (1997), presented the modular manipulator system (MMS), which is a reconfigurable manipulator consisting of joints (linear and revolute) and links which can be assembled to form a manipulator of any complexity.

Ji [11] (1998) considered the design and planning issues of an experimental reconfigurable parallel manipulator, which was constructed to aid their research on design and planning issues of reconfigurable parallel manipulators.

Hui, Kircanski, Goldenberg, Zhou, Kuzan, Wiercienski, Gershon and Sinha [12] (1993) present the design of the IRIS facility. The IRIS facility is a reconfigurable

manipulator system which incorporates two arms with up to four joints per arm. It was designed to test theories on grasping and manipulation.

1.7.2 Controls work

There has been a great deal of relevant research completed in the area of control of manipulators. A great deal of this research is in optimal control of manipulators undergoing contact with surroundings. Since the RPPM when redundantly actuated can be considered to be cooperating serial manipulators, the research is valid. Provided is a sample of those works which influenced the implementation of the redundantly-actuated RPPM, more specifically the classical hybrid position/force controller:

Raibert and Craig [13] (1981) first proposed the hybrid force controller. This controller typically has two elements, a desired trajectory of the end effector and a desired direction of force to be applied. Errors in the actual position and force from the desired are used to create a correction to minimize errors. This is referred to as classical hybrid position/force control.

Yoshikawa [14] (2000), provides a summary of the basic concepts and methodology behind the two major approaches to force control in use, hybrid and impedance control. He summarizes that unless there is switching between contact control and non-contact control, hybrid position/force controllers are better suited to providing more accurate output position and force.

An and Hollerbach [15] (1989), showed that the hybrid control may lead to an unstable responses. The lack of inclusion of detailed dynamics of the manipulator in the controller was shown to be one reason. This led to a great deal of research in

what has been called dynamic hybrid position/force control, which was not studied in the research of this thesis.

Fisher and Mujtaba [16] (1992) showed that the kinematic instability is not inherent in hybrid force controllers, but is actually due to an incomplete formulation and the inverse of the manipulator Jacobian. They show the inverse of the manipulator Jacobian should not be used in hybrid force control.

Wu, Wu and Li [17] (2001) used the dynamics of the manipulator to apply a PD controller to a 2-DOF redundantly-actuated parallel manipulator. Their method requires no force feedback, and they manage to eliminate the internal forces on the platform using a theory based on static force transmission.

1.7.3 Manipulator Kinematics and Associated Work

Kinematics and the use of screw coordinates for serial and parallel manipulators is not a new concept. The use of redundancy in parallel manipulators has also been studied. The following is but a brief sample of the work done in this field, specifically work that directly related to the research in this thesis:

Gosselin and Angeles [18] (1988), present work on the design of 3-DOF planar parallel manipulators from a kinematic view point and establish criteria to produce desired characteristics.

Merlet [19] (1998), presents a geometrical approach for determining the workspace of planar parallel manipulators.

Gosselin and Jean [20] (1996), presents an algorithm for determining the workspace of planar parallel manipulators with the inclusion of joint limits by creating arcs and lines to determine a boundary.

Merlet [21] (1996), showed the benefits of redundant actuation in parallel manipulators. He shows that actuation and sensing redundancy can be used for tasks such as solving the kinematics, singularity avoidance, and constructing geometric trusses.

Gosselin and Merlet [22] (1994) complete the study on the direct kinematics for non-redundantly-sensed planar parallel manipulators similar to the RPPM.

1.7.4 Force Capabilities

The work on force capabilities for a parallel manipulator is similar in some ways to the act of cooperating serial manipulators and to multi-fingered grasping. The difference is that grasping typically has constraints of friction requirements to support the grasped object. The force capabilities for a lone serial manipulator is unique, as there is a direct unique solution for the required joint torques for revolute joints (or force for prismatic joints) to sustain or apply a load at the end effector. Some work which is relevant to the research presented is provided:

Kumar and Waldron [23] (1988) noted that the Moore-Penrose pseudo-inverse, of what is referred to in this thesis as the weighted matrix of associated reciprocal screw quantities, yields no internal forces in grasping.

Kerr, Griffis, Sanger, and Duffy [24] (1992) showed that grasping a rigid object creates a system which is identical to a redundantly-actuated parallel manipulator, where the "grasped" object is the common payload.

Buttolo and Hannaford [25] (1995) present a direct-drive redundantly-actuated parallel manipulator. They introduced an algorithm to compute the force capabilities of the device. They also state that a redundantly-actuated device has the ability of choice of joint torques to achieve a homogeneous force output in the workspace.

Beiner [26] (1997) considers a redundantly-actuated 2-DOF parallel manipulator. He derives a non-linear optimization problem, with equality and inequality constraints, for the minimization of the joint torques to increase the output force. He then presents a closed-form solution to compute the joint torques.

Nahon and Angeles [27] (1991) discuss the problem of a hand grasping an object. They consider the hand grasping the object as a redundantly-actuated parallel manipulator. They formulate the problem of minimizing the internal forces on the grasped object.

1.8 Summary of Thesis Chapters

1.8.1 Chapter 2 - Design of the RPPM

Chapter 2 outlines the design of the RPPM. The initial design criteria are specified. The methodology for meeting the criteria are discussed. Then, the design itself is the discussed in detail. All of the hardware and sensing used by the RPPM is presented. The inherent sources of error in the design are discussed.

1.8.2 Chapter 3 - Implementation of the RPPM

Chapter 3 presents the issues surrounding the implementation of the RPPM. The basic theory behind the control algorithms is presented. General implementation issues are also presented, including the structure of the control programs. The application of the two controllers in the program are also presented. Finally, results of implementation of the RPPM in the 6-Bar configuration are presented, along with a discussion of those results.

1.8.3 Chapter 4 - RPPM Kinematics

Chapter 4 considers the kinematics of the RPPM. Both the forward and inverse displacement solutions are presented. A consideration of screw coordinates and associated-reciprocal screw coordinates, and how they can be applied to the RPPM is discussed. The construction of the associated-reciprocal screw matrix is shown, followed by the determination of a weighted associated-reciprocal screw matrix, which converts a vector of joint torques to an output force.

1.8.4 Chapter 5 - Force Capabilities

Chapter 5 presents work on force capabilities, for the non-redundantly and redundantly actuated configurations of the RPPM. For the non-redundant case, the problem of the determining the force capabilities is straight forward. For the redundantly-actuated cases, the DOR of the manipulator creates orders of infinity of solutions to the joint torques able to sustain or apply a load. Two methods are presented to overcome this, the first uses the Moore-Penrose pseudo-inverse solution and the second uses a minimization of the maximum joint torque. The three solution methods are compared using a simulation of the 8-Bar configuration of the RPPM.

1.8.5 Chapter 6 - Conclusions Recommendations for Future Work

Chapter 6 concludes the research presented in the thesis. Major conclusions from each of previous chapters are presented. Recommendations for future work are discussed.

1.9 Major Contributions

The major contributions of this research are as follows:

- The design of the Reconfigurable Planar Parallel Manipulator (RPPM) including:
  - complete reconfigurability in three different mechanism types, i.e., a 3-DOF 8-Bar mechanism, a 3-DOF 6-Bar mechanism, and a 2-DOF 5-Bar mechanism,
  - complete reconfigurability in actuation, allowing any shoulder or elbow joint of any branch to be actuated or replaced by a passive revolute joint,
  - sensing of the forces being applied to the platform from each of the branches at the wrist centres.
- The implementation of the RPPM, including:
  - design of a control program structure for implementation of the motor controllers,
  - implementation of both a PID controller for non-redundantly actuated cases and a hybrid position/force controller for the redundantly-actuated cases.
- The determination of force capabilities for the RPPM, including:
  - the use of scaling factors to determine the maximum possible sustainable or applicable force at the end effector,

- the use of an optimization algorithm to optimize the sustainable loads for the redundantly-actuated cases using the internal forces of the platform,
- a comparison of how the optimized use of internal forces improves the force capabilities of the manipulator.

Chapter 2

Design of the RPPM

2.1 Overview

This chapter discusses the design of the Reconfigurable Planar Parallel Manipulator (RPPM). Section 2.2 considers the objectives of the design, including the criteria and constraints laid out in the initial design stages. Kinematic proportions of the design and the solutions chosen to achieve the desired reconfigurability are then discussed in Sections 2.3 and 2.4. The chapter then presents the design itself, including all of the hardware, in Sections 2.5 and 2.6. There is also a discussion of the design as it relates to the initial criteria and constraints, and a presentation of the inherent errors of the design and hardware in Section 2.7.

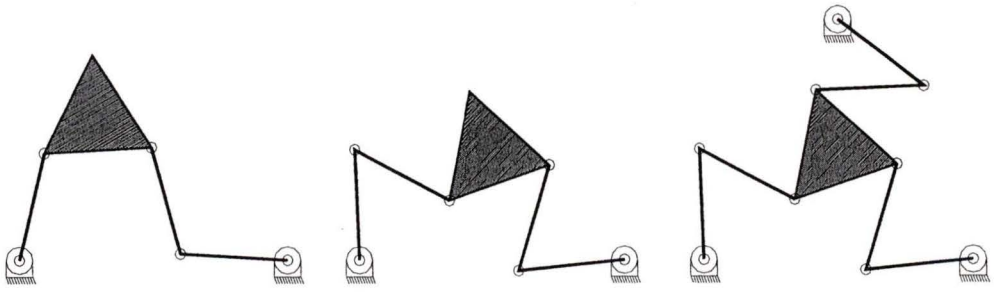

Figure 2.1: The desired configurations of the RPPM. From left to right: 2-DOF 5-Bar mechanism, 3-DOF 6-Bar mechnism, 3-DOF 8-Bar mechanism.

2.2 Design Objectives

2.2.1 General

The main goal of the design of the RPPM is to create a reconfigurable planar mechanism capable of acting as a testbed for theories on redundant-actuation in parallel manipulators. The design should allow for experimentally accurate and repeatable results.

2.2.2 Reconfigurability

Mechanism Type

It was decided that there are three planar manipulator configurations which are desirable. The RPPM should configure into a 2-DOF 5-Bar Mechanism, a 3-DOF 6-Bar Mechanism, and a 3-DOF 8-Bar Mechanism. The three desired mechanisms are shown in Figure 2.1. It is desired that the RPPM be able to reconfigure from

mechanism type to mechanism type simply and quickly, with minimal effort from the user.

Actuation

The RPPM should be able to facilitate actuation at any shoulder or elbow joint of any branch. Each joint should also be able to act as a free (passive) revolute joint. Wrists were decided not to be actuated to minimize the need to manipulate base distal masses.

2.2.3 Other Criteria and Constraints

Several other factors were taken into account in the design of the RPPM. The other necessities for the design included:

- the existing Micro-Mo series 3557 motors and their associated hardware already existing in the Robotics and Mechanisms (RAM) lab would be used,
- and the forces being applied to the payload from the branches would be sensed.

Other factors which were taken into consideration during the design of the RPPM, though not critical, included:

- the workspace and the joint limits should be maximized,
- the design must be as light as possible, to minimize the inertia seen by the actuators,
- and the device should be simple and inexpensive to manufacture.

2.3 Kinematic Design

2.3.1 Link Lengths

The ratio of link lengths and distance of the bases were chosen based on the optimum kinematic design of a planar 3-DOF parallel manipulator. The link lengths would be equal to achieve symmetry and maximization of the global workspace [18]. The base distances were chosen to be on an equilateral triangle, to also achieve a nice symmetric design. The distance between the bases was chosen to be 2.5 times the link length. The link lengths were all chosen to be 200mm, and the base distance was therefore chosen to be 500mm.

The platform edge length was chosen to be a combination of maximizing the global workspace, of facilitating the physical necessity of the force sensing, and of allowing simplicity in the overall design. From these criteria it was decided the platform edge length should be chosen to be 200mm, equal to the link lengths.

2.3.2 Workspace Analysis

With the link length and base distances chosen, it is possible to calculate the workspace of the RPPM. This is done by setting the orientation of the platform and solving for the workspace area at that particular angle, and then varying the angle to give a full workspace in terms of X versus Y for all possible orientation angles. The calculated workspace will be diminished later when the joint limits are taken into account. Figure 2.2 shows the workspace of the RPPM as a graph of the workspace in X and Y of the centre of the platform with respect to the orientation of the platform. It is evident that the majority of the workspace area is when the platform orientation

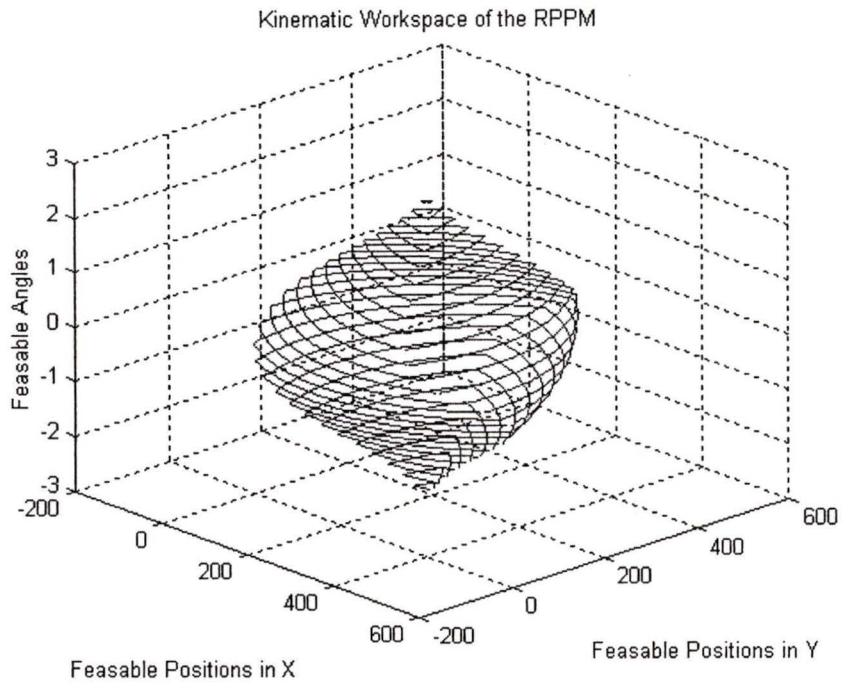

Figure 2.2: The kinematic workspace of the RPPM.

angle is within ± 1 radian of zero. In fact, approximately 75% of kinematic workspace of the RPPM lies between -1 and 1 radians, as illustrated in Figure 2.3.

2.4 Design for Reconfigurability

2.4.1 Of Mechanism Type

To reconfigure the RPPM into three different mechanism types, it was decided to begin with the 3-DOF 8-Bar device. It was noted that by removal of any one of the branches, the 3-DOF 6-Bar mechanism can be achieved. The 5-Bar device can formed by locking the platform to the forearm of any one of the two remaining

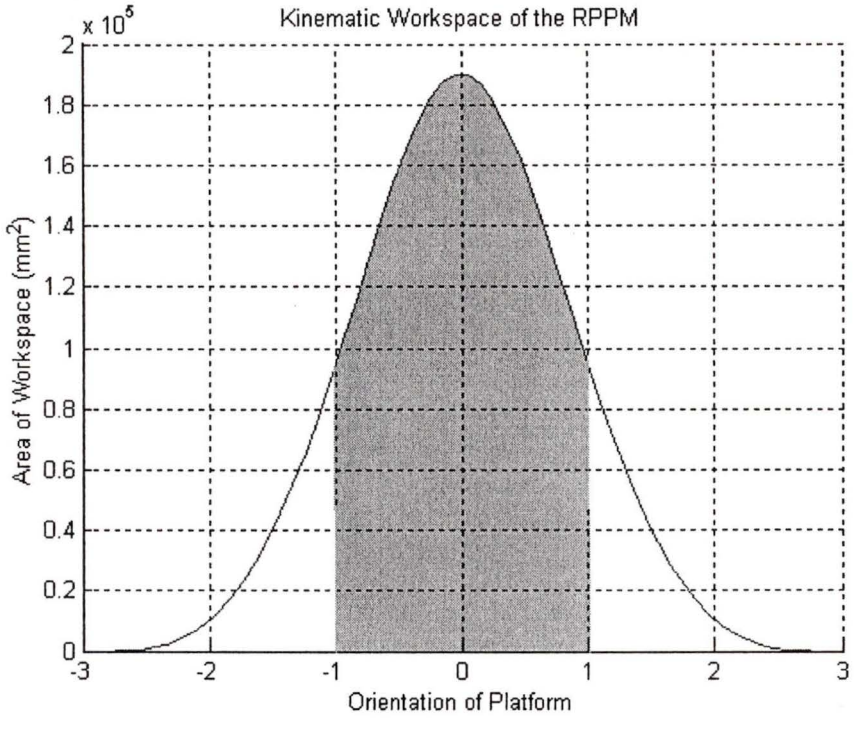

Figure 2.3: The area of workspace of the RPPM versus the orientation of the platform.

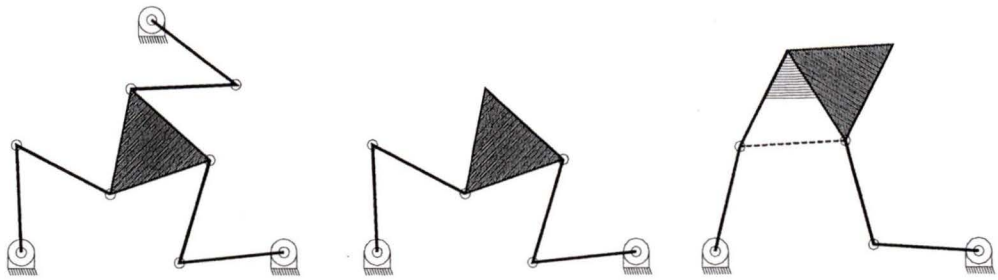

Figure 2.4: The three configurations of the RPPM, from left to right: the 8-Bar, 6-Bar, and the 5-Bar.

branches, resulting in an equivalent link of length equal to the other links. Figure 2.4 shows schematics of the RPPM as the 8-Bar device, as the 6-Bar device, followed by the 5-Bar device formed by locking the platform to the forearm of the left branch.

A major benefit of the proposed design is the ease of reconfiguration. When in the 8-Bar device, simply unhooking one branch and removing the corresponding base of the branch leaves the 6-Bar device. To then configure into the 5-Bar device a single bolt can be placed through the forearm link of one of the remaining branch and into the platform. To reconfigure from the 5-Bar to the 8-Bar, the reverse of this procedure is followed.

2.4.2 In Actuation

The major benefit of reconfigurability in actuation is the ability to test different non-redundant as well as different redundant-actuation configurations. For example, Figure 2.5 shows the 8-Bar device with all four possible desired non-redundant actuation configurations. In 2.5(a) all the shoulder joints are actuated, while all the

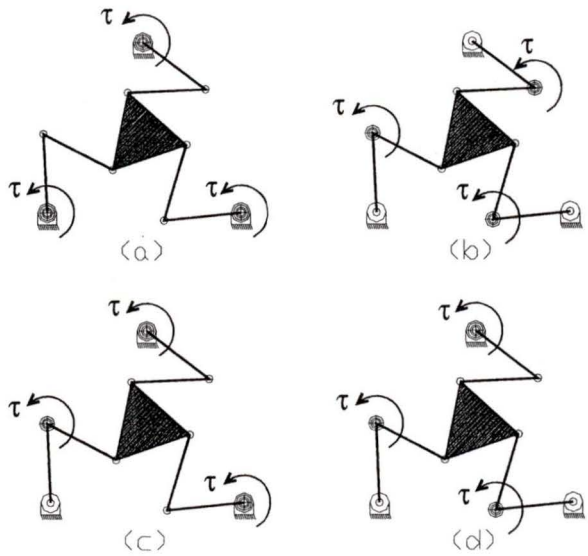

Figure 2.5: The four actuation configurations possible for the non-redundatly actuated RPPM.

elbow joints have free passive bearings. In 2.5(b) the shoulder joints have the free passive bearings and the elbow joints are actuated. In 2.5(c) two shoulder joints and one elbow joint are actuated, and in 2.5(d) two elbow joints and one shoulder joint are actuated.

Figure 2.6 shows all of the redundantly-actuated configurations desired for 8-Bar configuration of the RPPM. In 2.6(a) there is one extra actuator for a 1-degree of redundancy (1-DOR) mechanism. All of the shoulder joints and one elbow joint are actuated. The remaining two elbow joints are passive bearings. In 2.6(b) there is also a 1-DOR mechanism, but here two shoulder joints and two elbow joints are actuated. The remaining elbow joint and shoulder joint are free passive bearings. 2.6(c) shows the remaining possible 1-DOR mechanism available. Here all of the elbow joints and one of the shoulder joints are actuated. The remaining two elbow

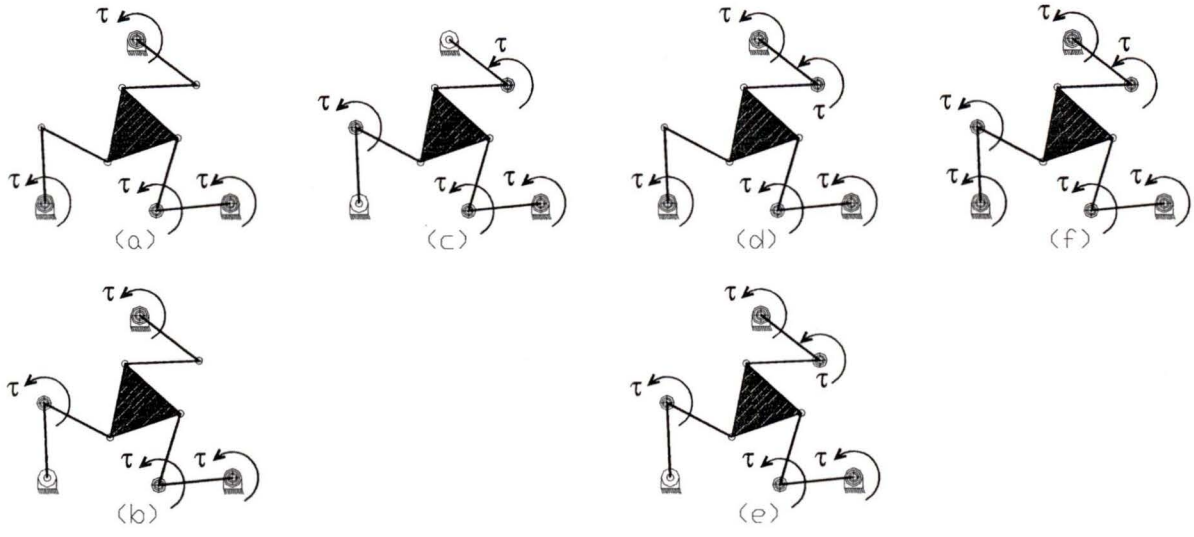

Figure 2.6: The redundantly actuated configurations for the RPPM.

joints have free passive bearings. In 2.6(d) there are two extra actuators for a 2-DOR mechanism. All of the shoulder joints and two of the elbow joints are actuated. The remaining elbow joint is a free passive bearing. 2.6(e) shows the only other possible 2-DOR mechanism. Here all of the elbow joints and two of the shoulder joints are actuated, and the only joint with a free passive bearing is a shoulder joint. Finally, 2.6(f) shows the only possible 3-DOR mechanism desired, where all shoulder joints and elbow joints are actuated. Here there are no free passive main-arm joints in the branches.

All of the devices shown in Figure 2.5 and Figure 2.6, while still of the same mechanism type (the 8-Bar mechanism), have different kinematic and dynamic properties, e.g., different singularities.

To satisfy desired reconfigurability in actuation, it was noted only the shoulder and elbow joints of the branches need to be actuated and reconfigurable. Therefore,

using a single and simple joint design makes it easier to facilitate the reconfiguration. To be able to reconfigure, a passive bearing replacement must be designed to allow substitution for the actuators at the joints.

2.4.3 Of Sensing Arrangements

As each actuator is equipped with an encoder, reconfigurability in actuation directly yields reconfigurability in sensing. Equipment to sense the displacement of the unactuated joints is not critical for the control of the actuated joints.

It was desired that the force sensors located on the payload (as will be discussed further in Section 2.5.7) can be replaced and removed as desired. This allows operation of the RPPM with or without the force sensing at the payload. For example, during the initial PID control experiments the RPPM was run without the force sensors, so that if any unforeseen errors occurred the resulting forces could not damage the force sensors in any way.

2.5 Physical Design

2.5.1 General Design

General Layout

It was first decided to use a cascading type of design to maximize the available joint limits. The first link of each branch would sit on top of the second link, and the second link would sit on top of the payload (platform). This was slightly modified with the second link in each branch being changed into a yoked link, having the platform sit inside the yoke, to allow more even force application from the branch to

Table 2.1: Important secifications of the DC motors

	Regular	**Supra**	
Output Power	14.5	26.1	W
No Load Speed	4800	5400	RPM
Stall Torque	16.3	26.2	oz-in

the payload.

Actuators

The existing actuators in the RAM Lab are Micro-Mo Series 3557 12 volt DC motors. There are two sub-types of these actuators, the regular and the supra. The important specifications of the regular and the supras are shown in Table (2.1). These motors have Micro-Mo 30/1 planetary gear reducers installed which give a 134:1 gear reduction. The complete manufacturers data sheets for the motors and gear reducers are contained in Appendix A.

2.5.2 Elbow and Shoulder Joint Design

The basic joint design is simple. The cascading design allows one link to sit on top of the subsequent link. The motor is bolted to this upper link and is held accurately by creating a precision fit hole for the boss of the motor. The shaft of the motor is attached to the lower link. To attach the motor shaft to this second link an adapter sleeve is used, which attaches to the motor shaft. This adapter sleeve is then attached to the lower link with a set screw.

To facilitate the use of a bearing instead of an actuator, bearing mounts were designed to be attached where the actuators are attached. The bearing sits in a

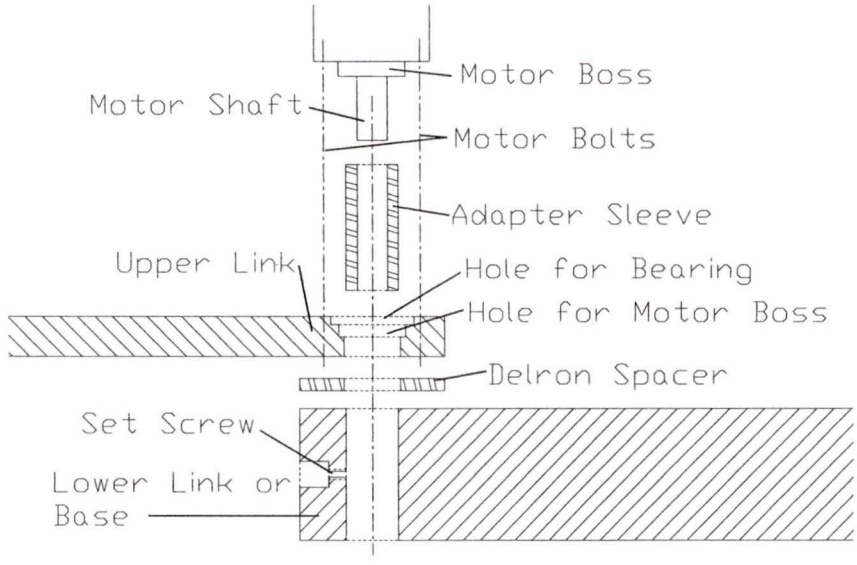

Figure 2.7: The general joint layout of the RPPM

precision fit hole on the link. The bearing bore is identical to the motor shaft. Thus small shafts were designed to fit through the bearing and into the adapter sleeves. The technical drawings of all the parts are located in Appendix B.

As all of the material being used is aluminum, spacer rings were made out of delron to fit between any two successive moving parts to keep the aluminum from "gumming up". A schematic of the general joint design is shown in Figure 2.7.

2.5.3 Base Design

The bases were designed to be the same height as the top surface of the second link is off the table surface. This was quite simple as roller bearings (discussed later in Section 2.5.5) are attached to the second link and are of known dimension. The middle of each base has the hole into which the shaft and adapter sleeve from the actuator are fitted. There is also a hole that fits a set screw which fixes the shaft and

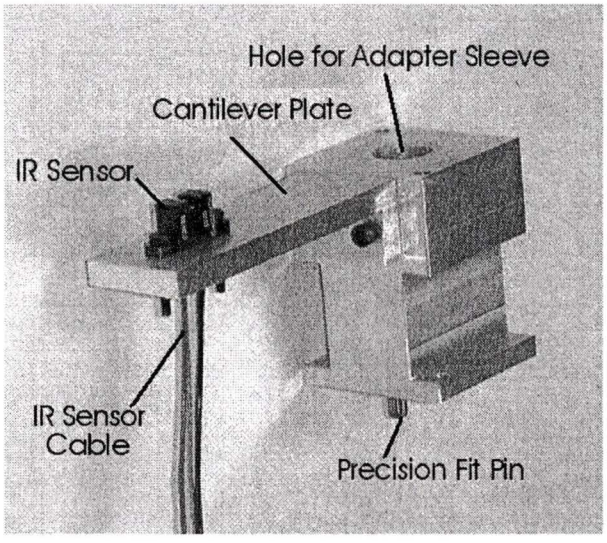

Figure 2.8: A base of an RPPM branch.

sleeve to the base. The bases also have an outreaching cantilever plate that attaches to hold an IR sensor used in homing the actuators. The homing based on the IR sensors will be discussed in further detail later in Section 2.5.7. A base (detached from the table surface) is shown in Figure 2.8, and the technical drawings are located in Appendix B.

The bases bolt onto the table top with two bolts. Two pins are on the bottom of each of the bases which fit into corresponding holes on the table surface precisely. The two pins are used to allow the bases to be removed and replaced accurately and repeatably. They are a precision fit. There is no play or movement of the base regardless of the bolts being tightened. The bolts are simply used to hold the bases to the table surface.

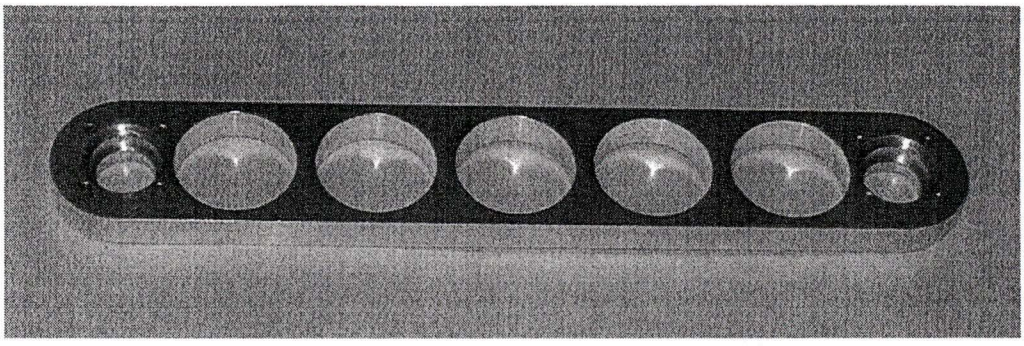

Figure 2.9: Link 1 of the RPPM.

2.5.4 Link 1

The first link of each branch must hold the actuator for both the elbow and shoulder joint. Since both the shoulder and elbow joint are to be the same, there is no need to make the shoulder and elbow joint sides of Link 1 different. Therefore, Link 1 is symmetric allowing its installation in either way. The actuators bolt on from underneath through countersunk holes in the link, and the link is designed with a hole to hold the boss of the motors accurately. There is a recess equal to the outer diameter of the bearings. The recess is used to hold the bearing accurately in case a non-actuated joint is desired. Finally, the link is laced with large holes to reduce the weight and inertial effects. Link 1 is shown alone in Figure 2.9. The technical drawing of Link 1 is located in Appendix B.

2.5.5 Link 2

The second link of each branch is not symmetrical like the first link. One end of Link 2 houses a hole for the motor shaft and a set screw similar to the base design. The link is yoked to hold the platform from either side at the wrist, so the only forces

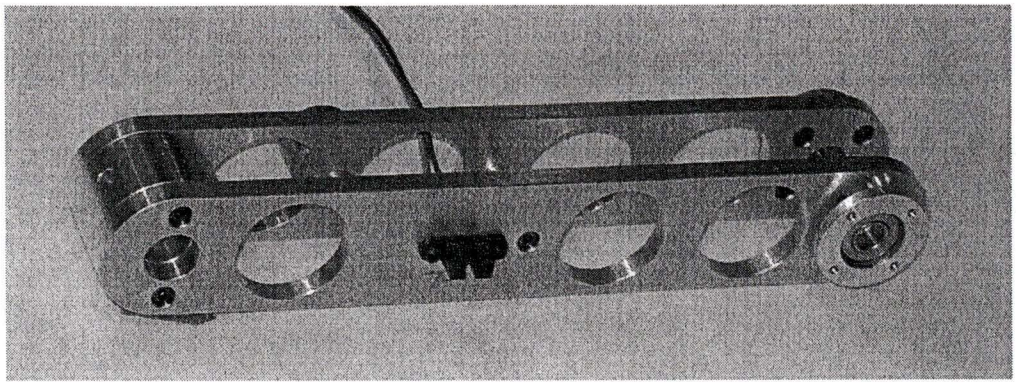

Figure 2.10: Link 2 of the RPPM.

being transmitted to the payload are in the desired plane of motion. The yokes are held apart in the centre of the link by a peg. A threaded hole allows a roller bearing to be placed underneath Link 2. This roller bearing sustains loads perpendicular to the plane of motion of the links, without creating a great deal of friction. Similar to the first link, the second link is filled with large holes to reduce the weight and inertial effects. Link 2 also houses a location for an IR Sensor, as will be discussed later in Section 2.5.7. Link 2 is shown in Figure 2.10. The technical drawings of all the parts required to assemble Link 2 are located in Appendix B.

Located at the wrist side of Link 2 is a counter-sunk hole. On the platform side of the wrist there is a corresponding threaded hole. This hole is used for a bolt to lock the wrist solid so that the second link and the platform configure into one large link for the 5-Bar mechanism. The resulting link length is the same as the length of the other links, i.e., 200mm.

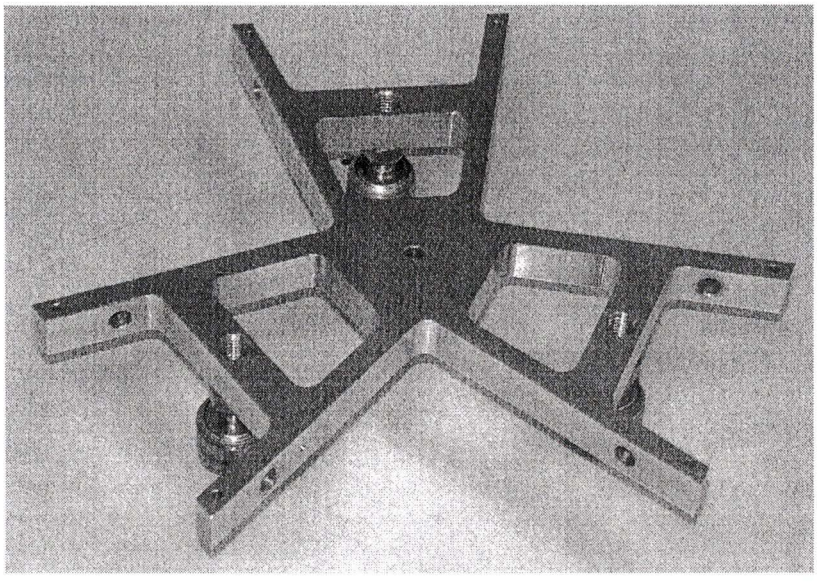

Figure 2.11: The RPPM platform.

2.5.6 Platform

The platform itself is designed around an equilateral triangle, with a wrist located at each vertex. The design is very simple, providing surfaces for force sensors to be mounted. This will be discussed further in Section 2.5.7. The platform possesses three threaded holes for roller bearings to take the load perpendicular to the plane of motion out of the platform. The platform is shown in Figure 2.11, devoid of wrists but with the roller bearings installed. The technical drawing of the platform is located in Appendix B.

2.5.7 Sensing Design

Position Sensors

The arrangement of the position sensing for the RPPM is extremely simple. Hewlett Packard (HEDS-5540) optical encoders are located on the motors. The encoders give 512 counts per motor revolution. With a gear reduction of 134:1, and quadrature encoding, 274,432 counts per revolution of the output shaft can be resolved. This allows for a resolution of 2.289×10^{-5} radians. The limitation of the positional sensing is that an actuator must be used to sense the displacement of the joint. No method of sensing a passive joint has been investigated. For more information on the optical encoders, please see [28].

Homing Sensors

The encoders are an incremental type of encoder, not an absolute type. Each time the RPPM is powered the joint angles need to be set (homed). To accomplish this homing, Hewlett Packard HOA 1881 infrared sensors are located on the RPPM at known locations, and each actuated joint has a cutter plate attached at a known angle. The specification sheets provided with the sensors are included in Appendix A. For the shoulder joint, the IR sensors are located on a cantilever beam that sticks out from the bases. An image of this is shown in Figure 2.12. For the elbow joints, the sensors are located on the second link. The cutter plate will interrupt the IR beam at a known angle (which can be varied by changing the orientation of the cutter plate with respect to the actuator) and triggers the sensor. A close up image of the cutter plate and IR sensor for the elbow joint on the second link are shown in Figure 2.13.

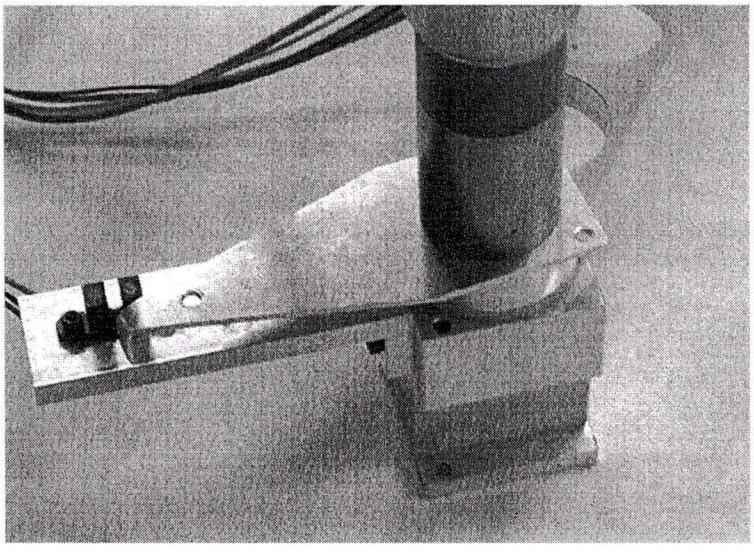

Figure 2.12: The shoulder homing arrangement of the RPPM, with the IR sensor and the cutter plate.

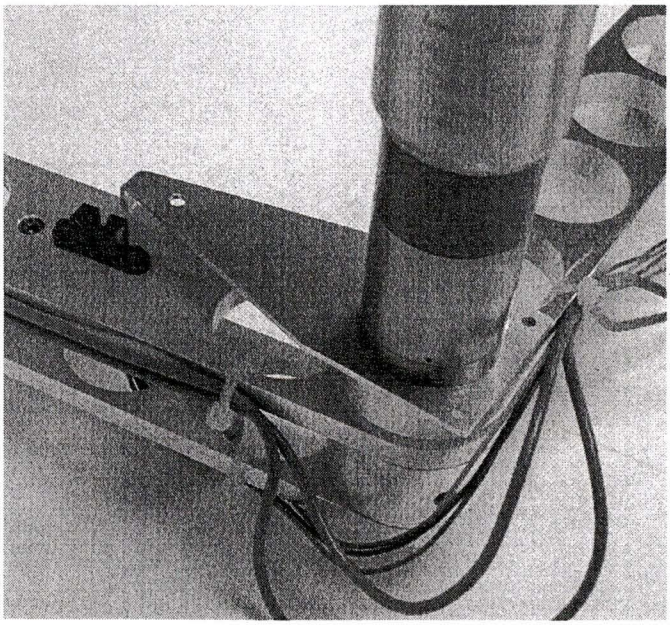

Figure 2.13: The elbow homing arrangement of the RPPM.

Force Sensing

Equipment: The force sensors chosen to be used on the RPPM are Transducer Techniques MLP-25 load cells. These are one-dimensional strain-gauge load cells. They boast a ± 25 pounds capacity. This translates to just over ± 111 Newtons capacity. The specification sheets for the force sensors are provided in Appendix A.

To condition the signal and translate the loads at the sensor into voltages, Transducer Techniques TMO-1 Amplifier/Condition Modules are used. They output ± 8 Volts and have two potentiometers which can be set to adjust the gain and the balance of the output signal. They are set so that 0 Newton load = 0 Volts, and a 10 Newton load = 0.75 Volts. This allows the ± 8 Volts output of the amplifiers to provide a range of sensing of ± 106 Newtons. The specification sheets for the conditioner modules are provided in Appendix A.

The A/D board chosen to read these signals into the control computer is a CIO-DAS16/Jr/16. This is a 16 channel A/D board. It was chosen for two reasons. The first reason is that this same board is currently being used in the RAM Lab, and therefore the majority of the software infrastructure exists. The second reason it was chosen, was that as a 16 channel board any new analog sensing that is added to the RPPM at a later date will not require any additional hardware, as there will be 10 channels not used by the six load cells. Set up with an input range of ± 10V, and with a resolution of 16 bits (65536 counts), this translates to a voltage resolution of 3.05×10^{-4} Volts. This yields a theoretical force resolution of 4.07×10^{-3} Newtons. For more information on the A/D boards used, please see [29].

Layout: Since the wrist consists of a passive revolute joint in the $\hat{\mathbf{z}}$ direction, only forces in $\hat{\mathbf{x}}$ and $\hat{\mathbf{y}}$ can be applied to the payload by each branch, i.e., no moment can

be applied at the wrist centre. To measure the $\hat{\mathbf{x}}$ and $\hat{\mathbf{y}}$ directional force at this point, two force sensors, for each branch, are aligned so that their corresponding axes of sensing intersect at the wrist centre. To keep the software work simple, the axes of sensing are aligned perpendicular to each other.

Preliminary testing was done to see how well two fixed perpendicular sensors would function before the design was finalized. A mock up of the wrist was built and known loads and directions of loads were compared to the sensed results. The sensed results, while not varying greatly in magnitude from the applied, had directional errors which were unacceptable. These errors were hypothesized to be due to shear forces being sensed and distorting the sensed force. To test this theory, one Del-Tron RD1 (see Appendix A for the specification sheets) linear slide was placed between each force sensor and the wrist. The linear slides were oriented to give a free motion perpendicular to the sensed force for the sensor, and were sized so that they could sustain the loads equal to the force sensor capabilities. When force sensing with linear slides was tested, it was clear that the original hypothesis of shear forces was correct, as the errors in direction were greatly reduced. The results of the force testing are show in Figure 2.14.

The resulting wrist design is shown in Figure 2.15, with all discussed features labelled.

2.6 Hardware System

The hardware associated with the actuators of the RPPM was already in possession of the RAM lab. It is also of a modular nature. Each motor is controlled by a PMDI MFIO-3A motor controller board, with each motor controller board capable

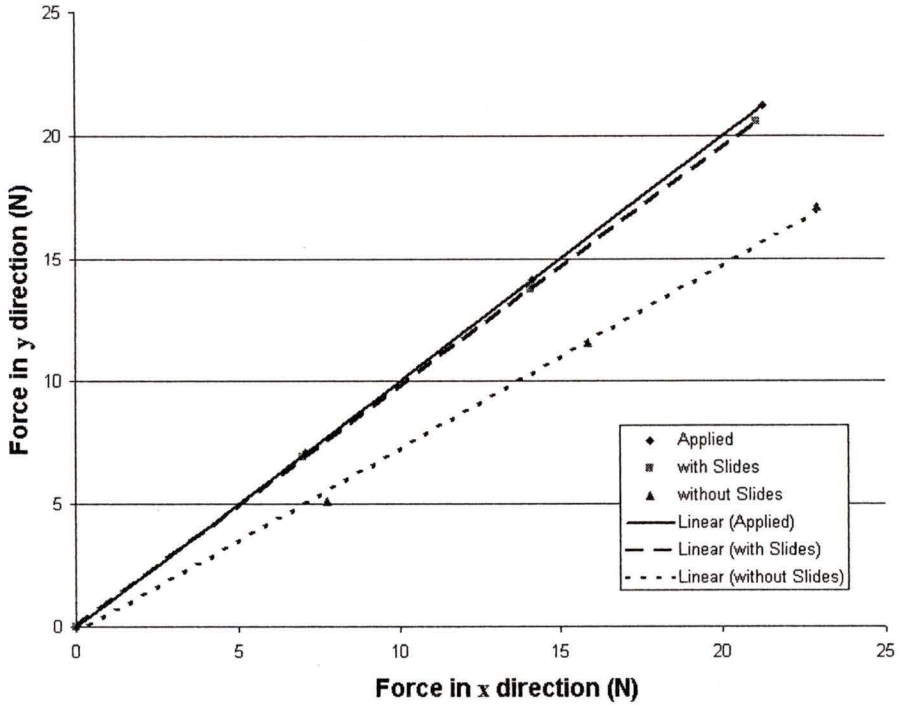

Figure 2.14: Graph of force applied and sensed (with and without linear slides).

of controlling up to three motors. For more information on the MFIO-3A boards, please see [30]. Each motor controller board runs through an interface board (see Appendix C) and then to linear amplifiers [31] that provide the power to the motors. An interface board, along with three linear amplifiers and a power supply are located in a linear amplifier/power supply boxes[1]. Two boxes are required for the up to six actuated axes of the RPPM. The encoders and IR homing sensors are also connected through the linear amplifier/power supply boxes. Each box also has an emergency stop switch.

[1]Mr. Scott Nokelby, M.A.Sc. and Mr. Paul Sobejko, M.A.Sc. are thanked for constructing the linear amplifier/power supply boxes.

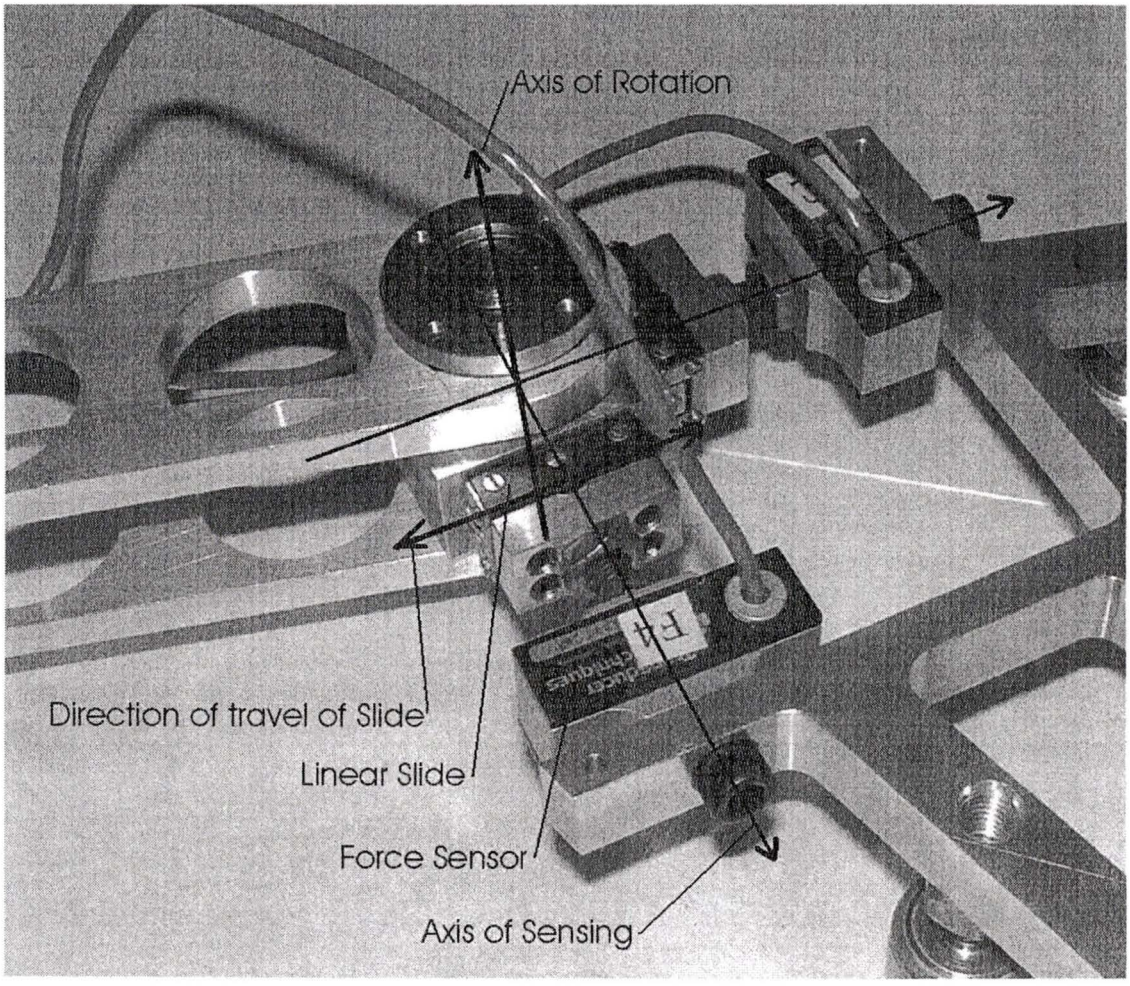

Figure 2.15: The final wrist layout of the RPPM.

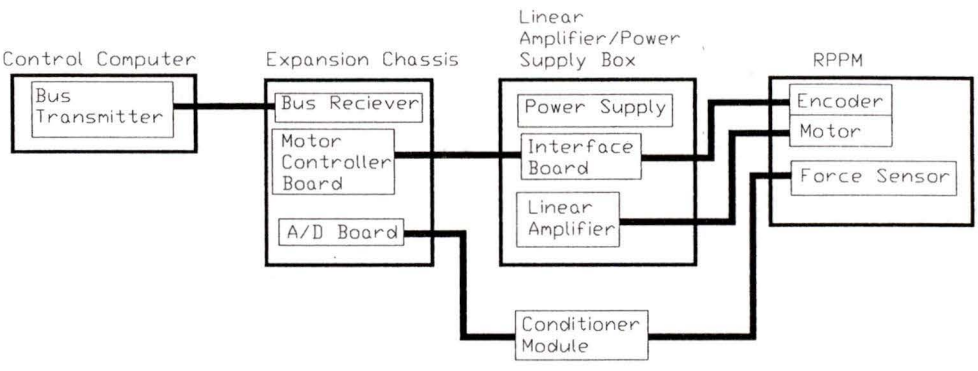

Figure 2.16: A schematic of the hardware for the RPPM.

The force sensors are hooked up directly to the A/D board on the computer. Running the RPPM with six motors requires the use of two motor controller boards and the A/D board. The computer does not have enough ISA slots to accommodate these cards. Therefore an ICS Advent OMNIX 400 series expansion chassis [32] for the computer is used. The expansion chassis is connected to the computer using an ICS Advent ECIK-2001 AT bus expansion kit [33]. This bus expansion kit has a transmitter which is placed into an open ISA slot in the computer and a receiver which is placed in an ISA slot in the expansion chassis. This allows the remaining 14 ISA slots in the expansion chassis to be used for the cards of the RPPM. A schematic of the hardware system is shown in Figure 2.16.

The computer is running QNX, a real time operating system. All of the software for the control programs is done in ANSI C. The control programs will be discussed further in Chapter 3. The motor controller boards and the A/D board came with existing libraries and functions. The existing libraries and functions simplify the use of the controller boards.

2.7 Discussion of Design

2.7.1 Comparison of Final Design to Initial Criteria

Reconfigurability

Reconfigurability in mechanism type has been successfully achieved. To reconfigure from the 8-Bar mechanism to the 6-Bar mechanism requires the removal of the two bolts which hold the force sensors of one branch to the payload. The removal of the two bolts completely removes the corresponding branch's wrist from the remainder of the mechanism. Removal of the two bolts for the corresponding base will facilitate complete removal of the branch from the table surface. All of the corresponding wiring is done with quick connectors. Removal and replacement of a branches wiring is simple. To reconfigure into the 5-Bar device, the bolt must be placed through the 2nd link and into the wrist. To reconfigure back, the reverse of this process is done. The RPPM is shown in the 8-Bar configuration in Figure 2.17. The RPPM is shown in the 6-Bar configuration in Figure 2.18. The RPPM is shown in the 5-Bar configuration in Figure 2.19.

Reconfigurability in actuation has also been achieved, though not as simply as reconfiguration of mechanism type. To change an actuated joint to a passive joint, the joint must be disassembled by undoing the shaft and sleeve from the lower link. The actuator must be then removed from the first link, and the bearing housing, with the bearing, must be put in place of the actuator. A shaft and adapter sleeve must be added and this new joint must then be reconnected to complete the reconfiguration to a passive joint from an actuated joint. Figure 2.20 shows both an actuated joint and the replacement passive bearing.

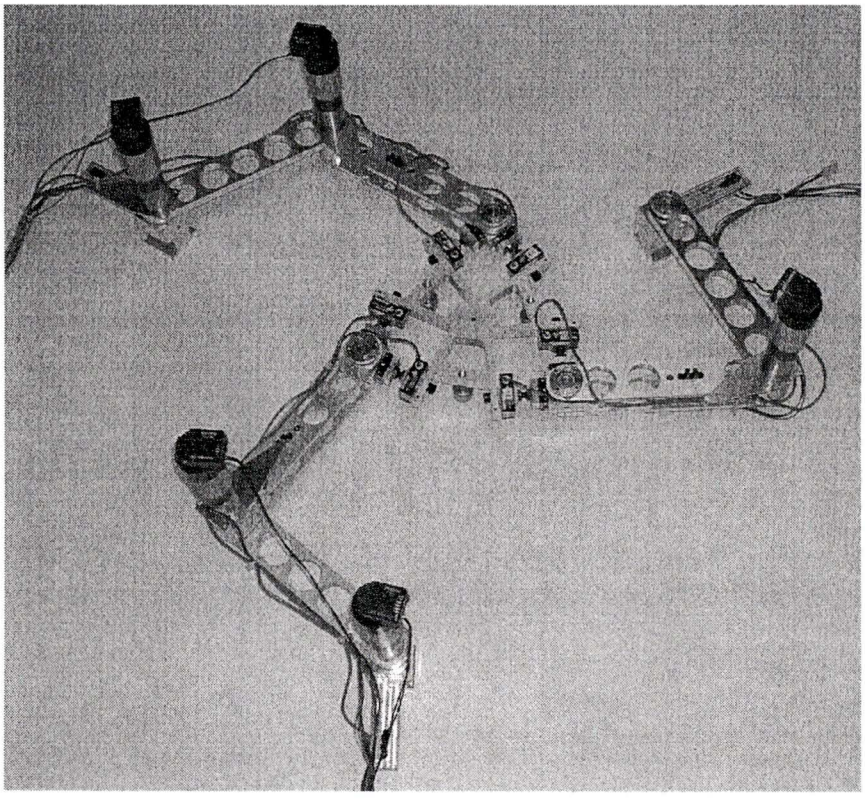

Figure 2.17: The 8-Bar configuration of the RPPM.

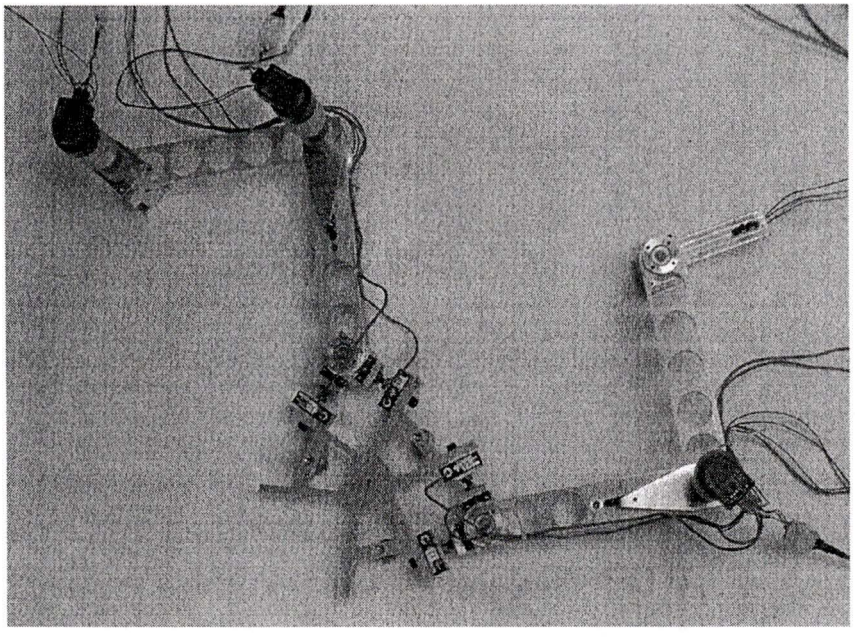

Figure 2.18: The 6-Bar configuation of the RPPM.

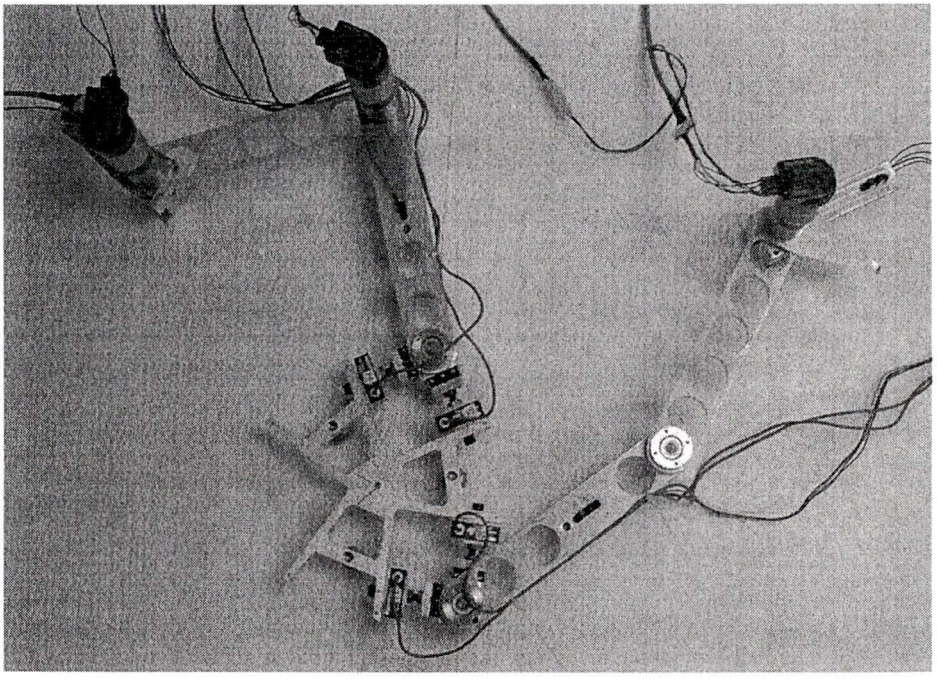

Figure 2.19: The 5 Bar configuration of the RPPM.

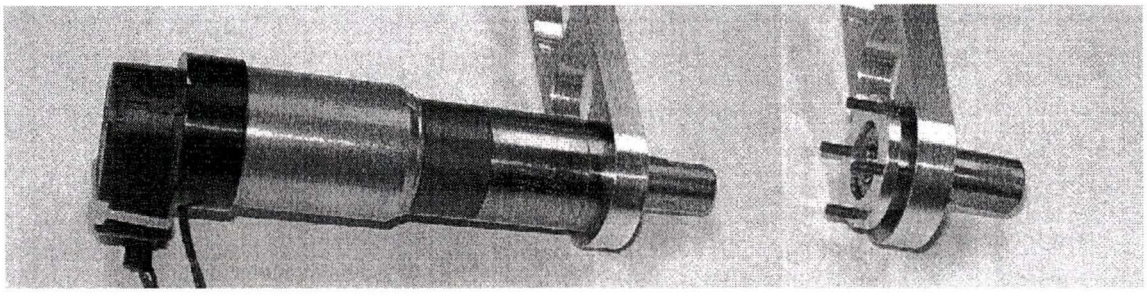

Figure 2.20: The replacement of an actuator with a passive bearing.

Reconfigurability of the force sensing is also achievable. The force sensors can be removed, and in their place bolts can be used. Figure 2.21 shows a wrist with one force sensor installed and one bolt installed in lieu of the other sensor.

Other Criteria and Constraints

The other criteria and constraints in the design were achieved:

- the existing Micro-Mo series 3557 motors and gearheads of the RAM lab are used in the design. No additional actuators are required,
- the forces being applied to the payload from the branches can be sensed accurately, as proven with the test rig,
- the design was kept as light as possible, to minimize the inertia seen by the actuators. Large holes were placed in the links to keep them light,
- the resulting design is simple and inexpensive to manufacture and to implement,
- and maximization of the kinematic workspace was achieved as discussed in Section 2.3.2. The workspace and joint limits of the actual design will be discussed in Section 2.7.2.

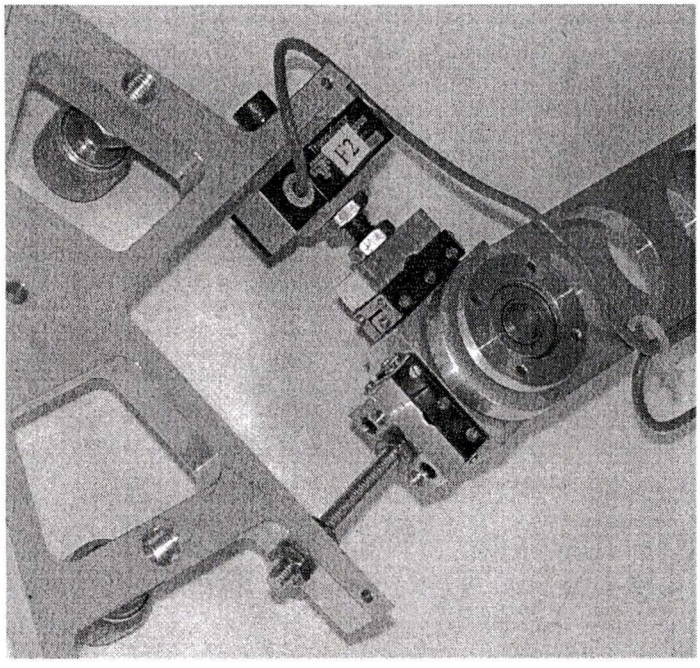

Figure 2.21: The replacement of a force sensor with a bolt.

2.7.2 Joint Limits And Workspace

The workspace of the physical RPPM is different than that of just the kinematic model of the RPPM. This is caused by the limits on the joint displacement values and by any physical interference between any of the links. For the shoulder joint, the IR sensor located on the cantilever plate can interfere with the first link. This interference creates an angle of approximately 0.62 radians (35 degrees) which Link 1 cannot enter. This leaves approximately 325 degrees of motion of Link 1 with respect to the base. The motion of Link 2 with respect to link 1 is also limited by the IR sensor. Since both the shoulder IR sensor and the elbow IR sensor are located at equal distance from the joint, the elbow sensor also creates an angle of 0.62 radians which Link 2 cannot enter with respect to Link 1.

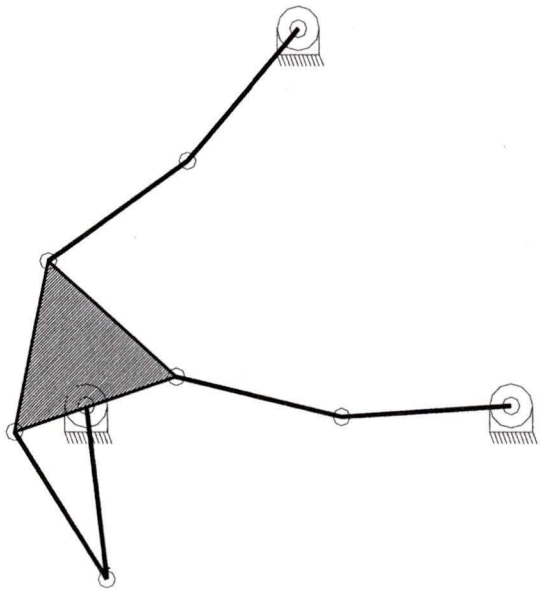

Figure 2.22: The platform interfering with a base.

Motion of the platform with respect to the second link is also limited by physical interferences. With the force sensors installed, it is the cable connecting them that interferes with the second link. This interference causes 2 radians of space which the platform may not enter with respect to the second link, leaving approximately a 245 degree joint limit. Without the force sensors installed, the interferences are much less, and over 270 degrees of motion is achievable.

Another interference that can limit the actual workspace of the RPPM is interference between the platform and the bases. It is possible, in some positions, for the branches to be able to reach the wrists but where the platform will be "in" the base. Figure 2.22 shows an example of this where all the joint angles are within their limits, yet the platform is interfering with a base.

The final, diminished workspace is then less that the initial kinematic workspace.

A method for solving the actual workspace has been shown by Gosselin and Jean [20]. They solved the problem by creating arcs and lines that each of the kinematic chains can reach and intersecting them to form the boundary of the workspace.

2.7.3 Errors

The main objective of the RPPM is to create an accurate and reliable testbed manipulator, therefore, sources of errors in the system are of great concern. To deal with errors requires not only minimization of them, but also acknowledgment of them when there is no chance of minimizing them. A known source of error that may be considered "large" and unavoidable may be easier to deal with for the researcher than a "small", but unknown, source of error. Knowledge of unavoidable errors will at least keep results repeatable and understandable, and will give the end user the ability to make appropriate inferences about experiments and a fair comparison of simulated and actual results.

It should be noted that the errors that are being discussed here are errors due to the physical system, design and hardware. They are not the total errors of the RPPM. They are the errors where the sensed values being read by the control system are not the actual values. The errors associated with the control system will be discussed in Chapter 3. The total errors are the summation of the errors presented here and the errors due to the controller. However, the errors being discussed here are of greater importance to note. These errors exist regardless of the controller being used, and are quite often unknown to the user.

Homing

Any errors in the homing of the joints will obviously result in inaccurate position readings of the RPPM. The homing sensors, being digital on/off sensors, result in an extremely repeatable response. The mounting of the cutter plate is a possible source of error in the homing. The cutter plate is not pinned accurately as it uses the bolts to mount the motor for positioning. Measuring the play in the mounting, an extremely conservative estimation of the error in cutter plate mounting was found to be approximately $\pm 1.25 \times 10^{-2}$ radians per joint.

Position

Errors in position, other than from homing, stem from several factors. The first factor, though rather minor, is in the resolution of the encoders. Considering the 134:1 reduction ratio of 512 counts per motor revolution and the use of quadrature encoders, can attribute to a error of $\pm 2.29 \times 10^{-5}$ radians.

The second and largest source of error in position, is the backlash of the gear boxes. The specifications of the gear boxes boast a backlash of $\leq 1°$, which translates to $\pm 1.75 \times 10^{-2}$ radians of possible error for each joint.

Summing the possible errors in homing, and the possible errors due to the encoder resolution and the backlash of the gear boxes results in a total error possibility of $\pm 3.0 \times 10^{-2}$ radians per joint, regardless of the control system being used. To observe this error during operation of the RPPM, some form of external position sensing such as a visual system would be required.

Force

Sources of errors in the force sensing system can be tracked from the sensors to the reading at the control computer. The load cells boast a zero balance accuracy of 1.0% full scale, and a non-repeatability of 0.05% full scale, which when summed translates to ± 1.17 Newtons.

The amplifiers are set manually and as they have two setting, they can have two errors. The first of which is an offset error, the second of which is an error in slope. Assuming they are set to perfectly however, they boast a maximum error of 1% fullscale, which translates to an error of ± 1.07 Newtons. The A/D Board digitization adds a error of resolution of 4.07×10^{-3} Newtons.

When summed, a total possible error in the force sensed of ± 2.24 Newtons is conservatively estimated.

Chapter 3

Implementation of the RPPM

3.1 Overview

Implemention of the RPPM contains many issues. Development of an overly complex and specific control system is not a goal of this research. This chapter considers the development of a control system which allows the user to obtain repeatable and predictable results within an experimental error. To accomplish this, there are two simple and effective control schemes which are applied. This chapter presents the basic theory and the implementation issues surrounding a PID controller for application of the non-redundantly actuated RPPM and a hybrid position/force controller for application of the redundantly-actuated RPPM. For further detail, this work presented on PD, PID and hybrid position/force control is derived mainly based from [4], [34], [35] and [36].

Section 3.2 presents the basic theory behind the PD, PID and hybrid/position force controllers. Section 3.3 considers the general implementation issues surrounding application of the RPPM. Section 3.4 specifically considers the issues involved in

implementation of the two controllers. Section 3.5 presents results of testing the two controllers on the non-redundantly actuated 6-Bar for the PID controller, and the redundantly-actuated 6-Bar for the hybrid position/force controller. Finally, Section 3.6 provides a discussion of the results, including a discussion of the errors in the controller.

3.2 Theory of Control Algorithms

3.2.1 PD and PID Control Theory

The voltage of an armerature-controlled DC motor (as are the actuators of the RPPM) can be shown to be

$$V = K_{Emf}\dot{\theta} + L_A\dot{I} + R_A I \tag{3.1}$$

where K_{Emf} is the back emf constant of the motor, L_A is the armerature inductance, R_A is the armerature resistance, and I is the current.

In general, a torque τ supplied to a motor produces a response of

$$\tau = J\ddot{\theta} + B\dot{\theta} \tag{3.2}$$

where J is the moment of inertia, B is the friction and $\ddot{\theta}$ and $\dot{\theta}$ are the acceleration and velocity of the motor, respectively. Also, the torque of a motor can be shown to be

$$\tau = K_T I \tag{3.3}$$

where K_T is the torque constant of the motor. Solving for the current I using

Equations 3.2 and 3.3

$$I = \frac{J\ddot{\theta} + B\dot{\theta}}{K_T} \tag{3.4}$$

Substituting Equation 3.4 into Equation 3.1 yields

$$V = K_{Emf}\dot{\theta} + L_A\left(\frac{J\dddot{\theta} + B\ddot{\theta}}{K_T}\right) + R_A\frac{J\ddot{\theta} + B\dot{\theta}}{K_T} \tag{3.5}$$

By neglecting the third order terms and setting the friction term $B = 0$, Equation 3.5 simplifies to

$$V = K_{Emf}\dot{\theta} + R_A\frac{J\ddot{\theta}}{K_T} \tag{3.6}$$

The basic theory behind a PD control loop for a motor, is that for an error in position

$$\theta_{Err} = \theta_{Desired} - \theta_{Actual} \tag{3.7}$$

and an error in velocity of the motor

$$\dot{\theta}_{Err} = \dot{\theta}_{Desired} - \dot{\theta}_{Actual}$$

can be corrected by a torque τ_{Pos}

$$\tau_{Pos} = J\ddot{\theta} = (K_P\theta_{Err} + K_V\dot{\theta}_{Err}) \tag{3.8}$$

where K_P and K_V are the control constants to be chosen. In Equation 3.8, friction has been neglected. Placing Equation 3.8 into Equation 3.6 yields

$$V = K_{Emf}\dot{\theta} + R_A\frac{(K_P\theta_{Err} + K_V\dot{\theta}_{Err})}{K_T} \tag{3.9}$$

Equation 3.9 is used to find the voltage to supply to the motors for the PD control algorithm.

The basis of a PID controller is the addition of a steady state error integral term. More specifically, the torque τ_{Pos} to correct the θ_{Err} and $\dot{\theta}_{Err}$ is

$$\tau_{Pos} = J\ddot{\theta} = (K_P\theta_{Err} + K_V\dot{\theta}_{Err}) + K_I \int \theta_{Err}dt \tag{3.10}$$

where K_I is a third constant to be chosen for the controller. Substituting Equation 3.10 into Equation 3.6 yields

$$V = K_{Emf}\dot{\theta} + R_A \left(\frac{(K_P\theta_{Err} + K_V\dot{\theta}_{Err}) + K_I \int \theta_{Err}dt}{K_T} \right) \tag{3.11}$$

Equation 3.11 is used to find the voltage to supply to the motors for the PID control algorithm.

3.2.2 Hybrid Position/Force Control Theory

A hybrid force controller is derived from taking a position control scheme and adding a force control scheme in parallel This force control scheme is added to correct for errors with any external loading that may be desired from the actuator. This means a hybrid controller supplies a torque τ_{Pos} to correct for position errors, and a torque τ_{For} to correct for force errors. The torque τ_{For} will deal with the desired output torque of the actuator while τ_{Pos} will deal with desired position output of the actuator. More specifically, the torque to be supplied to an actuator is

$$\tau_{Tot} = \tau_{Pos} + \tau_{For} \tag{3.12}$$

Yoshikawa [14] presents that for a error in output torque of

$$\tau_{Err} = \tau_{Desired} - \tau_{Actual} \tag{3.13}$$

τ_{For} should be

$$\tau_{For} = K_F \int \tau_{Err} dt \tag{3.14}$$

where K_F is a constant to be chosen. Since this term is an integral term, it is not recommended to use the PID controller to create τ_{Pos}. If the PID controller were to be used, it is possible that the two integral terms would be countering each other, creating an unstable controller. Instead, using the PD controller to create τ_{Pos} leaves only the one integral term in τ_{For}. More specifically, placing Equation 3.8 and Equation 3.14 into Equation 3.12 yields

$$\tau_{Tot} = (K_P \theta_{Err} + K_V \dot{\theta}_{Err}) + K_F \int \tau_{Err} dt \tag{3.15}$$

Substituting Equation 3.15 into Equation 3.6 provides

$$V = K_{Emf} \dot{\theta} + R_A \frac{\left((K_P \theta_{Err} + K_V \dot{\theta}_{Err}) + K_F \int \tau_{Err} dt\right)}{K_T} \tag{3.16}$$

Equation 3.16 is used to find the voltage to supply to the motors for the hybrid position/force control algorithm.

3.3 Implementation Issues

3.3.1 Structure of Control Programs

For each configuration of mechanism and actuation there is a different main control program. Each program however, is very similar in structure and share many sub-programs. The overall program procedure is the same. Each program contains one main program. Used by all the main programs are libraries and subprograms for use of all the associated hardware. There are also subprograms which are specific to the

RPPM. These include the displacement solutions of the RPPM, the motor control functions, and the torque solutions resolving the sensed forces into joint torques.

3.3.2 Procedure of Control Programs

The overall program procedure is the same for all programs. First, all hardware must be powered up. Then the program can be run. Initialization of all the hardware is done first. All of the hardware is synchronized and checked for errors. If anything does not initialize correctly, the program shuts down immediately.

Once all the hardware has been successfully initialized, the RPPM is ready to operate. Since the encoders on the actuators are incremental encoders, the initial starting position of the RPPM is not known. Therefore, the manipulator must be homed. The procedure for homing is explained in detail in Section 3.3.3.

Once all the joint angles are known from the homing sequence, the FDS for the RPPM is solved so the exact location of the platform can be found. When non-redundantly actuated, there are multiple solutions to this problem. However, the initial start position from homing typically yields one of the multiple solutions. The program chooses the FDS solution that is nearest to the typically found solution.

The first desired position of the RPPM is then this homed position. There is typically a desired trajectory to follow in position, and if desired, in force. The determination of the trajectory will be discussed in Section 3.3.4. Each pertinent piece of information is read and calculated in every iteration of the control loop. The hardware is latched to read and write to the encoders and actuators at the same time. The force sensors are read as soon as possible to this latching. All important control information is then calculated, and the controller calculates a voltage to supply to

the actuators. This voltage is supplied at the same time as the information for the next control loop is read. How the control is done in joint space will be discussed further in Section 3.3.5. The application of the control algorithms themselves will be discussed in greater detail in Section 3.4.

During operation of the RPPM, in each control loop, data is written to memory pre-allocated by the computer. The data typically contains both desired and actual joint positions, desired and actual forces, and voltages supplied to the actuators. At the termination of the program, this data is written into a data file for later examination using Matlab. The reason the data is written initially into memory is to minimize the length of time each control loop takes to execute.

At the beginning of each control loop, multiple checks are being done to ensure safe operation of the RPPM. These checks include loop execution time, joints exceeding limits, if the emergency stop switch is activated, hardware problems, or any other of the possible errors that demand immediate shut down of the RPPM. If any of these errors trigger, the RPPM is immediately shut down, displaying which error caused the shutdown.

As mentioned, during the shutdown procedure the data is transferred to a data file. This data file must be transferred off the QNX computer, which is the operational platform for the RPPM, to a computer with Matlab. This is done over the network. Matlab files have been written to analyze the data and produce graphs and important pieces of information.

3.3.3 Homing

As mentioned in Section 2.5.7 there are homing sensors located on the RPPM. The optical encoders that are used to track the joint position are relative (incremental) encoders, and are not absolute. This means that every time the RPPM is powered up they must first be homed. Homing consists of setting the joint angle to a known location and then setting the encoder counts to be at this location. When non-redundantly actuated this is quite simple. Since the system is not over constrained, each actuator can be moved independently of any other actuator. This allows the program to simply prompt the user which way to turn the actuators. Then, one at a time, the actuators are moved until they trigger the IR homing sensors. Since the triggering occurs at known angles, the displacement of that joint is now known. Once all the actuators have been homed, the joint displacements and corresponding position and orientation of the RPPM are known.

The problem when redundantly-actuated is that any one actuator cannot be moved without effecting the other actuators, as the RPPM is overconstrained in position. To turn one motor to search for its homing sensor, other actuators must turn as well. This is similar to how they must co-operate during run time. To overcome this, the user is prompted to set approximate values for the joint displacements. These approximate values are used by the program to carefully move the RPPM to home each actuator in turn. Once a minimum number of sensors have been homed, the remaining joint values can be solved. This is done by using the FDS for the homed joints to find the position and orientation of the platform, then using the IDS to solve for the remaining joints.

3.3.4 Inputs to Controller

Two different possibilities exist for the input to the controller of the RPPM. Both inputs provide a velocity to the end effector. The first input, which is only mentioned out of interest, is the use of the RSI Joystick [3] as an input to the non-redundantly actuated RPPM. The RSI Joystick is capable of providing a 6-DOF input. Since the RPPM is at most a 3-DOF device, only the 3-DOF planar motion of the joystick is used. The other information from the joystick is ignored. This setup was done because it provided an interesting demonstration for both the RPPM and the RSI Joystick.

The second, and normal input to the RPPM, is a predetermined trajectory which is programmed into the main program off-line. This is mainly used to provide repeatable desired trajectories so the results of experimentation would be easier to compare.

3.3.5 Joint Space Control

All of the control for the RPPM is done in joint space. This means that each joint is controlled independently of the others. The input velocity of the platform is integrated to yield a desired position and orientation of the platform, which is then converted into a new desired position for each joint, using the IDS. The new desired joint position, the desired joint position from the last control loop, and the execution time of a control loop are used to find a desired velocity for the joint. This method is not as accurate as using the Jacobian of the manipulator, but allows for a simpler solution which specifically avoids the use of the inverse of the Jacobian. The actual new position of each joint is measured, and the actual position of the joint from the

last control loop is used (along with the loop execution time) to provide an actual velocity of the joint.

The forces sensed at the wrists are translated into individual joint torques. Similarly, the desired joint torque values are resolved from the desired wrist forces. Therefore, each joint has all the errors it requires for the joint space control independent of the operation of any other joint.

3.4 Implementation of Joint Control Algorithms

3.4.1 PD and PID Control Implementation

The first obstacle to overcome is the choice of the constants K_P, K_V and K_I in the PID control loop. Craig [4] summarizes that the values of K_P and K_V should be

$$K_V = 2\sqrt{K_P} \tag{3.17}$$

It is also mentioned that typical the integral term K_I should be kept quite small so the system is "close" to the second order PD controller. For this reason, it was chosen that

$$K_I = \frac{K_P}{10} \tag{3.18}$$

In initial testing of the RPPM the constants were set to be extremely low so that any errors made would not cause any damage to the hardware. Slowly they were built up as the bugs were worked out of the control program. Final acceptable values were found to be $K_P = 100$, $K_V = 20$ and $K_I = 10$.

The program cycle when implemented with the PID control algorithm is quite simple, as no forces need to be dealt with. The control program loop is shown in a

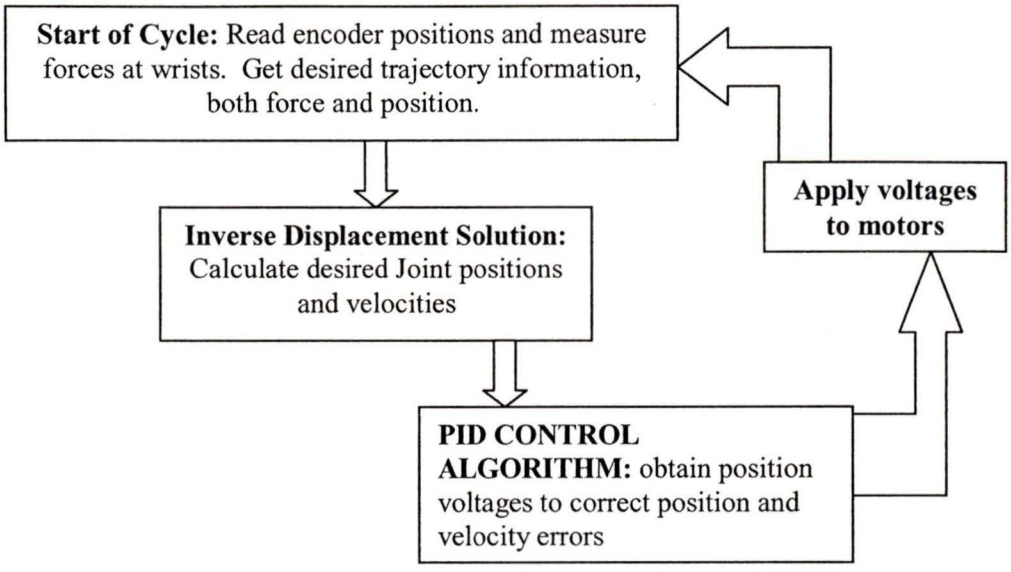

Figure 3.1: The flow chart depicting the PID control loop.

flow chart in Figure 3.1.

3.4.2 Hybrid Control Implementation

The first issue of implementation of the hybrid position/force controller is the choice of the control constants K_P, K_V and K_F. It was decided the position control constants K_P and K_V should be chosen according to Equation 3.17, and were set to the values of $K_P = 100$ and $K_V = 20$. K_F then had to be determined. It was decided to begin with, K_F should be set to 0 for initial testing. This PD-only control of the joint proved to give adequate responses. If K_F was increased to a large value, the controller became unstable in its position response to eliminate the dynamic forces sensed at the wrists. The maximum value found of K_F, without the controller creating large position errors, was approximately $K_F = 1$.

To determine the error in force of an actuator, a force feedback loop must be included. First, the desired force at each wrist is found. This is something that will vary greatly depending on what the user is trying to achieve or test. The desired forces at the wrist are used to solve for the desired joint torques.

The actual joint torques must then be found. This is done by first determining the actual pose of the platform. To accomplish this, the FDS is used with the actual sensed joint displacements. The measured forces at the wrist are then used to solve for the torques at the joints. It should be noted, however, that this "sensed actual torque" may in fact not be the "output actual torque" of the actuator. Issues such as friction may cause discrepancies between the two torques. This turns out to not be of great concern. What is actually desired by the user is the wrist force. Since the error term for force is an integral, the voltage and "output actual torque" will continue to increase until the error in "sensed actual torque" is zero. Therefore, the "output actual torque" may be different than the "sensed actual torque" for a joint, but the desired force at the platform is satisfied.

The program cycle for the hybrid controller is slightly more complex than that of the PID controller. The control loop is shown in a flow chart in Figure 3.2.

3.5 Results

3.5.1 Setups

For the Non-Redundantly Actuated PID Controller

Two setups are presented which show the effectiveness of the PID controller for the non-redundantly actuated 6-Bar mechanism. The first setup involved controlling the

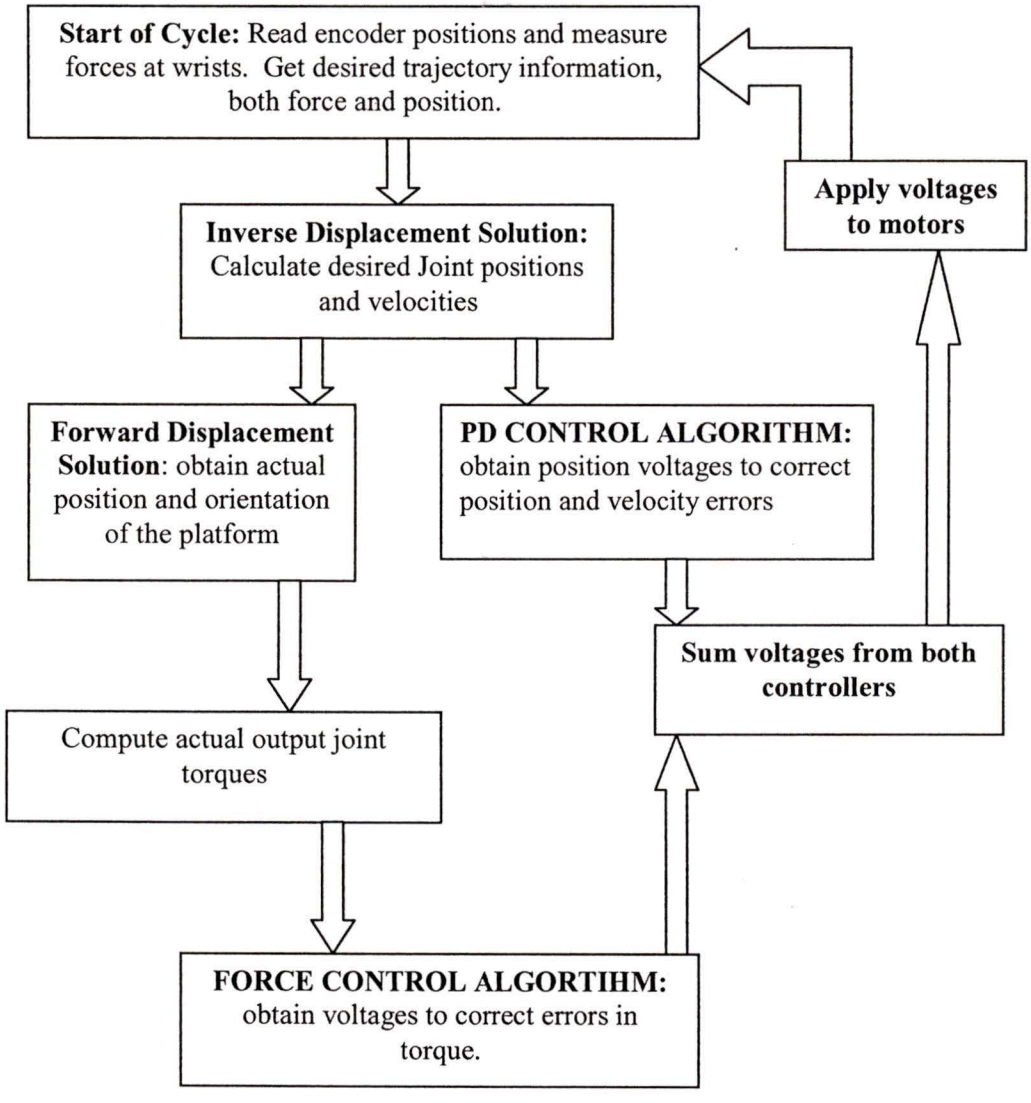

Figure 3.2: The flow chart of the hybrid position/force control scheme.

actuators over a desired trajectory when they were not hooked up to the RPPM. This was done because the controller does not include the dynamics of the RPPM, and will show the effects of the RPPM on the joint controllers. The second case tested with PID control was with the RPPM. Both cases used the values $K_P = 100$, $K_V = 20$ and $K_I = 10$. Both were actuated with a regular motor on the elbow of branch 1 ($\$_{2_1}$), a regular motor on the shoulder of branch 3 ($\$_{1_2}$), and with a supra motor on the elbow of branch 2 ($\$_{2_2}$). Note that only three joints were actuated for non-redundant actuation. The shoulder joint of branch 1 ($\$_{1_1}$) was unactuated.

For the Redundantly-Actuated Hybrid Controller

The setup for the redundantly-actuated 6-Bar configuration of the RPPM was the same as for the setup of the non-redundantly actuated 6-Bar configuration, with the addition of a supra motor on the shoulder joint of branch 1 ($\$_{1_1}$). The only free passive joints are the wrists. The constants used in the controller were $K_P = 100$, $K_V = 20$ and $K_F = .875$.

3.5.2 Desired Trajectory

The desired trajectories for all the results presented are the same. All the positions are for the centre of the RPPM platform. Initially, the trajectory begins with no motion (a pause) for 8 seconds. Then the RPPM moves with a sinusoidal velocity on a line in the direction of 225 degrees from the horizontal $\hat{\mathbf{x}}$ axis (downward, to the left at an angle of 45 degrees). This line is travelled in both senses in 4 seconds, with a maximum velocity of 0.11m/s. Travelling this line twice results in 8 seconds of motion. After completion of the line tracking there is a second pause for 4 seconds.

After the second pause, beginning at 20 seconds, the platform trajectory is a reorientation about its centre. The angular velocity of the platform follows a sinusoidal profile, the maximum being 0.15 radians/second. This reorientation is done twice, for 8 seconds of reorientation of the platform with no motion in $\hat{\mathbf{x}}$ or $\hat{\mathbf{y}}$. This reorientation is followed by a third pause for 4 seconds.

Beginning after the third pause, at 32 seconds, the platform moves with a sinusoidal velocity along a second line. This line is in the direction of 218 degrees from the horizontal $\hat{\mathbf{x}}$ axis. The maximum velocity reached is again approximately 0.11m/s. This line is travelled back and forth four times, for 16 seconds. This is followed by a fourth and final pause for 8 seconds.

After the fourth pause, the platform moves along a third line beginning at 56 seconds. This line is in the direction of 232 degrees from the horizontal $\hat{\mathbf{x}}$ axis. The program is ended at approximately 59 seconds.

3.5.3 PID Results

Only the Actuators, with PID Control

The desired and actual joint position through the trajectory as described are shown in Figure 3.3. The largest error of any of the joints through these trajectories was approximately 0.02 rads. The maximum error occurred for $\$_{2_2}$, the elbow joint of branch 2, at approximately 34 seconds.

The voltages supplied to the actuators are shown in Figure 3.4. The largest voltage supplied to any of the actuators was approximately 4.4V to $\$_{2_1}$ at approximately 8 seconds. This voltage corresponds to the high velocity of the joint at that instant.

As these desired motor trajectories were the same as in actual implementation,

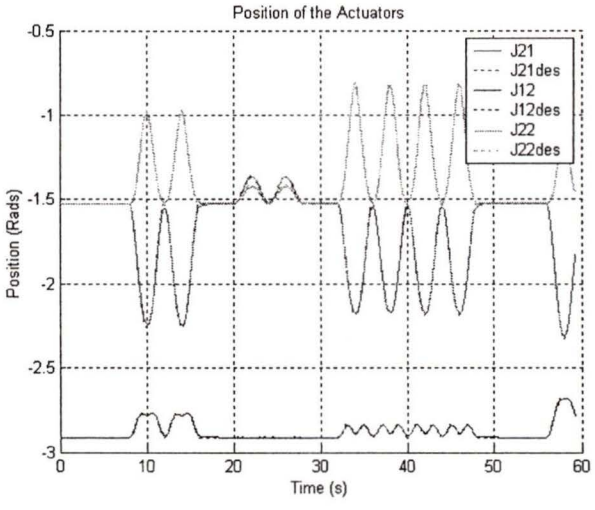

Figure 3.3: The joint position for the RPPM, actuators only.

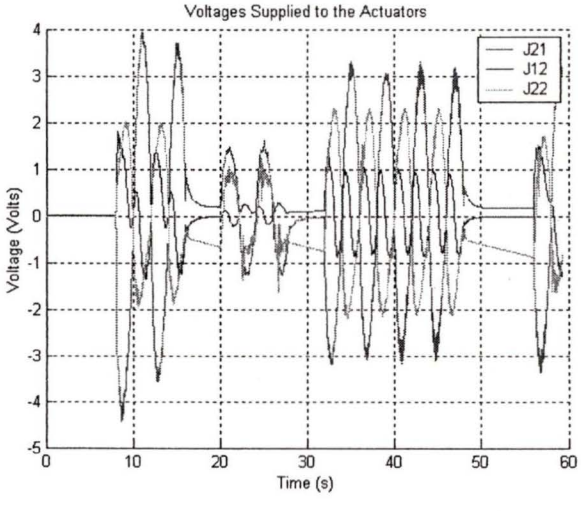

Figure 3.4: The voltages supplied to the actuators.

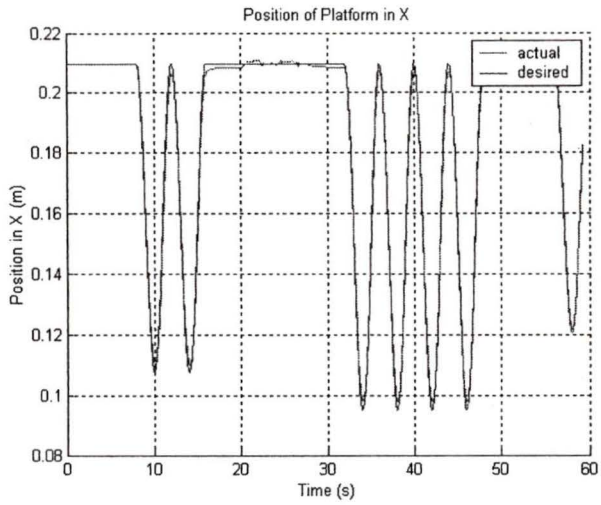

Figure 3.5: The theroetical x position of the RPPM, actuators only.

the actual motor trajectories can provide a theoretical position and orientation of the platform using the FDS. The desired trajectory of the RPPM platform and the theoretical trajectory that the RPPM would have followed are shown in Figure 3.5 for motion in the $\hat{\mathbf{x}}$ direction and in Figure 3.6 for motion in the $\hat{\mathbf{y}}$ direction. The largest theoretical error in position in the $\hat{\mathbf{x}}$ direction was approximately 0.003m, and occurred at about 34 seconds into the test. This corresponds to when the platform was undergoing constant position but was re-orientating. Largest position error in $\hat{\mathbf{y}}$ was approximately 0.004m and occurred at 58 seconds. This was when the platform was moving about on the third line.

The desired orientation of the platform and the theoretical orientation the RPPM would have followed are shown in Figure 3.7. The largest orientation error of platform was approximately 0.025 radians at about 34 seconds.

Putting the $\hat{\mathbf{x}}$ and $\hat{\mathbf{y}}$ trajectories into Cartesean paths, the RPPM would have moved as shown in Figure 3.8. As can be seen, the actual path the RPPM would

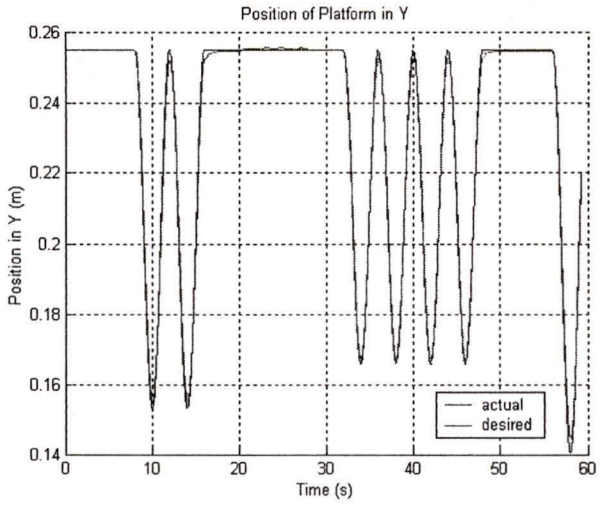

Figure 3.6: The theoretical y position of the RPPM, actuators only.

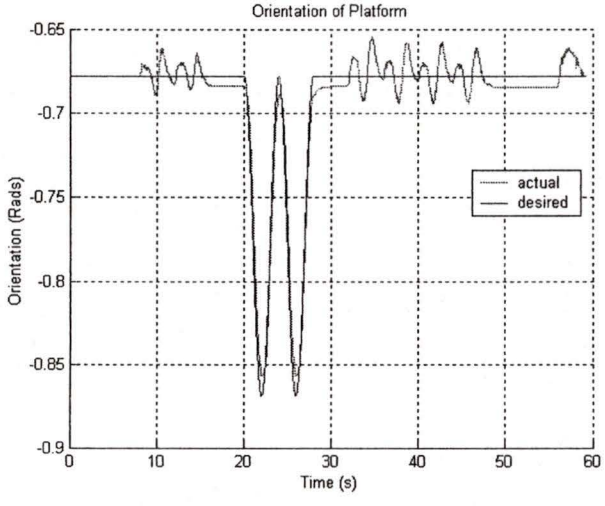

Figure 3.7: The theroetical orientation of the platform.

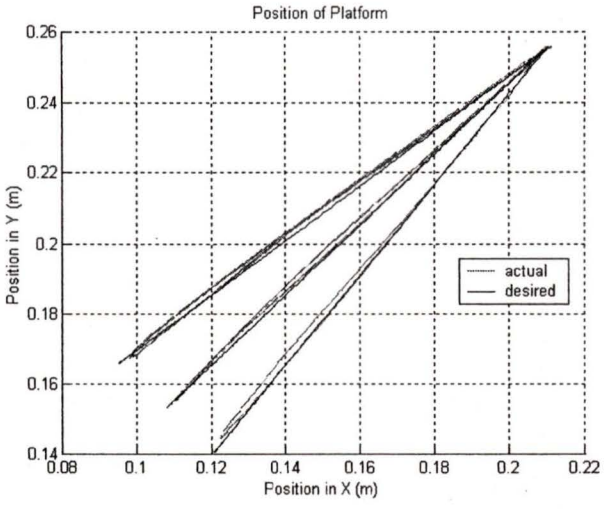

Figure 3.8: The theoretical path of the RPPM.

have followed was very close to the desired.

The RPPM with PID Control.

The actual positions of the actuators and the desired trajectories are shown in Figure 3.9. With the RPPM, the largest position error of a joint was approximately 0.025 radians in joint $\$_{2_2}$, and occurred at 34 seconds.

The voltages that were supplied to the actuators during the test are shown in Figure 3.10. The maximum voltage supplied to an actuator was approximately 4 Volts supplied to $\$_{2_1}$, and occurred at about 8 seconds.

The desired trajectory of the platform in $\hat{\mathbf{x}}$ and the actual trajectory in $\hat{\mathbf{x}}$ that the RPPM followed are shown in Figure 3.11. The largest position error in $\hat{\mathbf{x}}$ was approximately 0.0045m and occurred at 34 seconds.

The desired trajectory of the platform in $\hat{\mathbf{y}}$ and the actual trajectory in $\hat{\mathbf{y}}$ the RPPM followed are shown in Figure 3.12. Largest position error in $\hat{\mathbf{y}}$ was approxi-

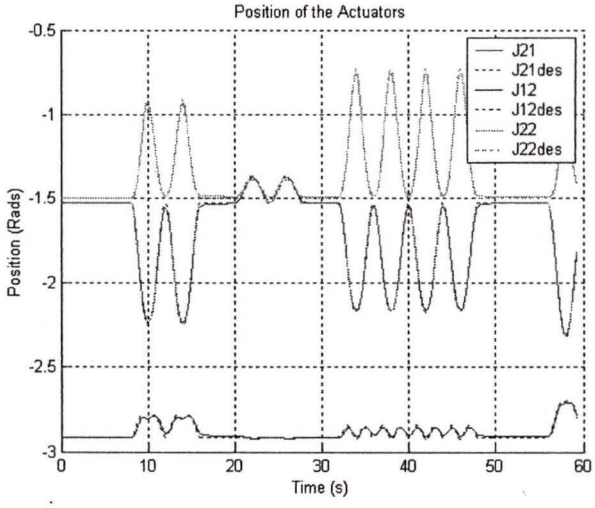

Figure 3.9: PID joint positions.

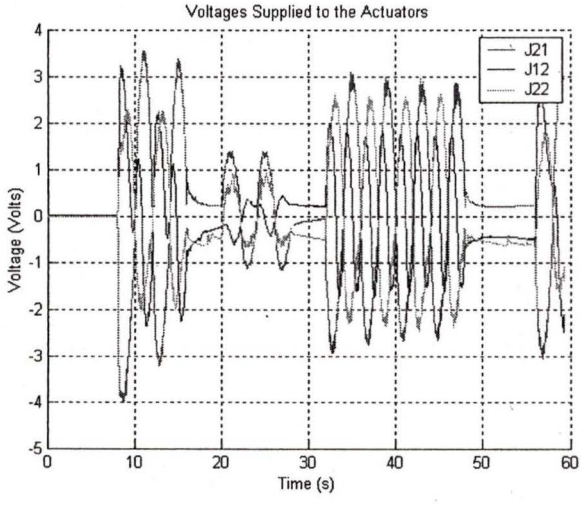

Figure 3.10: The voltages supplied during PID control.

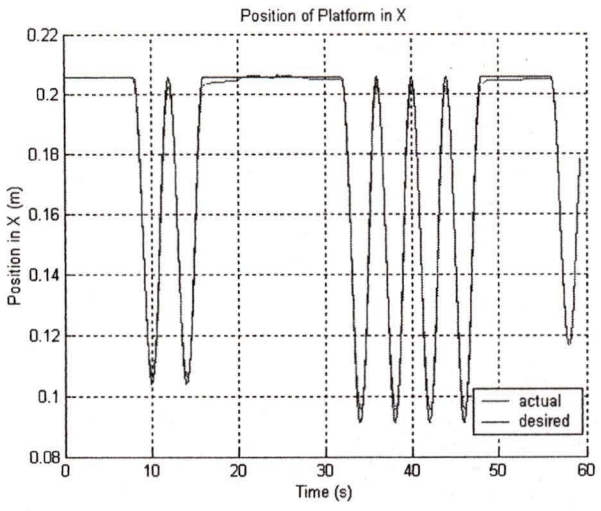

Figure 3.11: The poisition of the RPPM in X during PID control.

mately 0.006m, and occurred at 58 seconds.

The desired and actual orientation of the platform are shown in Figure 3.13. The largest error in orientation of platform was about 0.045rads at around 57 seconds.

It may be of interest to note the forces exerted on the platform while operating under PID control. These forces will show the dynamic forces of the platform and give a base for comparing to the hybrid controllers. Figure 3.14 shows the forces exerted by the branches to the platform in the $\hat{\mathbf{x}}$ direction of the platform frame. The maximum force applied in the $\hat{\mathbf{x}}$ direction was approximately -4N at wrist 2, at about 41 seconds.

Figure 3.15 shows the forces applied to the platform in the $\hat{\mathbf{y}}$ direction of the platform frame. The maximum force applied in the $\hat{\mathbf{y}}$ direction was approximately -1.9N at wrist 1, at about 11 seconds.

The net forces of the platform in $\hat{\mathbf{x}}$ and $\hat{\mathbf{y}}$ of the platform frame are shown in Figure 3.16. Notice how the direction of the net forces is in the direction of acceleration of

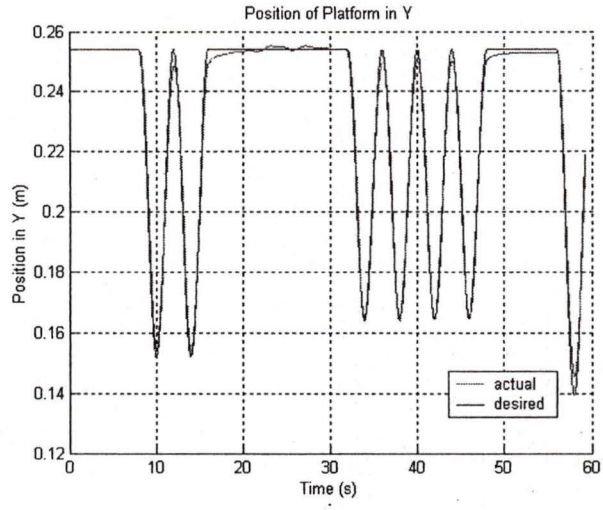

Figure 3.12: The position of the RPPM in Y during PID control.

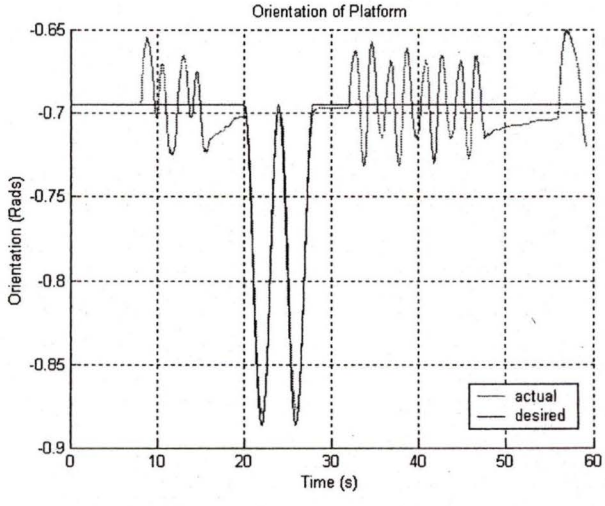

Figure 3.13: The orientation of platform during PID control.

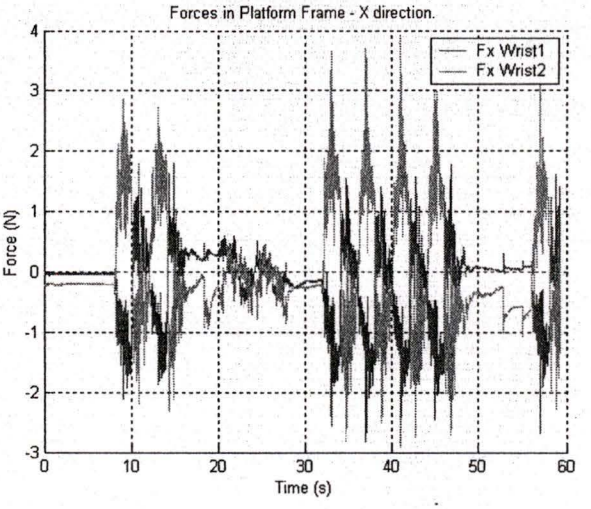

Figure 3.14: The forces sensed in X during PID control.

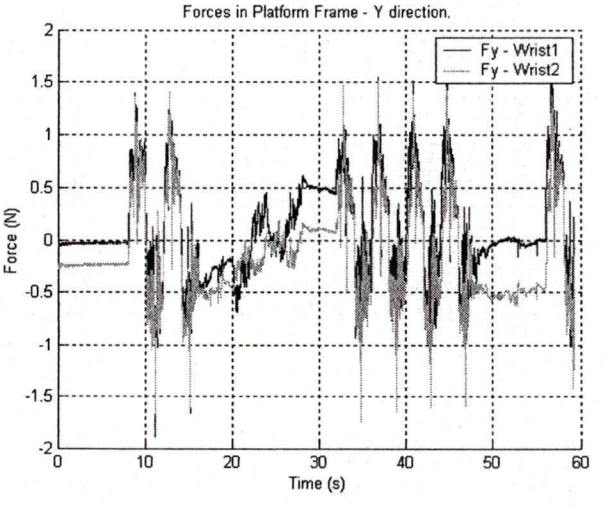

Figure 3.15: The forces sensed in Y during PID control.

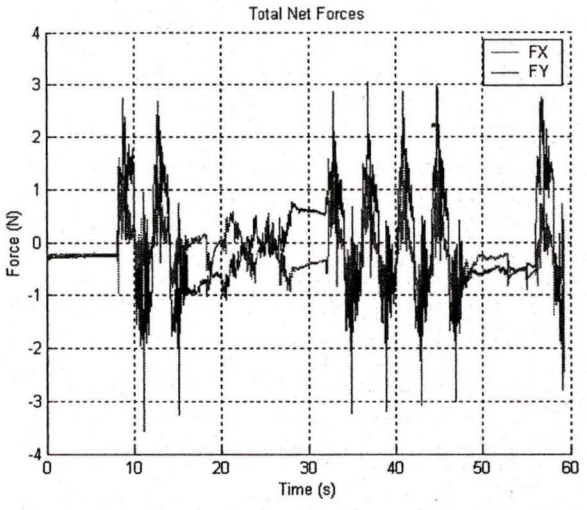

Figure 3.16: The net forces in the platfrom during PID control.

the platform.

3.5.4 Hybrid results

The hybrid controller attempted to move the RPPM in the exact same trajectory as the PID controller, with the addition of no desired wrist forces. The desired and actual joint displacements are shown in Figure 3.17. The largest joint displacement error was approximately 0.035 radians at $\$_{2_2}$ at about 46 seconds.

The voltages supplied to the actuators are shown in Figure 3.18. The maximum voltage supplied was about 2.7 Volts on $\$_{2_1}$, at 59 seconds.

The trajectory of the platform in the $\hat{\mathbf{x}}$ direction is shown in Figure 3.19. The largest position error of the platform in the $\hat{\mathbf{x}}$ direction was 0.004m, at approximately 50 seconds.

The trajectory of the platform in the $\hat{\mathbf{y}}$ direction is shown in Figure 3.20. The

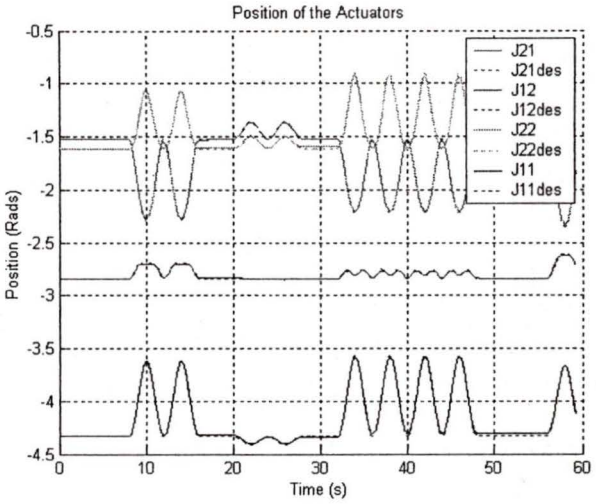

Figure 3.17: The joint displacements under hybrid control.

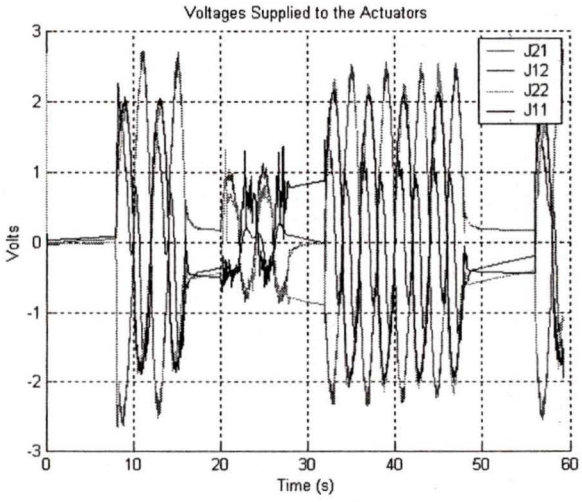

Figure 3.18: The votages supplied to the actuators during the hybrid control.

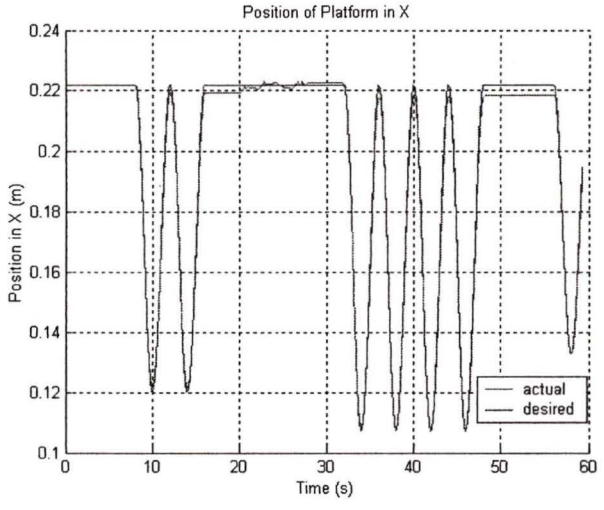

Figure 3.19: The position of the platform in X with hybrid control.

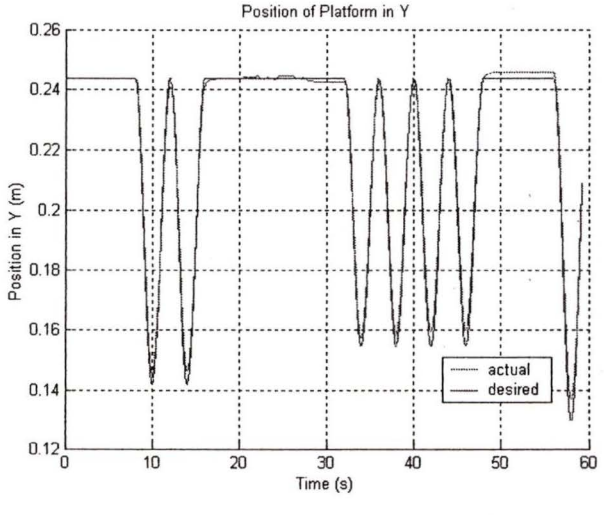

Figure 3.20: Position of the platform in Y at the RPPM moves using the hybrid controller.

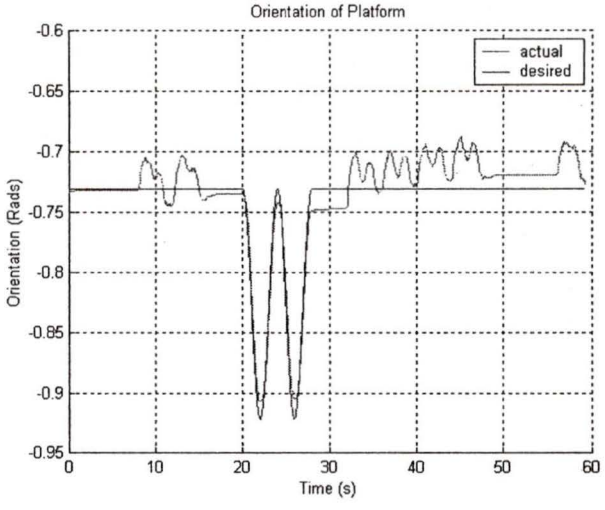

Figure 3.21: The orientation of the platform during hybrid control.

largest position error of the platform in the $\hat{\mathbf{y}}$ direction was 0.007m at 58 seconds.

The orientation of the platform is shown in Figure 3.21. The hybrid controller had a maximum orientation error of the platform of approximately 0.04 radians, which occurred at 45 seconds.

The forces sensed in the wrists of the RPPM during the motion in the platform frame of reference are shown in Figure 3.22 for the $\hat{\mathbf{x}}$ direction and in Figure 3.23 for the $\hat{\mathbf{y}}$ direction. The maximum sensed force in $\hat{\mathbf{x}}$ was - 3N, which occurred in wrist 1 at 58 seconds. The maximum sensed force in the $\hat{\mathbf{y}}$ direction was -1.8N, which occurred in wrist 2 at 33 seconds.

The "sensed actual torques" of the actuators calculated from the sensed forces are shown in Figure 3.24. The maximum joint torque was approximately 0.52Nm in $\$_{2_2}$ at 13 seconds.

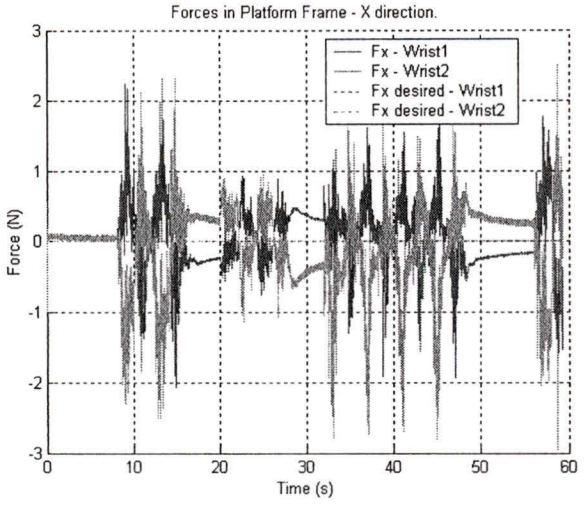

Figure 3.22: The forces applied to the payload in X during hybrid control.

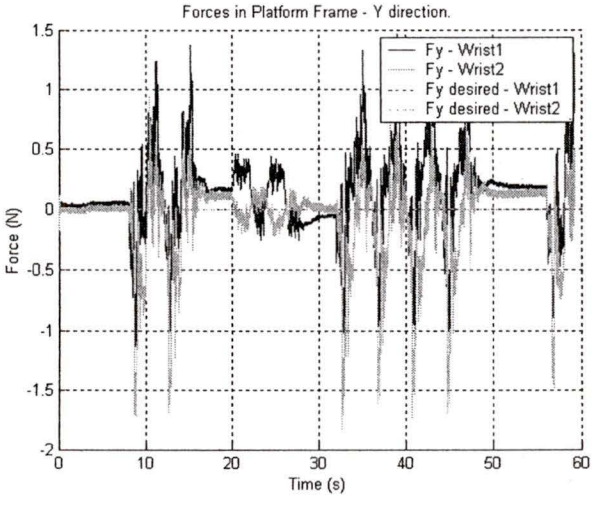

Figure 3.23: The Y direction forces during hybrid control.

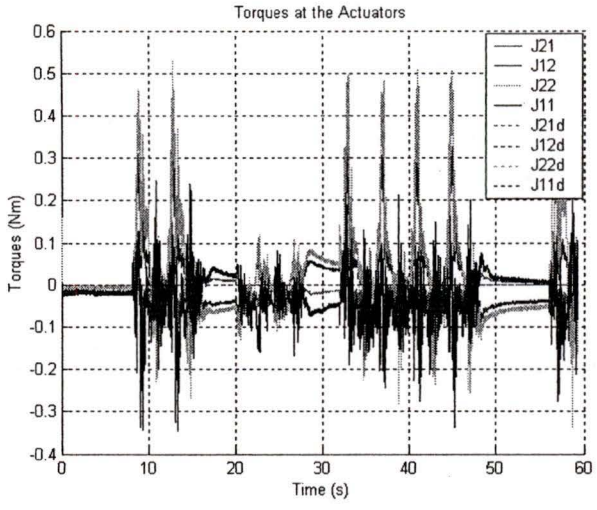

Figure 3.24: The "sensed actual torques" during hybrid control.

3.6 Discussion of Results

The PID controller was of greater accuracy when only controlling just the actuators, over when controlling the RPPM. This is as expected as the dynamics of the RPPM and the friction in the system would be expected to create greater errors in position. It is good to note that the joint displacement errors are typically quite small, the greatest error sensed was 0.025 radians. The accuracy of a sensed joint displacement was determined in Section 2.7.3 to be approximately 0.03 radians. These measured joint errors translated to approximately 0.008m of position error of the platform, and 0.045 radians of orientation error of the platform.

The hybrid force controller had greater joint displacement errors. This is due to the effect of the force integral portion of the controller. The motion of the RPPM creates inertial forces which are sensed, and since the desired forces at the wrists were zero, this creates joint torque errors which inhibit the position controllers ability to

match the desired trajectories in position accurately. The position error of the joint displacements increased from the 0.025 radians for the PID controller to 0.035 radians for the hybrid force/position controller.

The sensed inertial forces which create the position errors in hybrid control were also reduced by the hybrid controller. The PID controller, with only 3 actuators, actually created larger sensed forces in the platform than the hybrid controller, which is an overconstrained system. The maximum sensed force decreased from about 4N in the platform $\hat{\mathbf{x}}$ direction to 3N in the platform $\hat{\mathbf{x}}$ direction with the hybrid controller. A portion of the $\hat{\mathbf{x}}$ direction force is due to the required $\hat{\mathbf{x}}$ direction motion of the platform, but some is an internal self-cancelling force which creates no output force. The wrist forces are reduced by the hybrid controller due to the desired no wrist forces. This is shown by the reduction of voltages supplied to the actuators. In fact the PID controller had a maximum supplied voltage of 4V, and the hybrid controller had a maximum voltage of just 2.7V.

All of the tests show the effectiveness of the implementation of the RPPM. The accuracies of the sensed values from the desired values are all within or very close to the accuracy of the sensing.

Chapter 4

The Kinematics Associated with the RPPM

4.1 Overview

The joints of manipulators can be modelled with screw coordinates. This allows the velocities of points of interest on the manipulator to be found easily. It also allows for associated reciprocal screws to found. These associated-reciprocal screws describe the applicable forces of manipulators at loading points of interest. Screw coordinates are a convenient way to model the instantaneous kinematics of parallel manipulators. For a more thorough explanation of screw coordinates and associated-reciprocal screws, see [37].

This chapter considers the kinematics associated with the RPPM. Section 4.2 discusses the displacement solutions of the RPPM. Section 4.3 gives the basics of screw coordinates. Section 4.4 introduces associated-reciprocal screws that are associated with the joints of the RPPM, and Section 4.5 applies the associated-reciprocal screws

to the RPPM and derives the weighted associated-reciprocal screw matrix [$\$'^*$], which converts a vector of joint torques to an output load at the end effector.

4.2 Displacement Solutions

4.2.1 Forward Displacement Solution (FDS) for the RPPM

The Forward Displacement Solution (FDS) for the RPPM varies for each configuration of the mechanism and its actuation. The simplest case is where all possible joints are actuated and sensed. This allows each wrist location, x_{w_j} and y_{w_j}, for a branch j to be know as:

$$\begin{pmatrix} x_{w_j} \\ y_{w_j} \end{pmatrix} = \begin{pmatrix} x_{b_j} + l\left(\cos(\theta_{1_j}) + \cos(\theta_{1_j} + \theta_{2_j})\right) \\ y_{b_j} + l\left(\sin(\theta_{1_j}) + \sin(\theta_{1_j} + \theta_{2_j})\right) \end{pmatrix} \tag{4.1}$$

where l is the link length, and x_{b_j} and y_{b_j} are the locations of the base joint of branch j. Any two wrist locations can be used to determine the location and orientation of the platform. The orientation of the platform θ_{plat} can be found easily using the location of the first wrist and the second wrist by the two equations

$$\cos(\theta_{plat}) = \frac{x_{w_2} - x_{w_1}}{||\mathbf{r}_{w_2->w_1}||} \tag{4.2}$$

$$\sin(\theta_{plat}) = \frac{y_{w_2} - y_{w_1}}{||\mathbf{r}_{w_2->w_1}||}$$

and using the quadrant corrected arctangent function atan2,

$$\theta_{plat} = a\tan 2(\sin(\theta_{plat}), \cos(\theta_{plat})) \tag{4.3}$$

In Equations 4.2, $\mathbf{r}_{w_2->w_1}$ is a vector from w_2 to w_1.

With the orientation of the platform known, any known wrist location can be used to calculate the location of the centre of the platform.

The non-fully actuated (and sensed) FDS problem for the RPPM is more complex. However, for both the 5-Bar and the 6-Bar configurations the problem can always be shown to be an intersection of two circles. This yields two possible FDS solutions.

The solution for the intersection of two circles is as follows. Let p_x and p_y be the coordinates of the intersection point. Let circle "1" be defined by the centre point coordinates c_{x1} and c_{y1} with a radius r_1. Let circle "2" be defined by the centre point coordinates c_{x2} and c_{y2} with a radius r_2. The two equations of the circles are

$$(p_x - c_{x1})^2 + (p_y - c_{y1})^2 = r_1^2 \tag{4.4}$$

$$(p_x - c_{x2})^2 + (p_y - c_{y2})^2 = r_2^2 \tag{4.5}$$

Expanding and subtracting Equation 4.5 from Equation 4.4 and re-arranging terms yields

$$2p_x(c_{x2} - c_{x1}) + 2p_y(c_{y2} - c_{y1}) = r_1^2 - r_2^2 - {c_{x1}}^2 - {c_{y1}}^2 + {c_{x2}}^2 + {c_{y2}}^2 \tag{4.6}$$

which can be arranged into the form

$$p_x = \left(\frac{r_1^2 - r_2^2 - {c_{x1}}^2 - {c_{y1}}^2 + {c_{x2}}^2 + {c_{y2}}^2}{2(c_{x2} - c_{x1})}\right) - \frac{p_y(c_{y2} - c_{y1})}{(c_{x2} - c_{x1})} \tag{4.7}$$

To keep the equations simple, let

$$A = \left(\frac{r_1^2 - r_2^2 - {c_{x1}}^2 - {c_{y1}}^2 + {c_{x2}}^2 + {c_{y2}}^2}{2(c_{x2} - c_{x1})}\right)$$

and

$$B = -\frac{(c_{y2} - c_{y1})}{(c_{x2} - c_{x1})}$$

so that Equation 4.7 is simplified to

$$p_x = A + Bp_y \tag{4.8}$$

substituting Equation 4.8 into Equation 4.4 leaves a quadratic in terms of p_y, i.e.,

$$\left(A^2 + B^2p_y^2 + c_{x1}^2 + 2ABp_y - 2Bp_yc_{x1} - 2Ac_{x1}\right) + \left(p_y^2 - 2c_{y1}p_y + c_{y1}^2\right) = r_1^2 \tag{4.9}$$

and putting in standard form

$$p_y^2\left(B^2 + 1\right) + p_y\left(2AB - 2Bc_{x1} - 2c_{y1}\right) + A^2 + c_{x1}^2 - 2Ac_{x1} + c_{y1}^2 - r_1^2 = 0 \tag{4.10}$$

Equation 4.10 yields two solutions for p_y. Substituting the solutions for p_y into Equation 4.8 will yield a single solution for p_x for each solution of p_y.

As mentioned, the intersection of two circles can be used to yield FD solutions for the non-redundantly actuated 5-Bar and 6-Bar configurations of the RPPM. For example, take a 6-Bar mechanism that has branch one actuated at both the elbow and shoulder joint and has branch two with the elbow joint actuated. The location of the wrist of branch one is fully known from Equation 4.1. The platform is free to rotate about the wrist centre. Therefore, the centre point of the first circle is at the wrist, and the radius is the distance to the other wrist, i.e., the platform edge length l. The second branch has the elbow actuated, and therefore the centre point of the second circle is about the base joint. The second circle has a radius equal to the distance from the base joint to the wrist joint, which is determined by the angle of the elbow joint, and is equal to $\sqrt{l^2 + l^2 + 2l^2\cos(\theta_2)}$. The intersection of these two circles is the location of the second wrist point. The FDS can be completed for both of wrist location solutions. Table 4.1 shows the centre points and circle radii for the possible configurations of the 5-Bar and 6-Bar configurations.

Table 4.1: Circle centre points and radii for the FDS for the 5-Bar and 6-Bar configurations

Mechanism	Actuation Configuration	Centre 1	Radius 1	Centre 2	Radius 2
5-Bar	Two Shoulders	Elbow Location	l	Elbow Location	l
5-Bar	Two Elbows	Base Location	$\sqrt{l^2 + l^2 + 2l^2\cos(\theta_2)}$	Base Location	$\sqrt{l^2 + l^2 + 2l^2\cos(\theta_2)}$
5-Bar	One Shoulder; One Elbow	Elbow Location	l	Base Location	$\sqrt{l^2 + l^2 + 2l^2\cos(\theta_2)}$
6-Bar	One Branch; One Elbow	Wrist Location	l	Base Location	$\sqrt{l^2 + l^2 + 2l^2\cos(\theta_2)}$
6-Bar	One Branch; One Shoulder	Wrist Location	l	Elbow Location	l

Gosselin and Merlet outline a method of determining the FDS for the non-redundantly sensed 8-Bar configuration, and their work can be examined for more detail if desired [22]. For the 8-Bar with no DOR the problem is the answer to "How many ways can a triangle fit on three planar circles?". Gosselin and Merlet [22] used the standard equations for the FDS and eliminated the position of the platform in X and Y, leaving an equation in terms of only the angle of the platform, θ_{plat}. Using a half angle substitution they showed a minimum order polynomial of degree 6 which must be solved. That there are up to a possible of six solutions for the FDS of the 8-Bar was first shown by a geometric proof by K.H. Hunt in 1983 [38].

4.2.2 The Inverse Displacement Solution (IDS) for the RPPM

The Inverse Displacement Solution (IDS) for the RPPM is quite simple. The position and orientation of the platform are known, and the joint displacements are desired. The inverse is used because the typical input to the RPPM control programs is the desired position and orientation of the platform, and the joints must go to their corresponding required displacements.

The same IDS methodology can be applied to any configuration or mechanism assembly of the RPPM. This is done by taking the desired position and orientation of the platform and solving for the corresponding desired positions of the wrists. The inverse solution problem for each branch then becomes a system of two equations with two unknowns, i.e., the displacement of the elbow and shoulder joint. These equations can be solved for the required elbow and shoulder joint displacements. More specifically, from Equation 4.1 from the FDS, the two equations for any branch,

(without the index of the branch shown), are

$$x_w = x_b + l\cos(\theta_1) + l\cos(\theta_1 + \theta_2) \tag{4.11}$$

$$y_w = y_b + l\sin(\theta_1) + l\sin(\theta_1 + \theta_2) \tag{4.12}$$

where the unknowns at this point are θ_1 and θ_2, the angles of the shoulder and elbow joints, respectively. Equations 4.11 and 4.12 can be rearranged and simplified to

$$\frac{x_w - x_b}{l} = \cos(\theta_1) + \cos(\theta_1 + \theta_2) \tag{4.13}$$

$$\frac{y_w - y_b}{l} = \sin(\theta_1) + \sin(\theta_1 + \theta_2) \tag{4.14}$$

By squaring and adding Equations 4.13 and 4.14, and taking note of trigonometric identities and simplifications, it can be found that

$$\cos(\theta_2) = \frac{(x_w - x_b)^2 + (y_w - y_b)^2 - 2l^2}{2l^2} \tag{4.15}$$

This yields two solutions for the elbow displacement angle θ_2. One of these solutions corresponds to an "elbow up" and one corresponds to an "elbow down".

Typically in application the user can choose which solution they might desire to be running on. For example, in Chapter 2 all solutions used were of the "elbow down" configuration. With θ_2 known from Equation 4.15, the solution for θ_1 begins with taking Equations 4.13 and 4.14 and expanding and sorting in terms of θ_1 yielding

$$\frac{x_w - x_b}{l} = -\sin(\theta_1)\left(\sin(\theta_2)\right) + \cos(\theta_1)\left(1 + \cos(\theta_2)\right) \tag{4.16}$$

$$\frac{y_w - y_b}{l} = \sin(\theta_1)\left(1 + \cos(\theta_2)\right) + \cos(\theta_1)\left(\sin(\theta_2)\right) \tag{4.17}$$

which gives two equations and two unknowns, $\sin(\theta_1)$ and $\cos(\theta_1)$. These can be solved for algebraically, and by using the quadrant corrected arctangent function $\text{atan2}(\sin(\theta_1), \cos(\theta_1))$ a unique solution for θ_1 is found for each solution of θ_2. Regardless of what actuation scheme is being used by the RPPM, this solution method will provide the required joint angles, as long as the user can specify whether they desire the "elbow up" or "elbow down" configuration.

4.3 Screw Coordinates

4.3.1 Definition and Properties of Screw Coordinates and Screw Quantities

A screw is a geometric entity which consists of a line in space having an associated pitch. Screws can be represented by unit screw coordinates as

$$\$ = (\$_p; \$_0) = (\mathbf{l}; \mathbf{l}_0 + p\mathbf{l})^T$$

where $\$_p$ is a 3×1 vector called the primary vector and $\$_0$ is a 3×1 vector called the secondary vector, $\mathbf{l}$ and $\mathbf{l}_0$ are the Plücker coordinates of a line, and p is the associated pitch. As long as the pitch is not equal to infinity, unit screw coordinates have the constraints of

$$\$_p \cdot \$_p = 1 \tag{4.18}$$

and

$$\$_p \cdot \$_0 = p \tag{4.19}$$

If the pitch of a unit screw is equal to infinity, then $\$_p$ is a zero vector, and $\$_0$ becomes a unit vector

Equations 4.18 and 4.19 imply that of the seven parameters contained in screw coordinates (three for each vector plus the pitch), only five of those parameters are independent. Physically, the vector $\mathbf{l}$ is the direction of a line in space and $\mathbf{l}_0$ is the moment of that line about a reference point.

A general screw quantity $\mathbf{S}$ has the form

$$\mathbf{S} = \begin{pmatrix} \mathbf{s_p} \\ \mathbf{s_0} \end{pmatrix}$$

where $\mathbf{s_p}$, the primary vector is

$$\mathbf{s_p} = \begin{pmatrix} s_x \\ s_y \\ s_z \end{pmatrix}$$

and

$$\mathbf{s_0} = \begin{pmatrix} s_{0x} \\ s_{0y} \\ s_{0z} \end{pmatrix}$$

This can be broken into unit screw coordinates and an amplitude by

$$\mathbf{S} = \begin{pmatrix} \mathbf{s_p} \\ \mathbf{s_0} \end{pmatrix} = \alpha\$ = \alpha \begin{pmatrix} \$_p \\ \$_0 \end{pmatrix}$$

A screw can be used to describe a velocity. As mentioned, the vector $\mathbf{s_p}$ is the direction of a line in space with an associated amplitude, more specifically $\mathbf{s_p} = \alpha\$_p = \alpha\mathbf{l}$, and as long as the screw is not infinite pitch, can be used to describe an angular

velocity. The vector $\mathbf{l_0}$ describes a moment of that line about a point, and can be used to describe a linear velocity. This linear velocity is perpendicular to vector $\mathbf{s_p}$ because of the constraint of Equation 4.19. The associated pitch p yields a linear velocity in the direction of $\mathbf{l}$. The scalar $\boldsymbol{\alpha}$ therefore represents the magnitude of the angular velocity, with the vector $\$_0$ normalized with respect to α. More specifically, a general velocity described with screw coordinates is

$$\mathbf{V} = \begin{pmatrix} \boldsymbol{\omega} \\ \mathbf{v} \end{pmatrix} = \alpha\$ = \alpha \begin{pmatrix} \$_p \\ \$_0 \end{pmatrix} = \alpha \begin{pmatrix} \mathbf{l} \\ \mathbf{l_0} + p\mathbf{l} \end{pmatrix} \tag{4.20}$$

If the pitch of a screw is infinite then the screw quantity will provide no angular velocity, i.e., $\boldsymbol{\omega} = 0$. Therefore the screw will be normalized with respect to the secondary vector. A screw of infinite pitch will have the form

$$\mathbf{S} = \begin{pmatrix} \mathbf{0} \\ \mathbf{s_0} \end{pmatrix} = \alpha\$ = \alpha \begin{pmatrix} \mathbf{0} \\ \$_0 \end{pmatrix}$$

4.3.2 Modelling Joints of a Manipulator with Screw Coordinates

When unit screw coordinates are used to model a revolute joint, it is apparent that the primary vector will be equal to the $\hat{\mathbf{z}}_{\mathbf{joint}}$ direction, i.e., the axis of rotation of the joint. The pitch will be equal to zero as there is no linear motion in the direction of the axis of rotation. These are called zero-pitch screws. The secondary vector will be equal to

$$\$_0 = \hat{\mathbf{z}}_{\mathbf{joint}} \times \mathbf{r}_{\hat{\mathbf{z}}\mathbf{->Oref}}$$

where $\mathbf{r}_{\hat{\mathbf{z}}\mathbf{->Oref}}$ is a vector from the axis of rotation to the origin of the reference frame. Therefore, the angular velocity $\boldsymbol{\omega}$ and the linear velocity $\mathbf{v}$ of a point that

is coincident with the origin of the reference origin and attached to a link rotating about the joint will be equal to

$$\mathbf{V} = \begin{pmatrix} \boldsymbol{\omega} \\ \mathbf{v} \end{pmatrix} = \dot{q}\$ = \dot{q} \begin{pmatrix} \$_p \\ \$_0 \end{pmatrix} = \dot{q} \begin{pmatrix} \hat{\mathbf{z}} \\ \hat{\mathbf{z}}_{\mathbf{joint}} \times \mathbf{r}_{\hat{\mathbf{z}}->\mathbf{Pt}} \end{pmatrix}$$

where $\dot{q}$ is the rotational velocity of the revolute joint. If the reference frame for the screw coordinates is taken to originate at the active point of the end effector, then the velocity of the end effector at that point due to the rotation of the joint will be found.

When modelling a prismatic joint with unit screw coordinates, the pitch will be equal to infinity, and the screw is called an infinite-pitch screw. The infinite pitch is due to the lack of rotational velocity provided by a prismatic joint. Therefore, the unit screw is normalized with respect to the secondary vector. The secondary vector is equal to $\hat{\mathbf{z}}_{\mathbf{joint}}$, the direction of the prismatic joint. The velocity provided is therefore

$$\mathbf{V} = \begin{pmatrix} \boldsymbol{\omega} \\ \mathbf{v} \end{pmatrix} = \dot{q}\$ = \dot{q} \begin{pmatrix} \mathbf{0} \\ \$_0 \end{pmatrix} = \dot{q} \begin{pmatrix} \mathbf{0} \\ \hat{\mathbf{z}}_{\mathbf{joint}} \end{pmatrix}$$

where $\dot{q}$ is now the linear velocity of the prismatic joint.

For a serial manipulator with n joints, the velocity of the end effector can be found to be

$$\mathbf{V} = \sum_{i=1}^{n} \mathbf{V}_i = \sum_{i=1}^{n} \dot{q}_i \$_i$$

or placed into matrix form

$$\mathbf{V} = [\$]\,\dot{\mathbf{q}} \tag{4.21}$$

where [$] is the matrix of screw coordinates of the joints and $\dot{\mathbf{q}}$ is the vector of joint rates. It should be noted that all screw coordinates need to be taken with respect to the same frame of reference.

4.4 Associated-Reciprocal Screws

4.4.1 Definition of and Properties of Associated-Reciprocal Screw Coordinates

An actuated joint can be modeled by a unit screw $\$_{i_j}$, where i corresponds to the joint number of the joint in the branch, and j corresponds to the branch number. The force that can be applied by that joint can be modeled as an associated-reciprocal screw quantity $w_{i_j}\$'_{i_j}$. $\$'_{i_j}$ is defined as being the unit associated-reciprocal screw coordinates. $\$'_{i_j}$ is reciprocal to all of the joints in branch j except for joint i. The scalar w_{i_j} is the intensity of the associated-reciprocal screw, i.e., the wrench intensity of $\$'_{i_j}$. It should be noted that if an associated-reciprocal screw represents a force it is not capable of causing work to be performed by the joints (screws) to which it is reciprocal. The force will only cause work to be performed by the motion of the joint to which it is associated.

Unit associated-reciprocal screw coordinates have the same form as unit screw coordinates, that is:

$$\$' = \begin{pmatrix} \$'_p \\ \$'_0 \end{pmatrix} = \begin{pmatrix} \mathbf{l} \\ \mathbf{l_0} + p\mathbf{l} \end{pmatrix}$$

They also have similar properties, such as

$$\$'_p \cdot \$'_p = 1$$

and

$$\$'_p \cdot \$'_0 = p$$

as long as the pitch is not equal to infinity. This means that they have five independent variables. If the pitch of an associated reciprocal screw is equal to infinity, the screw quantity is normalized with respect to the secondary vector, i.e.,

$$w\$' = w \begin{pmatrix} \mathbf{0} \\ \$'_0 \end{pmatrix}$$

where

$$\$'_0 \cdot \$'_0 = 1$$

As mentioned, associated-reciprocal screw coordinates can be used to describe a force. The primary vector describes a direction, and can be used to describe the direction of linear force. The associated scalar w is equal to the magnitude of the linear force component. The vector $\mathbf{l}_0$ describes a moment (or torque) of that line about a reference point. The associated pitch p describes the magnitude of the moment or torque about the primary vector $\$'_p$. The combination of $\$'_0 = \mathbf{l}_0 + p\mathbf{l}$ describes the total moment (or torque) component of the force, normalized with respect to w. More specifically

$$\mathbf{F} = \begin{pmatrix} \mathbf{f} \\ \mathbf{m} \end{pmatrix} = w\$' = w \begin{pmatrix} \$'_p \\ \$'_0 \end{pmatrix} = w \begin{pmatrix} \mathbf{l} \\ \mathbf{l}_0 + p\mathbf{l} \end{pmatrix}$$

where w is the wrench intensity required to describe the force $\mathbf{F}$.

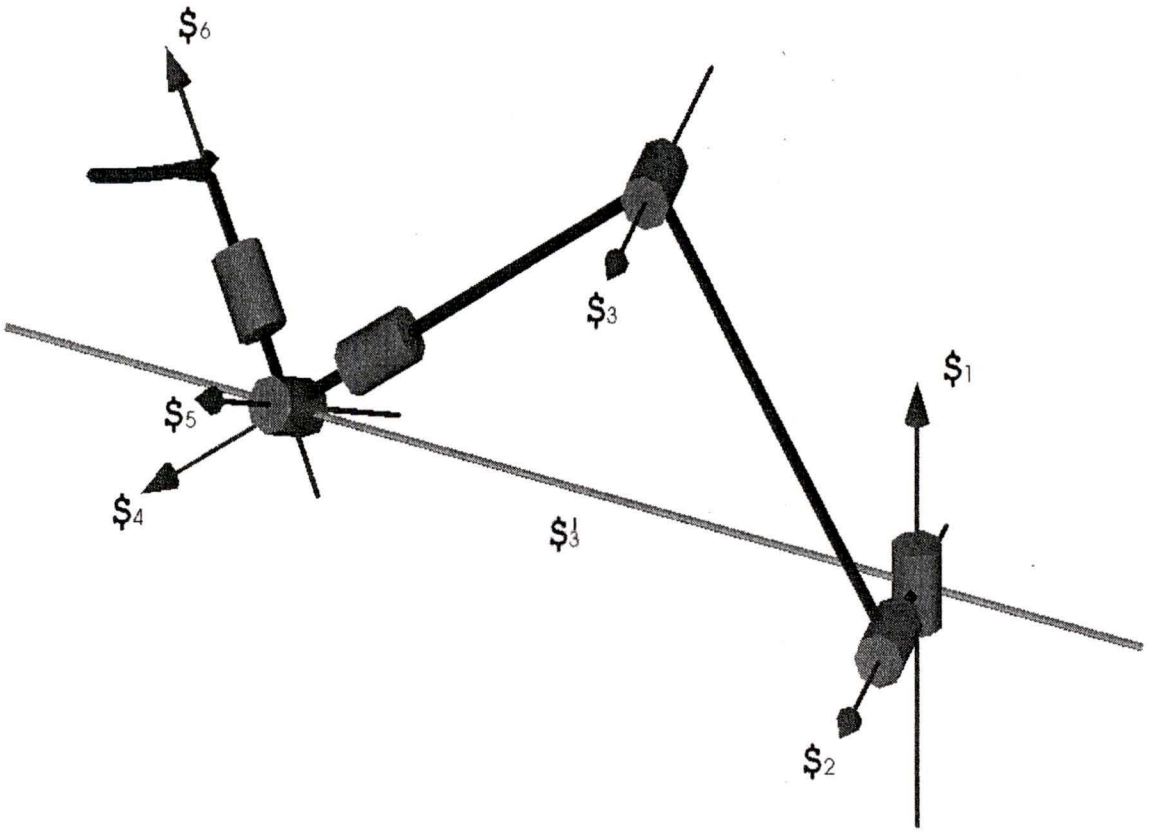

Figure 4.1: A general serial manipulator, showing the joints modelled with screw cooridnates and the associated-reciprocal screw of the third joint.

4.4.2 Associated-Reciprocal Screws for an Example Spatial Main-Arm

A spatial main-arm with a spherical wrist is shown in Figure 4.1. The joint at the elbow is modelled as the screw $\$_3$. It is desired to find the associated-reciprocal screw $\$_3'$. By the definition of an associated-reciprocal screw only motion caused by $\$_3$ can perform work subject to a force described by $\$_3'$. By noting that at the wrist there is an intersection of three zero-pitch screws, which can only perform motion in

orientation about the intersection point, it is apparent that to be reciprocal to these three joints $\$'_3$ must also be a zero-pitch screw, providing no moment, and intersect the wrist centre. To be reciprocal to the first two joints, which form a pointer pair of joints, it must also intersect them. The only point at which it can intersect these two joints is at their respective intersection. This defines $\$'_3$ to be a zero-pitch screw, intersecting both the wrist centre and the intersection of the first two joints, as illustrated in Figure 4.1. If a reference frame is taken to be located at the wrist centre, $\$'_3$ will then have the form

$$\$'_3 = \begin{pmatrix} \$'_p \\ \mathbf{0} \end{pmatrix}$$

where $\$'_p$ is a unit vector in the direction described.

4.4.3 Associated-Reciprocal Screws for a Planar Main Arm

For a revolute-only-jointed planar manipulator such as the RPPM the associated-reciprocal screw $\$'_{1j}$ for each shoulder joint $\$_{1j}$ can be defined as a pure force which intersects both the elbow joint $\$_{2j}$ and the wrist $\$_{3j}$. This implies $\$'_{1j}$ lies along the forearm of branch j and only $\$_{1j}$ does work against a force $\$'_{1j}$. Similarly, the associated-reciprocal screw of $\$_{2j}$ can be found to be a pure force intersecting the wrist and the shoulder joints. Figure 4.2 shows an arbitrary 6-Bar mechanism with the left branch 1 having both the elbow actuated and the shoulder actuated, and the right branch 2 having only the shoulder actuated. The reciprocal screws are shown for all three actuated joints.

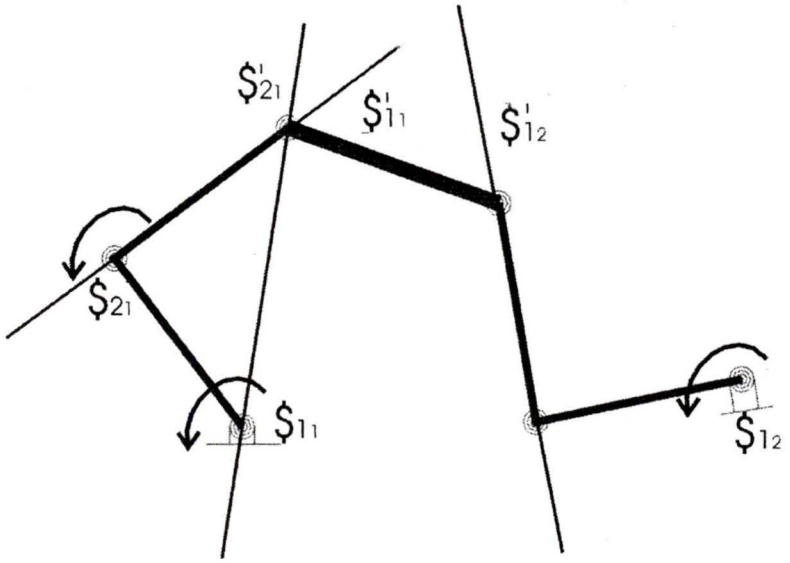

Figure 4.2: Reciprocal Screws for a 6-Bar

A planar unit reciprocal screw described in the full six dimensions is

$$\$'_{ij} = \begin{pmatrix} \$'_{xi_j} \\ \$'_{yi_j} \\ 0 \\ 0 \\ 0 \\ \$'_{0zi_j} \end{pmatrix} \tag{4.22}$$

By eliminating the zero elements of the unit associated-reciprocal screw, a more compact form for the planar case is (called the abbreviated 3-D form)

$$\$'_{ij} = \begin{pmatrix} \$'_{xi_j} \\ \$'_{yi_j} \\ \$'_{0zi_j} \end{pmatrix} \tag{4.23}$$

If a reference frame $refj$ for each branch is located at its respective wrist centre, and is aligned with the global reference frame, then because the unit associated-reciprocal screw is zero-pitch, there will be no moment, and

$$^{refj}\$'_{ij} = \begin{pmatrix} \$'_{xi_j} \\ \$'_{yi_j} \\ 0 \end{pmatrix} \tag{4.24}$$

and $\$'_{xi_j}$ and $\$'_{yi_j}$ form a unit vector in the direction of the applicable force $\$'_{i_j}$.

The force that can be applied due to the unit associated reciprocal screw $\$'_{i_j}$ is

$$\mathbf{F}_{appi_j} = w_{i_j}\$'_{i_j}$$

where w_{i_j} is the wrench intensity of the unit associated-reciprocal screw $\$'_{i_j}$. As long as all associated-reciprocal screws are taken with respect to the same frame of reference, the total force applied by the manipulator is the summation of the force from all the actuated joints in all the branches, i.e.,

$$\mathbf{F}_{app} = \sum_j \sum_i w_{i_j}\$'_{i_j}$$

4.4.4 The Reciprocal Product

An associated-reciprocal screw $\$'_{i_j}$ for the joint modelled as $\mathbf{\$}_{i_j}$ must satisfy

$$\$'_{i_j} \circledast \$_{k_j} = 0 : k \neq i \tag{4.25}$$

and

$$\$'_{i_j} \circledast \$_{i_j} \neq 0 \tag{4.26}$$

where the $\circledast$ operator indicates a reciprocal product. This ensures the associated-reciprocal screw is reciprocal to all joints in the branch except to the joint to which

it is associated. The reciprocal product is defined as the sum of the dot products of the primary and secondary vectors of the screws. Mathematically, the reciprocal product of two screws **A** and **B** is

$$\mathbf{A} \circledast \mathbf{B} = \mathbf{a_p} \cdot \mathbf{b}_0 + \mathbf{a}_0 \cdot \mathbf{b_p} \tag{4.27}$$

and physically **A**⊛**B** can be considered as the rate of work a force **A** does on a velocity **B**.

4.5 Application of the RPPM

4.5.1 Screw Coordinates for the RPPM

As we are dealing with a planar case and revolute-only joints the screws describing the joints will have the form

$$\$_{i_j} = \begin{pmatrix} \hat{\mathbf{z}}_{\$_{ij}} \\ \mathbf{r}_{Oref->\$_{ij}} \times \hat{\mathbf{z}}_{\$_{ij}} \end{pmatrix} = \begin{pmatrix} 0 \\ 0 \\ 1 \\ \$_{0xi_j} \\ \$_{0yi_j} \\ 0 \end{pmatrix} \tag{4.28}$$

where $\hat{\mathbf{z}}_{\$_{ij}}$ is a unit vector in the direction of the joint $\$_{i_j}$ and $\mathbf{r}_{Oref->\$_{ij}}$ is a vector from the reference origin to $\$_{i_j}$.

Figure 4.3 shows a schematic of the RPPM in the 8-Bar configuration. The reference frame $refG$ is the global reference frame for the RPPM. The reference frame for branch j is called $refj$, and is located at the wrist for branch j, and oriented

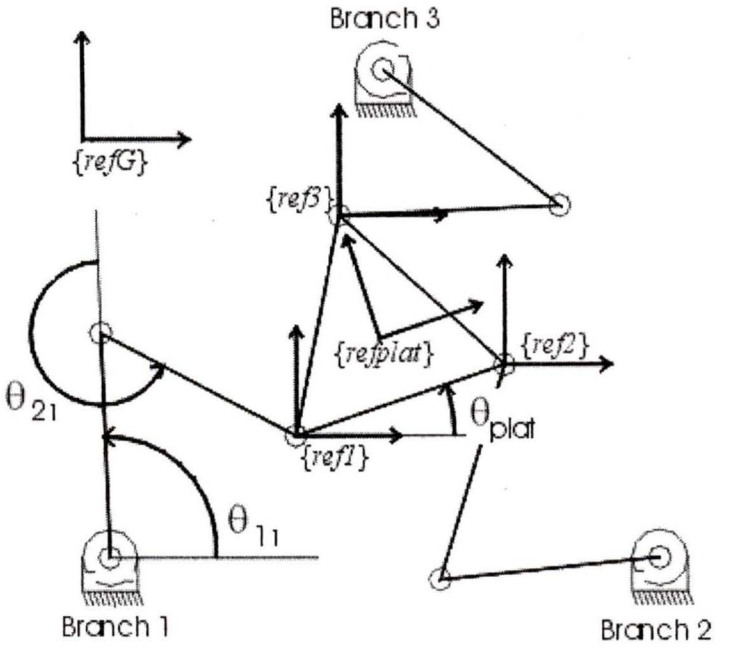

Figure 4.3: The Reference Frames for the RPPM.

the same as the global reference frame. The reference frame for the platform $refplat$, is located at the centre of the platform and is oriented an angle θ_{plat} with respect to the global reference frame, as defined by the FDS in Section 4.2.1.

Shoulder Joint

For the reference frame $refj$ for each branch j located at the wrist centre and aligned with the global reference frame $refG$, the screw coordinates can be found. The vector from the reference frame origin (the respective wrist centre) to the shoulder

joint, using Equation 4.1 is

$$ {}^{refj}\mathbf{r}_{Oref->\$_{1j}} = \begin{pmatrix} -l\left(\cos(\theta_{1_j}) + \cos(\theta_{1_j} + \theta_{2_j})\right) \\ -l\left(\sin(\theta_{1_j}) + \sin(\theta_{1_j} + \theta_{2_j})\right) \\ 0 \end{pmatrix} $$

The screw coordinates for each shoulder joint can be found as

$$ {}^{refj}\$_{1_j} = \begin{pmatrix} 0 \\ 0 \\ 1 \\ -l\left(\sin(\theta_{1_j}) + \sin(\theta_{1_j} + \theta_{2_j})\right) \\ l\left(\cos(\theta_{1_j}) + \cos(\theta_{1_j} + \theta_{2_j})\right) \\ 0 \end{pmatrix} $$

Elbow Joint

If the same reference frame $refj$ for each branch j is taken to be located at the wrist centre and aligned with the global frame of reference, then for an elbow joint

$$ {}^{refj}\mathbf{r}_{Oref->\$_{2j}} = \begin{pmatrix} -l\cos(\theta_{1_j} + \theta_{2_j}) \\ -l\sin(\theta_{1_j} + \theta_{2_j}) \\ 0 \end{pmatrix} $$

and the screw coordinates for each elbow joint can be found as

$$ {}^{refj}\$_{2_j} = \begin{pmatrix} 0 \\ 0 \\ 1 \\ -l\sin(\theta_{1_j} + \theta_{2_j}) \\ l\cos(\theta_{1_j} + \theta_{2_j}) \\ 0 \end{pmatrix} $$

4.5.2 Associated-Reciprocal Screws for the RPPM

Shoulder Joint

As mentioned in Section 4.4.3, the associated-reciprocal screw for the shoulder joint of any branch will lie along the forearm of that branch, intersecting the elbow joint and the wrist joint. The associated-reciprocal screw can be found geometrically using this knowledge and the knowledge of the FDS, or by using the screw coordinates of the joints and Equations 4.25 and 4.26. Either method will result in the unit associated-reciprocal screw for the shoulder joint (shown in the abbreviated 3-D form) of

$$ {}^{refj}\$'_{1_j} = \begin{pmatrix} \cos(\theta_{1_j} + \theta_{2_j}) \\ \sin(\theta_{1_j} + \theta_{2_j}) \\ 0 \end{pmatrix} \tag{4.29} $$

where the reference frame $refj$ is the frame located at the wrist centre for that branch and aligned with the global reference frame as illustrated in Figure 4.3.

Elbow Joint

As mentioned in Section 4.4.3, the associated-reciprocal screw for the elbow joint of any branch j on the RPPM will intersect the wrist centre and the base joint of the branch. Taking a reference frame $refj$ for branch j to be located at the branches wrist centre and oriented with a global frame of reference, the planar associated-reciprocal screw $\$'_{2_j}$ can be found either from geometric inspection or from using the screw coordinates of the joints and Equations 4.25 and 4.26. Both methods will

result in

$$ {}^{refj}\$'_{2_j} = \begin{pmatrix} \frac{x_{w_j} - x_{b_j}}{\|\mathbf{r}_{w_j->b_j}\|} \\ \frac{y_{w_j} - y_{b_j}}{\|\mathbf{r}_{w_j->b_j}\|} \\ 0 \end{pmatrix} \tag{4.30} $$

The magnitude of the vector from the wrist location to the base location for the branch j, $\mathbf{r}_{w_j->b_j}$, can be solved for in terms of the joint variables θ_1 and θ_2 by noting that

$$ \|\mathbf{r}_{w_j->b_j}\| = \left((x_w - x_b)^2 + (y_w - y_b)^2\right)^{\frac{1}{2}} $$

and rewriting Equation 4.15 gives

$$ \|\mathbf{r}_{w_j->b_j}\| = \left(2l^2\cos(\theta_2) + 2l^2\right)^{\frac{1}{2}} $$

Using Equation 4.1 to solve for the remainder of the terms in Equation 4.30, ${}^{refj}\$'_{2_j}$ can be expressed in terms of the joint variables only (and shown in the abbreviated 3-D form) as

$$ {}^{refj}\$'_{2_j} = \begin{pmatrix} \frac{\cos(\theta_{1_j}) + \cos(\theta_{1_j} + \theta_{2_j})}{(2 + 2\cos(\theta_{2_j}))^{\frac{1}{2}}} \\ \frac{\sin(\theta_{1_j}) + \sin(\theta_{1_j} + \theta_{2_j})}{(2 + 2\cos(\theta_{2_j}))^{\frac{1}{2}}} \\ 0 \end{pmatrix} \tag{4.31} $$

4.5.3 Derivation of [$'] using Screw Transforms

To find the total external force being applied from the manipulator,

$$ \mathbf{F}_{app} = \sum_j \sum_i w_{i_j} \$'_{i_j} \tag{4.32} $$

where w_{i_j} is the intensity applied for the unit associated-reciprocal screw $\$'_{i_j}$. It is required however, for all reciprocal screws to be taken with respect to the same reference point and frame of orientation.

In matrix form, this can be rewritten as

$$\mathbf{F}_{app} = [\$']\,\mathbf{w} \tag{4.33}$$

where $[\$']$ is the matrix of associated-reciprocal screws and $\mathbf{w}$ is a vector of wrench intensities.

For the RPPM, the associated-reciprocal screws are originally formed with respect to their branch frame $refj$. To arrange in matrix form, all associated-reciprocal screw coordinates must be transformed into a common reference frame. The common reference frame used is positioned at the centre of the platform and oriented with the platform as shown in Figure 4.3, and is called $refplat$.

A screw transformation taking a six dimensioned $\$'_{i_j}$ from reference frame a to frame b, and from a point c to point d is defined as

$${}^{b}_{a}\mathbf{T}_{c->d} = \begin{bmatrix} {}^{b}_{a}[\mathbf{R}] & [\mathbf{0}]_{3\times3} \\ {}^{b}\tilde{\mathbf{r}}_{d->c}\,{}^{b}_{a}[\mathbf{R}] & {}^{b}_{a}[\mathbf{R}] \end{bmatrix} \tag{4.34}$$

where ${}^{b}_{a}[\mathbf{R}]$ is a rotation matrix describing the orientation of frame a with respect to frame b, and ${}^{b}\tilde{\mathbf{r}}_{d->c}$ indicates the cross-product skew-symmetric matrix of ${}^{b}\mathbf{r}_{d->c}$. As noted above, since all branch frames are oriented the same, with the global frame of reference $refG$ as in Figure 4.3, all of the rotation matrices will be the same, a rotation about the $\hat{\mathbf{z}}$ axis by the angle θ_{plat}. This yields a rotation matrix for the

screw transforms of

$$ {}^{refplat}_{refj}[\mathbf{R}] = \begin{bmatrix} \cos(\theta_{plat}) & -\sin(\theta_{plat}) & 0 \\ \sin(\theta_{plat}) & \cos(\theta_{plat}) & 0 \\ 0 & 0 & 1 \end{bmatrix} \tag{4.35} $$

The matrix ${}^{b}\tilde{\mathbf{r}}_{d->c}$ is a cross-product skew-symmetric matrix of the vector ${}^{b}\mathbf{r}_{d->c}$, a vector from point d to point c. It should be noted that the skew-symmetric matrix forms an equivalent mathematical result as a cross product, i.e.,

$$ \tilde{\mathbf{r}}_{d->c}\,\mathbf{v} = \mathbf{r}_{d->c} \times \mathbf{v} \tag{4.36} $$

where $\mathbf{v}$ is an arbitrary 3×1 vector used only to show that the skew symmetric matrix accounts for a cross product. If the vector $\mathbf{r}_{d->c}$ is

$$ \mathbf{r}_{d->c} = \begin{pmatrix} r_x \\ r_y \\ r_z \end{pmatrix} $$

then the skew-symmetric matrix $\tilde{\mathbf{r}}_{d->c}$ to satisfy Equation 4.36 is [4]

$$ \tilde{\mathbf{r}}_{d->c} = \begin{bmatrix} 0 & -r_z & r_y \\ r_z & 0 & -r_x \\ -r_y & r_x & 0 \end{bmatrix} \tag{4.37} $$

The platform edge length of the RPPM is equal to the link length l, and the platform forms an equilateral triangle. Therefore, the vectors from the centre of the platform to the wrist centre j, ${}^{refplat}\mathbf{r}_{cplat->wj}$, are

$$ {}^{refplat}\mathbf{r}_{cplat->w1} = \begin{pmatrix} \frac{-l}{2} \\ \frac{-l}{2}\tan(\frac{\pi}{6}) \\ 0 \end{pmatrix} $$

$$ {}^{refplat}\mathbf{r}_{cplat->w2} = \begin{pmatrix} \frac{l}{2} \\ \frac{-l}{2}\tan(\frac{\pi}{6}) \\ 0 \end{pmatrix} $$

$$ {}^{refplat}\mathbf{r}_{cplat->w3} = \begin{pmatrix} 0 \\ \frac{l}{2\cos(\frac{\pi}{6})} \\ 0 \end{pmatrix} $$

and therefore the skew symmetric matrices are

$$ {}^{refplat}\tilde{\mathbf{r}}_{cplat->w1} = \begin{bmatrix} 0 & 0 & \frac{-l}{2}\tan(\frac{\pi}{6}) \\ 0 & 0 & \frac{l}{2} \\ \frac{l}{2}\tan(\frac{\pi}{6}) & \frac{-l}{2} & 0 \end{bmatrix} \tag{4.38} $$

$$ {}^{refplat}\tilde{\mathbf{r}}_{cplat->w2} = \begin{bmatrix} 0 & 0 & \frac{-l}{2}\tan(\frac{\pi}{6}) \\ 0 & 0 & \frac{-l}{2} \\ \frac{l}{2}\tan(\frac{\pi}{6}) & \frac{l}{2} & 0 \end{bmatrix} \tag{4.39} $$

$$ {}^{refplat}\tilde{\mathbf{r}}_{cplat->w3} = \begin{bmatrix} 0 & 0 & \frac{l}{2\cos(\frac{\pi}{6})} \\ 0 & 0 & 0 \\ \frac{-l}{2\cos(\frac{\pi}{6})} & 0 & 0 \end{bmatrix} \tag{4.40} $$

The transformation matrix to transform from a branch frame $refj$ to the platform frame $refplat$ can now be found by inserting the appropriate skew-symmetric matrix from Equations 4.38, 4.39 or 4.40 and the rotation matrix of Equation 4.35 into Equation 4.34. For example, the combined transformation matrix for the third branch to the platform ${}^{refplat}_{ref3}\mathbf{T}_{w3->cplat}$ is

$$ {}^{refplat}_{ref3}\mathbf{T}_{w3->cplat} = \begin{bmatrix} {}^{refplat}_{ref3}[\mathbf{R}] & [\mathbf{0}]_{3\times3} \\ {}^{refplat}\tilde{\mathbf{r}}_{w3->cplat}\,{}^{refplat}_{ref3}[\mathbf{R}] & {}^{refplat}_{ref3}[\mathbf{R}] \end{bmatrix} $$

$$
{}^{refplat}_{ref3}\mathbf{T}_{w3->cplat} = \begin{bmatrix}
\cos(\theta_{plat}) & -\sin(\theta_{plat}) & 0 & 0 & 0 & 0 \\
\sin(\theta_{plat}) & \cos(\theta_{plat}) & 0 & 0 & 0 & 0 \\
0 & 0 & 1 & 0 & 0 & 0 \\
0 & 0 & \frac{l}{2\cos(\frac{\pi}{6})} & \cos(\theta_{plat}) & -\sin(\theta_{plat}) & 0 \\
0 & 0 & 0 & \sin(\theta_{plat}) & \cos(\theta_{plat}) & 0 \\
-\cos(\theta_{plat})\frac{l}{2\cos(\frac{\pi}{6})} & \sin(\theta_{plat})\frac{l}{2\cos(\frac{\pi}{6})} & 0 & 0 & 0 & 1
\end{bmatrix} \tag{4.41}
$$

It is clearly evident that the associated reciprocal screw ${}^{refplat}\$'_{i3}$ is longer and more cumbersome than ${}^{ref3}\$'_{i3}$, regardless of whether it is the shoulder or elbow joint.

Once all of the associated-reciprocal screws have been transformed into the reference frame *refplat* they can be put into the abbreviated 3-D form and arranged in matrix form to satisfy Equation 4.33. The matrix is called the matrix of associated-reciprocal screws, [$'].

4.5.4 Derivation of [$'*]

While [$'] can be used to provide an output force for the planar parallel manipulator, it requires knowledge of the wrench intensities w_{i_j}. The weighted associated-reciprocal screw matrix [$'*] satisfies the equation

$$\mathbf{F}_{app} = [\$'^*]\boldsymbol{\tau}$$

where $\boldsymbol{\tau}$ is the vector of joint torques, not wrench intensities. To accomplish this a matrix [$*] is created which satisfies

$$\mathbf{w} = [\$^*]\boldsymbol{\tau} \tag{4.42}$$

and therefore

$$[\$'^*] = [\$'][\$^*]$$

To find $[\$^*]$ the physical properties of wrench intensities can be used. The wrench intensity w_{i_j} is the magnitude of the linear force component of $\$'_{i_j}$. This magnitude is caused by the torque τ_{i_j}. For each joint there is a scalar w'_{i_j} that satisfies

$$w_{i_j} = w'_{i_j}\tau_{i_j}$$

and therefore, to satisfy Equation 4.42, $[\$^*]$ will be a diagonal matrix of the scalars as

$$[\$^*] = [diag(...w'_{i_j}...)]$$

This scalar w'_{i_j} can be found by several different methods. The simplest is by noting that

$$\tau_{i_j} = \left\| \mathbf{r}_{\$_{i_j}->\$'_{i_j}} \times w_{i_j}\$'_{pi_j} \right\| \tag{4.43}$$

where $\$'_{pi_j}$ is the primary vector denoting only the linear force component of $\$'_{i_j}$ and $\mathbf{r}_{\$_{i_j}->\$'_{i_j}}$ is a vector from the joint $\$_{i_j}$ to the associated-reciprocal screw $\$'_{i_j}$. Here note that the torque is the magnitude of the cross product and not a vector. The RPPM is a planar manipulator and the resultant torque will only be in the $\hat{\mathbf{z}}$ direction. Therefore the magnitude of the $\hat{\mathbf{z}}$ component will be equal to the magnitude of the resultant of the cross product.

Equation 4.43 can be rearranged to solve for the scalar wrench intensity w_{i_j} in terms of the torque τ_{i_j} as

$$w_{i_j} = \frac{\tau_{i_j}}{\left\| \mathbf{r}_{\$_{i_j}->\$'_{i_j}} \times \$'_{pi_j} \right\|}$$

and therefore

$$w'_{i_j} = \frac{1}{\left\| \mathbf{r}_{\$_{i_j} -> \$'_{i_j}} \times \$'_{pi_j} \right\|} \tag{4.44}$$

The other method of determining w'_{i_j} is to utilize the principles of conservation of power. This method is more standard in robotics applications, as it is not specific to the planar case. In matrix form, conservation of power yields

$$([\$']\mathbf{w})^T \Delta \mathbf{V} = \boldsymbol{\tau}^T \dot{\mathbf{q}} \tag{4.45}$$

where $\mathbf{V}$ is the velocity of the end effector represented by a screw quantity, $\dot{\mathbf{q}}$ is the vector of joint rates, $\boldsymbol{\tau}$ is the vector of joint torques, and the applied force of the end effector as a screw quantity is $\mathbf{F} = [\$']\mathbf{w}$. In Equation 4.45, Δ denotes the Lipkins operator,

$$\Delta = \begin{bmatrix} \mathbf{0}_{3x3} & \mathbf{I}_{3x3} \\ \mathbf{I}_{3x3} & \mathbf{0}_{3x3} \end{bmatrix} \tag{4.46}$$

Since $\mathbf{V} = [\$]\,\dot{\mathbf{q}}$ for a serial branch, and Equation 4.45 is true for all $\dot{\mathbf{q}}$, we have

$$([\$']\mathbf{w})^T \Delta\,[\$] = \boldsymbol{\tau}^T \tag{4.47}$$

Transposing both sides of Equation 4.47 yields

$$[\$]^T \Delta([\$']\mathbf{w}) = \boldsymbol{\tau} \tag{4.48}$$

where it has been noted that $\Delta = \Delta^T$. It should also be noted that $\$_i^T \Delta \$'_k = \$_i \circledast \$'_k$, and since $\$_i \circledast \$'_k = 0$ for all $k \neq i$, the product $[\$]^T \Delta[\$']$ yields a diagonal matrix with the terms $\$_i \circledast \$'_k$ on its diagonal. Finally, rewriting Equation 4.48 provides

$$\mathbf{w} = \left([\$]^T \Delta[\$']\right)^{-1} \boldsymbol{\tau} \tag{4.49}$$

where the inverse of the matrix is also a diagonal matrix with the terms $\frac{1}{\$_i \circledast \$'_k}$ on its diagonal. Therefore, the elements of Equation 4.49 are

$$w_{i_j} = \frac{1}{\$_{i_j} \circledast \$'_{i_j}} \tau_{i_j}$$

where the subscript $_{i_j}$ again refers to the joint i in branch j. Therefore

$$w'_{i_j} = \frac{1}{\$_{i_j} \circledast \$'_{i_j}} \tag{4.50}$$

which will yield the same result as Equation 4.44.

For an example consider a shoulder joint of branch j. Equation 4.29 states the associated reciprocal-screw ${}^{refj}\$'_{2_j}$ and the vector $\mathbf{r}_{\$_{1_j} -> \$'_{1_j}}$ can be found using the FDS of Equations 4.1. Solving for w'_{1_j} using Equation 4.44 yields

$$w'_{1_j} = \frac{1}{\left\| \begin{pmatrix} l\left(\cos(\theta_{1_j}) + \cos(\theta_{1_j} + \theta_{2_j})\right) \\ l\left(\sin(\theta_{1_j}) + \sin(\theta_{1_j} + \theta_{2_j})\right) \\ 0 \end{pmatrix} \times \begin{pmatrix} \cos(\theta_{1_j} + \theta_{2_j}) \\ \sin(\theta_{1_j} + \theta_{2_j}) \\ 0 \end{pmatrix} \right\|}$$

which becomes when simplified

$$w'_{1_j} = \frac{1}{\left\| \begin{matrix} 0 \\ 0 \\ l\sin(\theta_{2_j}) \end{matrix} \right\|} = \frac{1}{l\sin\left(\theta_{2_j}\right)}$$

This is as expected, when one considers the force direction is along the second link, which acts as a binary link.

Similarly w'_{1_j} can also be found for the reciprocal product method of Equation

4.50. Where

$$
{}^{refj}\$_{1_j} \circledast {}^{refj}_{1_j}\$' = \begin{pmatrix} 0 \\ 0 \\ 1 \\ -l\left(\sin(\theta_{1_j}) + \sin(\theta_{1_j} + \theta_{2_j})\right) \\ l\left(\cos(\theta_{1_j}) + \cos(\theta_{1_j} + \theta_{2_j})\right) \\ 0 \end{pmatrix} \circledast \begin{pmatrix} \cos(\theta_{1_j} + \theta_{2_j}) \\ \sin(\theta_{1_j} + \theta_{2_j}) \\ 0 \\ 0 \\ 0 \\ 0 \end{pmatrix}
$$

$$
= \begin{pmatrix} 0 \\ 0 \\ 1 \end{pmatrix} \cdot \begin{pmatrix} 0 \\ 0 \\ 0 \end{pmatrix} + \begin{pmatrix} -l\left(\sin(\theta_{1_j}) + \sin(\theta_{1_j} + \theta_{2_j})\right) \\ l\left(\cos(\theta_{1_j}) + \cos(\theta_{1_j} + \theta_{2_j})\right) \\ 0 \end{pmatrix} \cdot \begin{pmatrix} \cos(\theta_{1_j} + \theta_{2_j}) \\ \sin(\theta_{1_j} + \theta_{2_j}) \\ 0 \end{pmatrix}
$$

which as expected, when simplified again yields

$$
w'_{1_j} = \frac{1}{l\sin\left(\theta_{2_j}\right)}
$$

Chapter 5

Force Capabilities

5.1 Overview

This chapter considers the force capabilities of the RPPM. In many robotics applications there is a known desired output force at the end effector. This desired force can be represented by a screw quantity $\mathbf{F}_{app}$. In other instances, it is useful to know the possible magnitude of the force that can be applied for a known direction requirement of both the force and moment. Determining the potential magnitude of the applicable force for all possible directions, will define the force capabilities of the manipulator. The purpose of determining the force capabilities of the RPPM is to answer the question, "For a known position and orientation of the RPPM, how much load can be sustained or applied by its end effector?".

Section 5.2 describes the analytical method for determining the force capabilities of the RPPM for both the non-redundantly actuated and redundantly-actuated cases. Section 5.3.1 explains the development of an objective function to optimize the force capabilities. Section 5.3.2 describes the Broyden-Fletcher-Goldfarb-Shanno (BFGS)

optimization algorithm [39], which is used to optimize the objective function. Section 5.4 presents the results of the methods, and Section 5.5 provides a discussion of the results, including a discussion of the optimization errors in Section 5.5.3.

5.2 Analytical Methods for Determining Force Capabilities for the RPPM

5.2.1 Forward Force Solution

The forward force solution method, as will be discussed further, may be used to create force capability plots for a manipulator. The output force $\mathbf{F}_{app}$ is calculated from

$$\mathbf{F}_{app} = [\$'^{*}]\boldsymbol{\tau}$$

where $\boldsymbol{\tau}$ is a vector of the input torques and $[\$'^{*}]$ is the weighted matrix of associated reciprocal screw quantities as described in Section 4.5. The input torques vary from their minimum to maximum values for each actuator, yielding a set of applicable forces. From the forward force solution it should be stressed that the result is an applicable force. This forward solution may be used to determine and create force capability plots. The forward force method requires knowledge of the joint torques to provide the output force, yet in real situations what are desired are the joint torques required to produce a desired magnitude of force in a given direction.

5.2.2 Inverse Force Solution

The inverse force solution solves for the input torques, $\boldsymbol{\tau}$, required to sustain (or apply) a known force, $\mathbf{F}_{app}$, for a known location and orientation of the end effector.

To determine the force capabilities, however, we want to find the maximum possible magnitude of force for a known direction of force $\$_{\mathbf{f}}$.

Non-Redundantly Actuated

The inverse solution works differently for the redundant and non-redundant actuation cases. For the non-redundant cases, $[\$'^*]$ is a square matrix, 2×2 for the 5-Bar and 3×3 for both the 6-Bar and 8-Bar configurations. Therefore $[\$'^*]$ is invertible and the solution begins with

$$\boldsymbol{\tau}_{\$_{\mathbf{f}}} = [\$'^*]^{-1}\$_{\mathbf{f}} \tag{5.1}$$

where $\$_{\mathbf{f}}$ is the unit force screw in the direction of a desired $\mathbf{F}_{app}$, i.e ,

$$\mathbf{F}_{app} = f_{app}\$_{\mathbf{f}}$$

where f_{app} is the scalar magnitude, i.e., the intensity, of $\mathbf{F}_{app}$. Equation 5.1 yields a vector of the torques, $\boldsymbol{\tau}_{\$_{\mathbf{f}}}$, required to create the unit force $\$_{\mathbf{f}}$ in the direction of the desired $\mathbf{F}_{app}$. Since all maximum joint torque capabilities, $\tau_{i_j\,\max}$, are known, scaling factors are created by

$$sf_{i_j} = \left| \frac{\tau_{i_j\,\max}}{\tau_{\$_{\mathbf{f}} i_j}} \right| \tag{5.2}$$

for all actuated joints i of each branch j.

The scaling factors of Equation 5.2 can be placed in a set. The scaling factor in this set which has a minimum absolute value is the maximum factor which all joint torques can be scaled by and still remain at or below their corresponding maximum value. More specifically,

$$SF = \min_{ij}(sf_{ij}) \tag{5.3}$$

Finally the maximum force $\mathbf{F}_{app}$ that can be applied in the force direction $\$_\mathbf{f}$ is

$$\mathbf{F}_{app} = SF[\$'^*](\boldsymbol{\tau}_{\$_\mathbf{f}}) \tag{5.4}$$

Since $[\$'^*](\boldsymbol{\tau}_{\$_\mathbf{f}})$ generates the unit force screw $\$_\mathbf{f}$, the maximum possible intensity f_{app} of the screw quantity $\mathbf{F}_{app}$ is

$$f_{app} = SF \tag{5.5}$$

To determine a force capability plot from this, the direction $\$_\mathbf{f}$ is varied through all possible directions. This method is useful in application as well, since as mentioned, often the direction of applied loading is known and the maximum possible magnitude of the load is desired. These maximum possible load magnitudes are the quantity that is directly yielded from the above minimum-scaling-factor based inverse force solution.

Redundantly-Actuated

For the redundantly-actuated cases, $[\$'^*]$ is not a square matrix. When all possible actuators on the RPPM are being used, $[\$'^*]$ has dimensions of 2×4 for the 5-Bar mechanism, 3×4 for the 6-Bar mechanism, and 3×6 for the 8-Bar mechanism. Since only square matrixes are invertible, the Moore-Penrose pseudo-inverse defined as

$$[\$'^*]^+ = [\$'^*]^T([\$'^*][\$'^*]^T)^{-1} \tag{5.6}$$

could be used, allowing the solution

$$\boldsymbol{\tau} = [\$'^*]^+\mathbf{F}_{app} \tag{5.7}$$

The same method of using scaling factors, to determine the maximum allowable force magnitude for the non-redundantly actuated cases, is used for the redundantly-actuated cases, i.e.,

$$\boldsymbol{\tau}_{\$_\mathbf{f}} = [\$'^*]^+ \$_\mathbf{f}$$

The smallest scaling factor is then found which determines the maximum amount that $\$_\mathbf{f}$ can be scaled.

It should be noted that the Moore-Penrose pseudo-inverse stems from a minimization of $\boldsymbol{\tau}^T\boldsymbol{\tau}$, the square of the magnitude of the torque vector. Therefore, the results are not expected to coincide with the actual maximum force capabilities of the manipulator.

5.3 Optimization Based Solution Method

5.3.1 The Objective Function

The goal of the optimization routine is to maximize the potential magnitude of the output force $\mathbf{F}_{app}$. This is accomplished by maximizing the scaling factor, i.e., maximizing the minimum from the set of scaling factors. The minimum of the scaling factors is attributed to the maximum joint torque in $\boldsymbol{\tau}_{\$_\mathbf{f}}$, since all $\tau_{i_j\,\max}$ are equal. Therefore, to maximize the magnitude of the output force, the maximum joint torque in $\boldsymbol{\tau}_{\$_\mathbf{f}}$ must be minimized.

To set up the problem for optimization techniques, the vector of torques $\boldsymbol{\tau}_{\$_\mathbf{f}}$ was broken up into

$$\boldsymbol{\tau}_{\$_\mathbf{f}} = \boldsymbol{\tau}_{\$_\mathbf{f} part} + \boldsymbol{\tau}_{\$_\mathbf{f}\,\mathrm{hom}} \tag{5.8}$$

where the particular solution, $\boldsymbol{\tau}_{\$_{\mathbf{f}}part}$, fulfills

$$\$_{\mathbf{f}} = [\$'^{*}]\boldsymbol{\tau}_{\$_{\mathbf{f}}part} \tag{5.9}$$

and $\boldsymbol{\tau}_{\$_{\mathbf{f}}\,\mathrm{hom}}$ is said to be a homogeneous solution and satisfies

$$[\$'^{*}]\boldsymbol{\tau}_{\$_{\mathbf{f}}\,\mathrm{hom}} = \mathbf{0}$$

$\boldsymbol{\tau}_{\$_{\mathbf{f}}\,\mathrm{hom}}$ can be found for any solution for $\boldsymbol{\tau}_{\$_{\mathbf{f}}part}$. To solve for the homogenous torque, Single Value Decomposition (SVD) is used on $[\$'^{*}]$. SVD on the matrix $[\$'^{*}]$ of size m×n and rank r provides a [**U**], [**S**], and a [**V**] matrix. The [**S**] matrix is a diagonal matrix of size m×n of the square roots of the non-zero eigenvalues of $[\$'^{*}][\$'^{*}]^{T}$ and $[\$'^{*}]^{T}[\$'^{*}]$. The [**U**] (size m×m) and [**V**] (size n×n) matrices are both orthogonal matrices and provide bases for the four fundamental subspaces of $[\$'^{*}]$ [40]. The last n-r (the DOR of $[\$'^{*}]$) columns of [**V**] can be taken to be [**V**′], and

$$\boldsymbol{\tau}_{\$_{\mathbf{f}}\,\mathrm{hom}} = [\mathbf{V}']\,\mathbf{v} \tag{5.10}$$

and **v** is any (n-r)×1 vector which is mapped though [**V**′] into the null-space torque for the given $[\$'^{*}]$. The columns of [**V**′] form a basis for the null-space of $[\$'^{*}]$. The resultant $\boldsymbol{\tau}_{\$_{\mathbf{f}}\,\mathrm{hom}}$ is physically a set of applicable torques which result in no output force from the payload. The torques are such that they only apply what is called an internal force. Kumar and Waldron in 1988 [23] noted that the pseudo-inverse solution corresponds to a solution with no internal force. The vector **v** is chosen to optimize the objective function of the manipulator.

The Moore-Penrose pseudo-inverse solution can be used to find $\boldsymbol{\tau}_{\$_{\mathbf{f}}part}$, as it satisfies Equation 5.9, and using Equation 5.10 for $\boldsymbol{\tau}_{\$_{\mathbf{f}}\,\mathrm{hom}}$ yields

$$\boldsymbol{\tau}_{\$_{\mathbf{f}}} = [\$'^{*}]^{+}\$_{\mathbf{f}} + [\mathbf{V}']\,\mathbf{v} \tag{5.11}$$

The objective is to then minimize the maximum torque in $\boldsymbol{\tau}_{\$_f}$ by manipulating the n-r sized vector $\mathbf{v}$ in Equation 5.11.

Power Norm

A power norm to the k^{th} power of a vector is equal to the k^{th} root of sum of the terms to the k^{th} power. More specifically, the k^{th} power norm of a vector $\mathbf{t}$ with i elements is

$$Pnorm(\mathbf{t},k) = (t_1^k + t_2^k + ... + t_i^k)^{\frac{1}{k}}$$

As the power of the norm increases, the solution approaches the maximum value of the scalar components of $\mathbf{t}$. It should be noted that since the maximum absolute value comes from a summation of power products, as long as k is even, the result will be a positive value.

5.3.2 Broyden-Fletcher-Goldfarb-Shanno (BFGS) Optimization Algorithm

The Broyden-Fletcher-Goldfarb-Shanno (BFGS) optimization algorithm [39] is used to minimize the objective function by varying $\mathbf{v}$. BFGS is a Quasi-Newton optimization routine. A matrix, $\mathbf{S}$, is used to approximate the inverse of the Hessian matrix of the objective function. The search direction at the k^{th} iteration, $\boldsymbol{\delta}_k$, is found as

$$\boldsymbol{\delta}_k = \frac{-\mathbf{S}_k\mathbf{g}_k}{\|\mathbf{S}_k\mathbf{g}_k\|}$$

where $\mathbf{g}_k$ is the gradient of the objective function at the current value of $\mathbf{v}_k$. The minimum value for the objective function is then found along the direction $\boldsymbol{\delta}_k$ using

a single-dimension search technique. For the work of this thesis the golden-section line search is used[1].

At the next iteration, the **S** matrix is found as

$$\mathbf{S}_{k+1} = \mathbf{S}_k + \left(1 + \frac{\boldsymbol{\gamma}_k^T \mathbf{S}_k \boldsymbol{\gamma}_k}{\boldsymbol{\gamma}_k^T \mathbf{S}_k}\right) \frac{\boldsymbol{\delta}_k \boldsymbol{\delta}_k^T}{\boldsymbol{\delta}_k^T \boldsymbol{\gamma}_k} - \frac{\boldsymbol{\delta}_k \boldsymbol{\gamma}_k^T \mathbf{S}_k + \mathbf{S}_k \boldsymbol{\gamma}_k \boldsymbol{\delta}_k^T}{\boldsymbol{\gamma}_k^T \boldsymbol{\delta}_k}$$

where

$$\boldsymbol{\gamma}_k = \mathbf{g}_{k+1} - \mathbf{g}_k$$

The BFGS optimization algorithm was chosen for several reasons. First, the **S** matrix will be positive definite as long as the single-dimension line search is done well and the previous **S** matrix is also positive definite. At the first iteration, (k=1), **S** is set to be an identity matrix, and therefore as long as the line search tolerance is good the **S** matrix will remain positive definite. The **S** matrix will approach closer to the inverse of the Hessian of the objective function at each iteration. For the implementation of the BFGS algorithm, the gradient at the k^{th} iteration $\mathbf{g}_k$ is found numerically at the point $\mathbf{v}_k$.

5.4 Results

5.4.1 Overview of Considered Location and Link Dimensions

The simulated results below were all found for the same arbitrary non-singular position and orientation of the 8-Bar manipulator. The centre of the platform is located at X=0.25 m,Y=0.18 m, with the bottom edge of the platform oriented at an angle

[1]Dr. W.S. Lu is thanked for providing the Matlab code for the golden-section line search.

of $\frac{-\pi}{12}$ radians from the horizontal. All link lengths match the RPPM design, i.e., the platform edge length and link lengths were taken to be 0.20 m. The maximum allowable actuator torques were all assumed to be 4.2 Nm. The distance between the base joints was set to be 0.50 m. Branch 1 is always the left branch, branch 2 is always the right branch, and branch 3 is the upper branch. Joint 1 is always the shoulder (base) joint, and joint 2 is always the elbow joint for each branch. The loading point of the end effector is always the centre of the platform.

5.4.2 Results of Non-Redundantly Actuated 8-Bar

Figure 5.1 shows the force polygon for the non-redundantly actuated 8-Bar configuration of the RPPM with the manipulator shown. The force polygon plot is centered around the loading point of the manipulator. Only the shoulder joint, joint 1, of each branch is actuated. Figure 5.2 shows the same force polygon as Figure 5.1, but without the manipulator. The grey scale of the plot shows the amount of applicable moment and the outer boundary lines indicate maximum force capabilities. For example, the manipulator can sustain a pure force in the $\hat{\mathbf{x}}$ direction of 34.7 N, with f_y=0 and m_z=0. Similarly, the manipulator can sustain a pure force in the $\hat{\mathbf{y}}$ direction of 36.8 N, with f_x=0 and $m_z = 0$. The maximum level of sustainable moment is approximately 5.54 Nm.

Figure 5.3 shows the joint torques of the non-redundantly actuated 8-Bar configuration versus the angle of applied loading for the manipulator. For this plot the moment applied about $\hat{\mathbf{z}}$ is always equal to 0. This graph shows how there is always only one joint torque that is maximized and limiting the applicable force of the manipulator. Each side of the force polygon corresponds to a specific joint being the

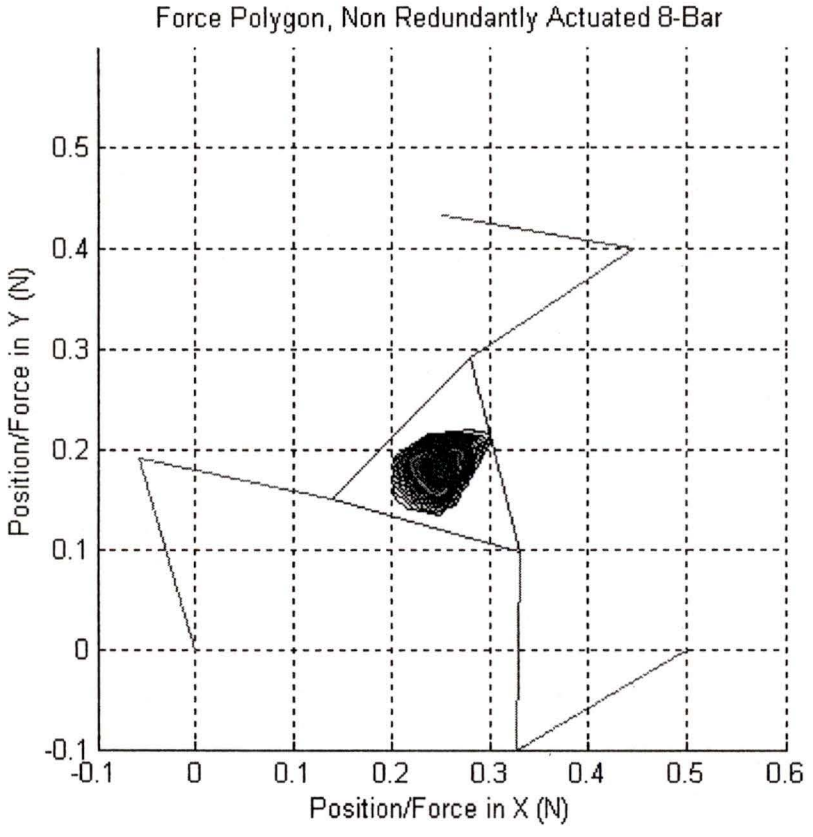

Figure 5.1: The force polygon for the non-redundantly actuated 8-Bar, shown with the manipulator.

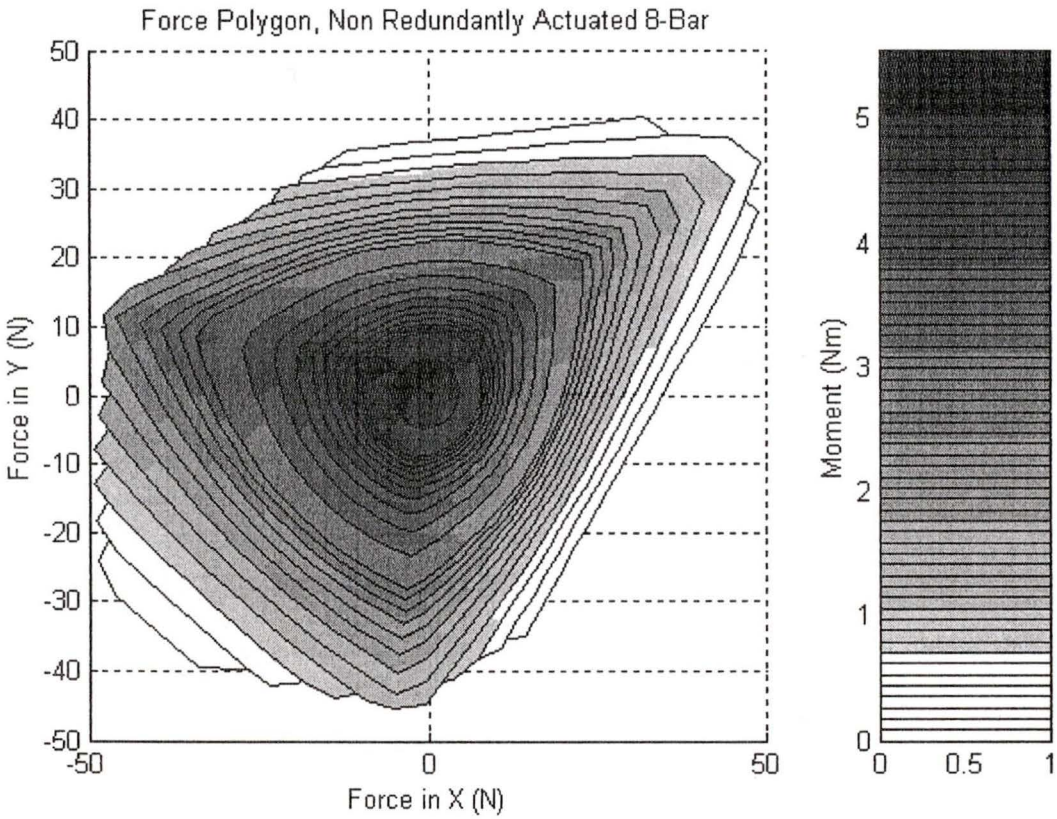

Figure 5.2: The force polygon of the non-redundantly actuated 8-Bar.

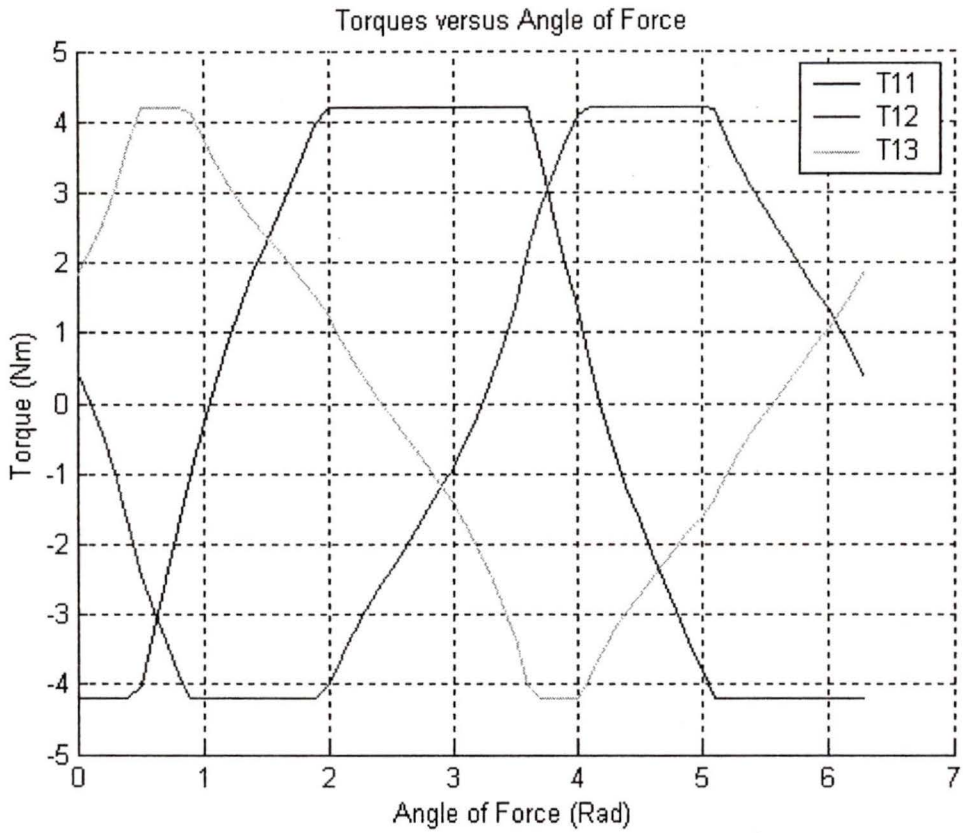

Figure 5.3: The joint torques of the non-redundantly actuated 8-Bar vs the angle of the applied load, with no moment being applied.

limiting factor in the capability. For example, when the angle of force is between one and two radians, $\$_{1_2}$ is the limiting joint. At almost two radians, the limiting joint becomes $\$_{1_1}$. Here on the force capability plot in Figure 5.2, there is a meeting of two sides of the force polygon.

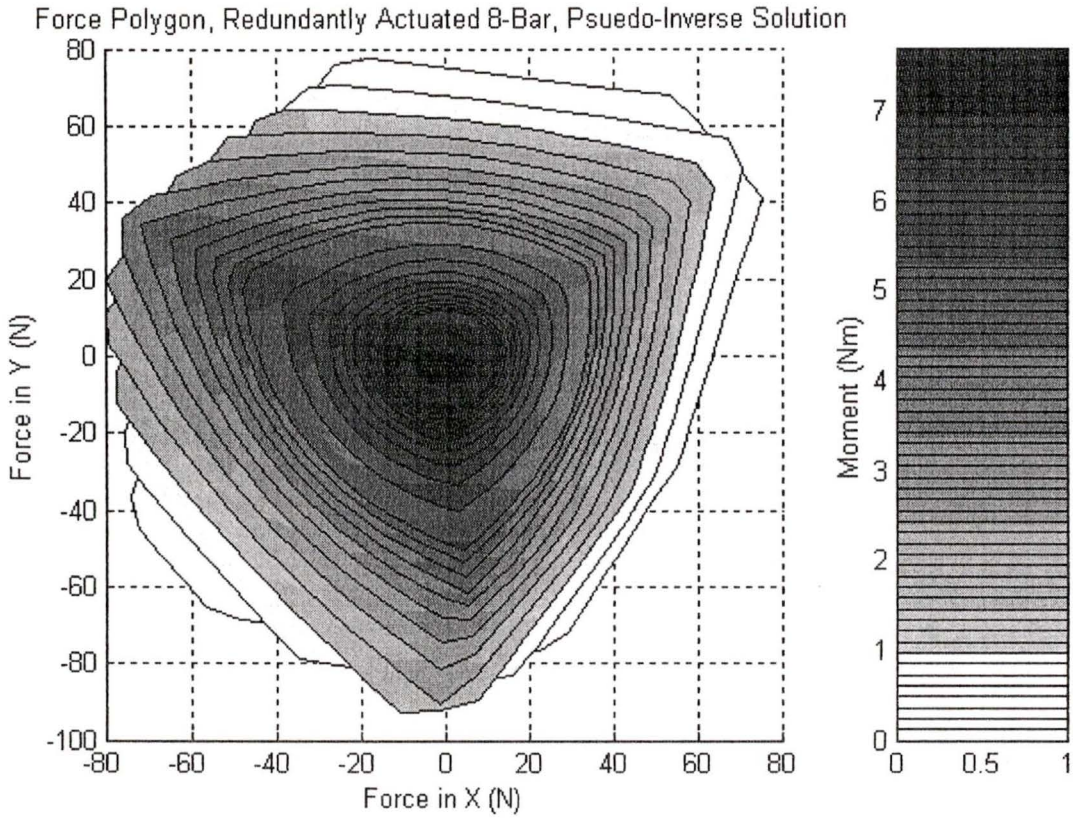

Figure 5.4: The force polygon of the redundantly-actuated 8-Bar with the pseudo-inverse solution.

5.4.3 Results of Redundantly-Actuated 8-Bar

Pseudo-Inverse Results

Figure 5.4 shows the force polygon for the redundantly-actuated 8-Bar configuration using the Moore-Penrose pseudo-inverse solution method. Here all possible joints are actuated, i.e., both the shoulder and elbow joint of each branch. The magnitude of the applicable moment is shown by grey-scale. The manipulator can sustain a pure force in the $\hat{\mathbf{x}}$ direction of 63.5 N, with f_y=0 and m_z=0. Similarly, the manipulator

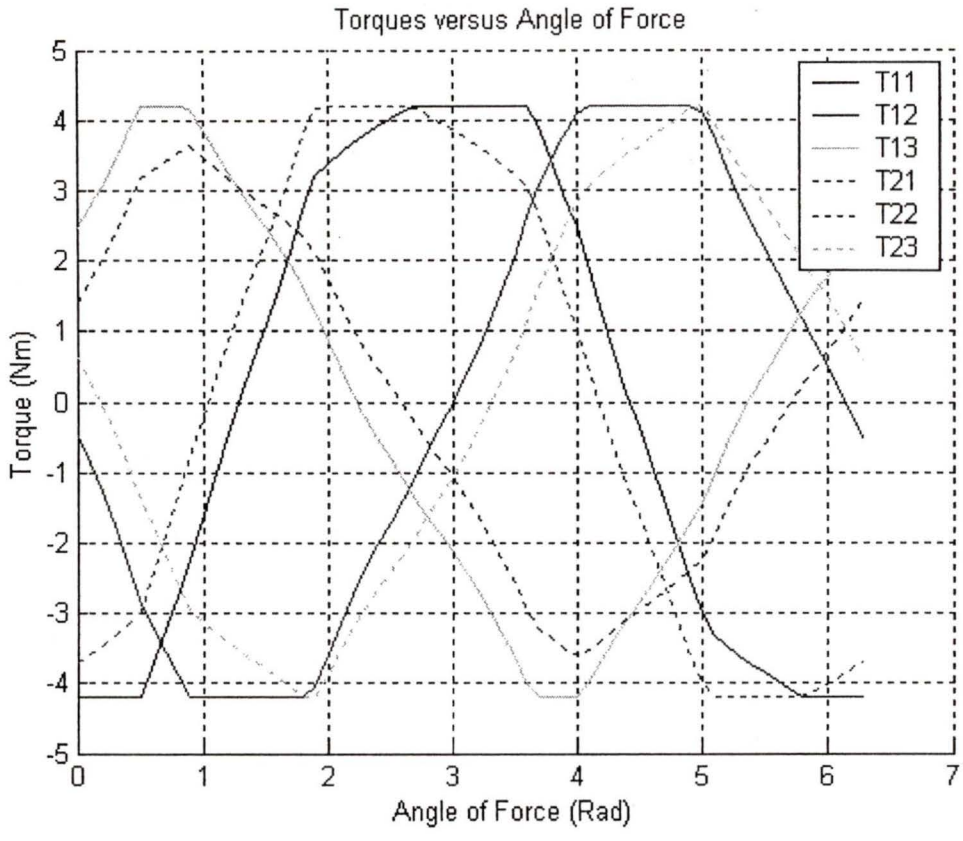

Figure 5.5: The joint torques of the redundantly-actuated (peudo-inverse solution) 8-Bar vs the angle of the applied load, with no moment being applied.

can sustain a pure force in the $\hat{\mathbf{y}}$ direction of 74.9 N, with f_x=0 and m_z=0. The maximum level of sustainable moment is approximately 7.68 Nm.

Figure 5.5 shows the joint torques versus the angle of applied load for the force polygon of the redundantly-actuated pseudo-inverse solution with no moment being applied by the manipulator. Notice how there is always only one joint being at a maximum at any given time. A joint torque being maximum once again corresponds to a side of the force polygon.

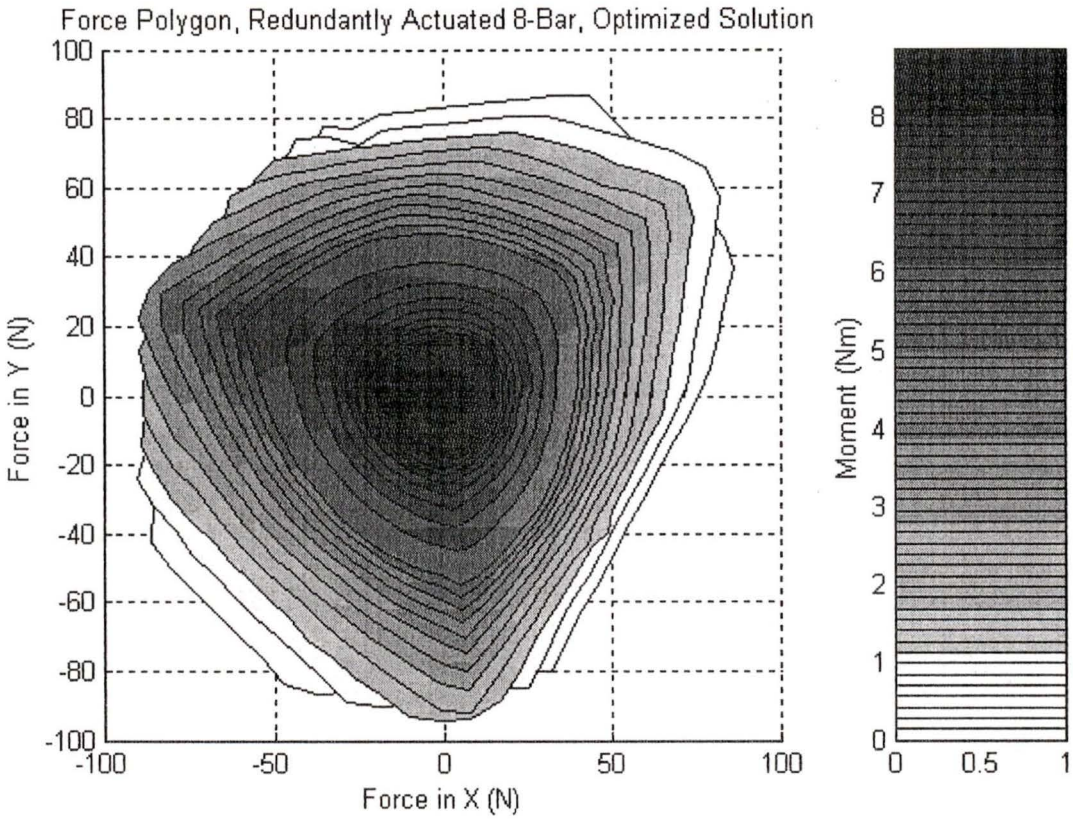

Figure 5.6: The optimized force polygon of the redundatly-actuated 8-Bar.

Optimized results

Figure 5.6 shows the force polygon for the redundantly-actuated 8-Bar configuration using the BFGS optimization solution method. Once again, both the shoulder and elbow joint of each branch are actuated. The magnitude of the applicable moment is shown by grey scale. The manipulator can sustain a pure force in the $\hat{\mathbf{x}}$ direction of 76.1 N, with f_y=0 and m_z=0. Similarly, the manipulator can sustain a pure force in the $\hat{\mathbf{y}}$ direction of 83.3 N, with f_x=0 and m_z=0. The maximum level of sustainable moment is approximately 8.86 Nm.

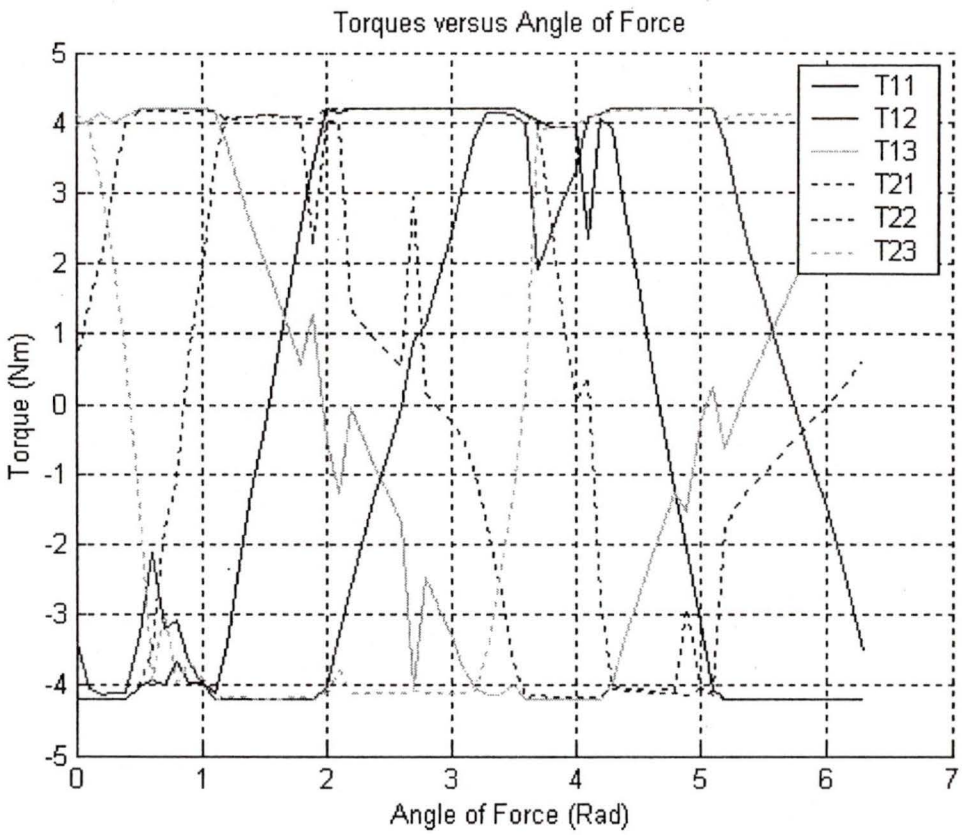

Figure 5.7: The joint torques of the optimized redundantly actuated 8-Bar vs the angle of the applied load, with no moment being applied.

Figure 5.7 shows joint torques versus the direction of applied load by the manipulator found using optimization. Here it should be noted that instead of just one joint being at the maximum value there are always at least two being maximum, and there are usually two others very close to the maximum. The other two joints are typically in transition from a maximum to a minimum joint torque.

Table 5.1: Comparison of the non-redundatly actuated 8-Bar and the redundantly-actuated 8-Bar force capabilities

	Non-Redundantly Actuated	Pseudo-Inverse Solution	Percent Difference
f_x	34.7	63.5	183%
f_y	36.8	74.9	204%
m_z	5.54	7.68	139%

5.5 Discussion of Results

5.5.1 Comparison of Non-redundant Actuation and Pseudo-Inverse Redundant-Actuation Solutions

There is quite a difference between the force capabilities of the non-redundantly actuated 8-Bar configuration and the redundantly-actuated 8-Bar configuration. A comparison of the results is shown in Table 5.1. Here it is clear that extremely large gains in force capabilities are made from redundantly actuating the parallel device. What is interesting in the comparison of the non-redundantly actuated device and the redundantly-actuated device with the pseudo-inverse solution, is that there is always only one joint torque which is limiting the force capabilities of the manipulator.

5.5.2 Comparison of the Optimized Solution and the Pseudo-Inverse Solution

Table 5.2 shows a comparison of the redundantly-actuated solution techniques. It is clear that gains are made in the instantaneous force capabilities by optimization. What is of great interest with this is in the joint torques. With the optimized joint

Table 5.2: Comparison of the force capabilities for the pseudo-invese and optimized solutions for the redundatly-actuated 8-Bar

	Pseudo-Iverse Solution	Optimized Solution	Percent Difference
f_x	63.5	76.1	120%
f_y	74.9	83.3	111%
m_z	7.68	8.86	115%

torques there is always more than one joint torque at the maximum value at any given instant. In fact, there are always two, with two others near their maximum value.

5.5.3 Optimization Errors

The analytical methods used to solve for the force capability plots contains only errors due to the computational accuracy of Matlab, which is extremely high and therefore they contain an insignificant amount of error. The optimization based method however, contains a much higher degree of error. By examining Figures 5.6 and 5.7, jaggedness in the edges of the force polygon and torque values instead of smooth edges and lines can be clearly seen. These are due to errors in the optimization routine. The first error of the optimization method can be attributed to the setting of the optimizational tolerances. The second is due to the use of a power norm of 50 in the objective function.

Optimizational Tolerances

The tolerances set on the optimization algorithm were a pertubation tolerance of 5×10^{-4}, a gradient tolerance of 5×10^{-4}, and a line search tolerance of 10^{-25}. The high tolerance on the line search was used to ensure a positive-definite **S** matrix.

These tolerances could be increased to increase the accuracy of the optimization based routine.

Power norm

The accuracy of the power norm of 50 can create an error in the objective function itself. The power norm is to return the maximum joint torque out of the vector. The higher the power norm, the closer to the actual maximum joint torque the objective function returns.

Example

For an example, the optimization routine with the current optimizational tolerances and a power norm of 50 was run for a $\$_\mathbf{f}$ of (1,0;0). The resulting torques to create the unit screw $\$_\mathbf{f}$ are

$$\boldsymbol{\tau}_{\$_f} = \begin{pmatrix} \tau_{1_1} \\ \tau_{1_2} \\ \tau_{1_3} \\ \tau_{2_1} \\ \tau_{2_2} \\ \tau_{2_3} \end{pmatrix} = \begin{pmatrix} -0.05528 \\ -0.04490 \\ 0.05213 \\ 0.00771 \\ -0.05517 \\ 0.05397 \end{pmatrix}$$

The Pnorm($\boldsymbol{\tau}_{\$_f}$, 50) = 0.05619, yet the actual maximum torque has a magnitude of -0.05528. A difference of 1.7%. By increasing the accuracy of the optimization routines to a pertubation tolerance of 10^{-10}, a gradient tolerance of 10^{-10}, and a line

search tolerance of 10^{-30}, the resulting torque vector becomes

$$\boldsymbol{\tau}_{\$_f} = \begin{pmatrix} \tau_{1_1} \\ \tau_{1_2} \\ \tau_{1_3} \\ \tau_{2_1} \\ \tau_{2_2} \\ \tau_{2_3} \end{pmatrix} = \begin{pmatrix} -0.05521 \\ -0.04498 \\ 0.05317 \\ 0.00627 \\ -0.05513 \\ 0.05374 \end{pmatrix}$$

which shows that the original optimizational tolerances result in a negligible difference from higher tolerances. In fact, the maximum torque has dropped from -0.05528 to -0.05521, an improvement of just 0.12%. The higher tolerances also require much more computational time to achieve. Running the routine with the high tolerances and with a power norm of 100 results in a torque vector of

$$\boldsymbol{\tau}_{\$_f} = \begin{pmatrix} \tau_{1_1} \\ \tau_{1_2} \\ \tau_{1_3} \\ \tau_{2_1} \\ \tau_{2_2} \\ \tau_{2_3} \end{pmatrix} = \begin{pmatrix} -0.05504 \\ -0.04563 \\ 0.05403 \\ 0.00514 \\ -0.05500 \\ 0.05431 \end{pmatrix}$$

where the maximum torque magnitude has decreased from -0.05528 in the original optimization routine, to -0.05504 in the fully improved optimization routine, an improvement of 0.42%. This small improvement is also considered negligible compared to the computational requirements of the higher tolerances and the higher power norm.

Chapter 6

Conclusions and Recommendations for Future Work

6.1 Overview

This chapter presents the major conclusions of the previous chapters. This chapter also recommends some future work to be continued in line with what was presented in the thesis. Section 6.2 presents the conclusions on the design, implementation, kinematics, and force capabilities of the RPPM. Section 6.3 provides the recommendations for future work, including design upgrades, implementation improvements, and implementation of the maximization of the force capabilities.

6.2 Conclusions

6.2.1 RPPM Design

A reconfigurable planar parallel manipulator (RPPM) has been successfully designed. The RPPM is capable of reconfiguring into 3 mechanism configurations: a 3-DOF 8-Bar mechanism, a 3-DOF 6-Bar mechanism, and a 2-DOF 5-Bar mechanism. Reconfigurability in actuation has also been achieved, any shoulder or elbow joint of the branches can be either an actuated or a passive revolute joint. This modularity was achieved by using a simple joint and link design. For the 8-Bar configuration, this allows four possible non-redundantly actuated configurations and six redundantly-actuated configurations.

The ability of the RPPM to sense the forces being applied to the platform by each of the branches was done by using linear force sensors which intersect at the wrist centres. With the use of linear slides aligned perpendicular to the axis of sensing, no shear forces are sensed and the result is an accurate sensing structure.

The RPPM design allows for a measured joint displacement with a worst case accuracy of $\pm 3.0 \times 10^{-2}$ radians per joint. The measured force worst case accuracy is approximately ± 2.24 Newtons per sensor.

6.2.2 RPPM Implementation

The implementation of the RPPM when non-redundantly actuated was accomplished with PID control. The dynamic effects of the manipulator increases the errors, but only slightly, and still leaves them within acceptable levels. The use of a hybrid position/force controller for the redundantly-actuated RPPM was also completed.

The accuracies decreased slightly from the PID controlled RPPM, but were still near the errors of the sensed values. The maximum joint displacement error was found in the hybrid controller, and was approximately 0.035 radians. Compared to the maximum error in the sensed value of approximately 0.03 radians, the controller was proven to be effective.

The accomplishment of the RPPM proves the manipulator as an effective testbed manipulator. Accurate control with the simple algorithms used successfully showed the capabilities and potentials of the RPPM.

6.2.3 RPPM Kinematics

It is possible to solve both the forward and inverse displacement solutions for the RPPM. For the FDS, when the RPPM is redundantly sensed, the solution is simple and unique, as all the wrist locations of the platform are known. With only minimal sensing, the FDS for the 5-Bar and the 6-Bar both can be solved with the intersection of two circles, yielding 2 possible solutions. When the 8-Bar is minimally sensed, the method is more complex, but it has been show that there exist up to 6 possible FDS solutions.

The IDS for all actuation configurations and mechanism types follow the same procedure. The location of the wrist for each branch is found, then the joint displacements are found for that branch to satisfy the corresponding wrist location. There exists, for each branch, two possible solutions, an "elbow up" solution and an "elbow down" solution. It is up to the user to specify which solution they desire.

With the joints of the RPPM modelled with screw coordinates, it is possible to create a matrix of associated-reciprocal screws. A weighted associated-reciprocal

screw matrix, which converts a vector of joint torques to an output force at the end effector, can then be found.

6.2.4 Force Capabilities

The force capabilities of the RPPM can be found for any position and orientation of the platform. The force capabilities, when non-redundantly actuated, are limited by the maximum torque required to create a force modelled by a unit screw in the desired direction. The same applies to using a Moore-Penrose pseudo-inverse solution to the redundantly-actuated configurations of the RPPM. Using an optimization routine, the internal forces of the platform (those which create no applied or sustained load) are utilized to decrease the maximum torque required to create the unit force. This causes more than one joint being the limiting joint, and increases the force capabilities of the manipulator. This was proven with a simulation of the fully-redundantly actuated 8-Bar mechanism modelled on the RPPM.

6.3 Recommendations for Future Work

6.3.1 RPPM Design Upgrades

One of the major sources of error in joint position for the RPPM is caused by the backlash of the gearboxes. In fact, over half of the possible joint error is in the backlash. Harmonic-drive gear reducers would provide a backlash-free alternative to the planetary gearboxes currently on the actuators. Some modification of the joints may be required.

The 5-Bar configuration for the RPPM can also be improved. The current locking

of the platform to a second link of a branch renders the force sensing at that wrist unusable due to the lack of a revolute joint. Design of a link for the application of better sensing in the 5-Bar mechanism is recommended.

6.3.2 Implementation and Control Improvements

There exists more work on the implementation of the RPPM that should be done. Specifically in two major areas. First, a more user friendly control program structure should be designed. The current method of using different programs for different configurations of mechanism type and actuation configuration is cumbersome. It may possible to create a program which would facilitate the researcher in a more general capacity.

Second, the controllers themselves are not optimal. While they are basic, simple, and demonstrate the capability of the RPPM to act as a testbed manipulator, optimal control theory in both the PID scheme and the hybrid scheme are possible. Use of the dynamics of the RPPM can greatly increase the controller capabilities, and possibly improve the experimental results.

6.3.3 Implementation of Force Capabilities

The implementation of the optimized force capabilities for the RPPM is possible. The RPPM was designed to test theories similar to optimizing force capabilities for redundantly actuated manipulators. The testing would be a beneficial demonstration of the capabilities of the RPPM, and to the theory itself.

With the use of a quasi-Newton optimization method, it may be possible that the calculated $\mathbf{S}$ matrix from the last control loop could be used to create the $\mathbf{S}$ matrix

for the current control loop. This may be possible due to the fact that the RPPM physically moves only small amounts in each control loop. Hence, only one or two optimization iterations need to be executed for each control loop of the RPPM. This theory could be tested in simulation prior to its application. This would drastically reduce the time required to optimize the force capability. A method for application of Single Value Decomposition has been presented by Golub and Van Loan [41]. Therefore, it would be possible to implement the optimization routine.

References

[1] M. Raghavan, "The stewart platform of general geometry has 40 configurations," *Journal of Mechanical Design*, vol. 115, no. 3, pp. 277–282, 1993.

[2] L. Notash and R. P. Podhorodeski, "On the forward displacement problem of three-branch parallel manipulators," *Mechanism and Machine Theory*, vol. 30, no. 3, pp. 391–404, 1994.

[3] P. Sobejko, *Implementation of Redundantly-Sensed Parallel-Manipulator-Based 6-DOF Joysticks.* MASc thesis, University of Victoria, Victoria B.C., Canada, Dec 2002.

[4] J. J. Craig, *Introduction to Robotics, Mechanics and Control - Second Edition.* Don Mills, Ontario: Addison-Wesley Publishing Company, 1989.

[5] R. P. Podhorodeski and S. B. Nokleby, "Reconfigurable main-arm for assembly of all revolute-only kinematically simple branches," *Journal of Robotic Systems*, vol. 17, no. 7, pp. 365–373, 2000.

[6] R. P. Podhorodeski and K. Pittens, "A class of parallel manipulators based on kinematically simple branches," *ASME Journal of Mechanical Design*, vol. 116, pp. 908–914, 1994.

[7] G.Yang, I.-M. Chena, W. K. Lim, and S. H. Yeo, "Kinematic design of modular reconfigurable in-parallel robots," *Autonomous Robots*, vol. 10, no. 1, pp. 83–89, 2001.

[8] H. Cheng, G. Liu, Y. Yiu, Z. Xiong, and Z. Li, "Advantages and dynamics of parallel manipulators with redundant actuation," in *Proceedings 2001 IEEE/RSJ International Conference on Intelligent Robotics and Systems*, (Hawaii, USA), pp. 171–176, 2001.

[9] G. Hamlin and A. Sanderson, "Tetrobot modular robotics: prototype and experiments," in *IEEE International Conference on Intelligent Robots and Systems*, (Osaka, Japan), pp. 390–395, 1996.

[10] W. Schonlau, "Modular manipulator system (mms), architecture and implementation," in *Proceedings of the 1997 8th International Conference on Advanced Robotics, ICAR'97*, (California, USA), pp. 901–906, 1997.

[11] Z. Ji, "Design of a reconfiurable plaform manipulator," *Journal of Robotic Systems*, vol. 15, no. 5, pp. 341–346, 1998.

[12] R. Hui, N. Kircanski, A. Goldenberg, C. Zhou, P. Kuzan, J. Wiercienski, D. Gershon, and P. Sinha, "Design of the iris facility. a modular, reconfigurable and expandable robot test bed," in *Proceedings of the IEEE International Conference on Robotics and Automation*, (Atlanta, USA), pp. 155–160, 1993.

[13] M. Raibert and J. Craig, "Hybrid position/force control of manipulators," *Transactions of the ASME, Journal of Dynamic Systems, Measurement and Control*, vol. 103, no. 2, pp. 126–133, 1981.

[14] T. Yoshikawa, "Force control of robot manipulators," in *Proceedings of the 2000 IEEE International Conference on Robotics and Automation*, (San Francisco, CA), pp. 220–226, 2000.

[15] C. An and J. Hollerbach, "The role of dynamic models in cartesian force control of manipulators," *Internation Journal of Robotics Research*, vol. 8, no. 4, pp. 51–72, 1989.

[16] W. D. Fisher and M. S. Mujtaba, "Hybrid position/force control: A correct formulation," *International Journal of Robotics Research*, vol. 11, no. 4, pp. 299–311, 1992.

[17] Y.-L. Wu, X.-Z. Wu, and S.-Y. Li, "Pd control of redundant parallel manipulators," *Journal of National University of Defense Technology*, vol. 23, no. 3, pp. 111–114, 2001.

[18] C. Gosselin and J. Angeles, "The optimum design of a planar three-degree-of-freedom parallel manipulator," *Journal of Mechanisms, Transmision, and Automation in Design*, vol. 110, no. 1, pp. 35–41, 1988.

[19] J.-P. Merlet, "Workspaces of planar parallel manipulators," *Mechanism and Machine Theory*, vol. 33, no. 1, pp. 7–20, 1998.

[20] C. Gosselin and M. Jean, "Determination of the workspace of planar parallel manipulators with joint limits," *Robotics and Autonomous Systems*, vol. 17, no. 3, pp. 129–138, 1996.

[21] J.-P. Merlet, "Redundant parallel manipulators," *Laboratory Robotics and Automation*, vol. 8, no. 1, pp. 17–24, 1996.

[22] C. Gosselin and J.-P. Merlet, "The direct kinematics of planar parallel manipulators: Special architectures and number of solutions," *Mechanism and Machine Theory*, vol. 29, no. 8, pp. 1083–1097, 1994.

[23] V. Kumar and K. Waldron, "Force distribution in closed kinematic chains," in *Proceedings of the IEEE 1988 International Conference on Robotics and Automation*, (Philidelphia, Pennsylvania), pp. 114–119, 1988.

[24] D. Kerr, M. Griffis, D. Sanger, and J. Duffy, "Redundant grasps, redundant manipulators, and their dual relationship," *Journal of Robotic Systems*, vol. 9, no. 7, pp. 973–1000, 1992.

[25] P. Buttolo and B. Hannaford, "Advantages of actuation redundancy for the design of haptic displays," in *ASME International Mechanical Engineering Congress and Exposition, Part 2 of (2)*, (California, USA), pp. 623–630, 1995.

[26] L. Beiner, "Redundant actuation of a closed-chain manipulator," *Advanced Robotics*, vol. 11, no. 3, pp. 233–245, 1997.

[27] M. Nahon and J. Angeles, "Optimization of dynamic forces in mechanical hands," *Journal of Mechanisms, Transmissions, and Automation in Design*, vol. 113, no. 2, pp. 167–173, 1991.

[28] H. Packard, "Quick assembly two and three channel optical encoders, technical data," tech. rep., Hewlett Packard, Feb 1990.

[29] C. Inc., "Pci-das1602/16 manual, revision 2," tech. rep., ComputerBoards Inc., January 1999.

[30] P. M. Inc., "Mfio-3a user's manual," tech. rep., Precision MicroDynamics Inc, 1997.

[31] P. M. Inc., "Bta-28v-6a linear power amplifier user's manual, revision 2.1," tech. rep., Precision MicroDynamics Inc, March 1997.

[32] I. Advent, "Omnix 400 series chassis user's guide," tech. rep., ICS Advent, 2000.

[33] I. Advent, "Model ecik-2000 and ecik-2001," tech. rep., ICS Advent, September 1997.

[34] J. VandeVegte, *Feedback Control Systems.* Englewood Cliffs, N.J.: Prentice Hall, Inc., 1986.

[35] T. Yoshikawa, *Foundations of Robotics, Analysis and Control.* Cambridge, Massachusetts: The MIT Press, 1988.

[36] K. Ogata, *Modern Control Engineering - Third Edition.* Englewood Cliffs, N.J.: Prentice Hall, Inc., 1997.

[37] K. Hunt, *Kinematic Geometry of Mechanisms.* Oxford: Clarendon Press, 1978.

[38] K. Hunt, "Structural kinematics of in-parallel-actuated robot-arms.," *Journal of Mechanisms, Transmision, and Automation in Design*, vol. 105, no. 4, pp. 705–712, 1983.

[39] A. Antonio, *Optimization: Theory and Practice.* Victoria, B.C., Canada: Dept. of Electrical and Computer Engineering, University of Victoria, 2000.

[40] G. Strang, *Linear Algebra and its Applications.* San Diego: Harcourt Brace Jovanovich, 1988.

[41] G. H. Golub and C. F. V. Loan, *Matrix Computations.* Baltimore, Maryland: The John Hopkins University Press, 1988.

Appendix A

Equipment Data Sheets for the RPPM

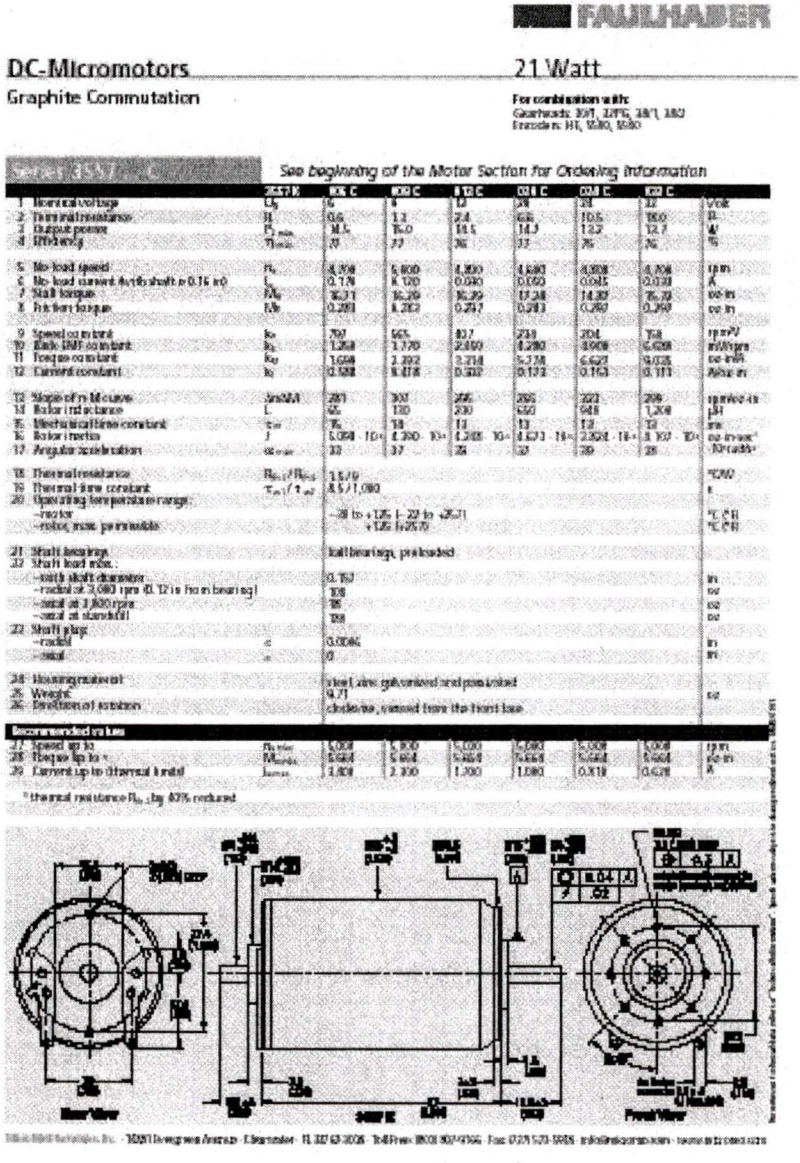

FAULHABER

DC-Micromotors 21 Watt

Graphite Commutation

For combination with:
Gearheads: 30/1, 32/1S, 38/1, 38/2
Encoders: IE3, IE3D, IE3D

Series 3557 ... C — See beginning of the Motor Section for Ordering Information

1 Nominal voltage	U_N	V	6	9	12	24	36	48
2 Terminal resistance	R	Ω	0.6	1.1	2.4	6.6	10.5	19.0
3 Output power	$P_{2\,max.}$	W	15.5	15.0	18.5	14.3	13.2	12.7
4 Efficiency	$\eta_{max.}$	%	77	77	76	77	76	76
5 No-load speed	n_0	rpm	4,950	5,600	4,800	4,680	4,900	4,700
6 No-load current (with shaft ø 0.16 in)	I_0	A	0.178	0.120	0.040	0.060	0.045	0.038
7 Stall torque	M_H	oz-in	16.71	16.29	16.29	17.38	14.30	16.29
8 Friction torque	M_R	oz-in	0.283	0.283	0.297	0.283	0.269	0.269
9 Speed constant	k_n	rpm/V	797	565	817	234	204	158
10 Back-EMF constant	k_E	mV/rpm	1.256	1.770	1.469	4.280	4.908	6.338
11 Torque constant	k_M	oz-in/A	1.656	1.392	1.714	5.138	6.427	8.035
12 Current constant	k_I	A/oz-in	0.598	0.718	0.583	0.193	0.153	0.113
13 Slope of n-M curve	$\Delta n/\Delta M$	rpm/oz-in	297	337	286	285	323	299
14 Rotor inductance	L	µH	66	130	230	550	948	1,200
15 Mechanical time constant	τ_m	ms	15	18	13	13	12	12
16 Rotor inertia	J	oz-in-sec²	5.09E-10	4.39E-10	4.26E-10	4.67E-10	2.82E-10	3.35E-10
17 Angular acceleration	$\alpha_{max.}$	10³ rad/s²	33	37	35	32	39	28
18 Thermal resistance	R_{th1} / R_{th2}	°C/W	3.5 / 9					
19 Thermal time constant	τ_{w1} / τ_{w2}	s	8.5 / 1,080					
20 Operating temperature range:								
–motor		°C (°F)	–30 to +125 (–22 to +257)					
–rotor, max. permissible		°C (°F)	+125 (+257)					
21 Shaft bearings			ball bearings, preloaded					
22 Shaft load max.:								
–with shaft diameter		in	0.157					
–radial at 3,000 rpm (0.12 in from bearing)		oz	108					
–axial at 3,000 rpm		oz	36					
–axial at standstill		oz	108					
23 Shaft play:								
–radial	c	in	0.0006					
–axial	a	in	0					
24 Housing material			steel, zinc galvanized and passivated					
25 Weight		oz	9.71					
26 Direction of rotation			clockwise, viewed from the front face					
Recommended Values								
27 Speed up to	$n_{N\,max.}$	rpm	4,000	5,300	4,000	4,000	3,000	3,000
28 Torque up to *	$M_{max.}$	oz-in	5.664	5.664	5.664	5.664	5.664	5.664
29 Current up to (thermal limit)	$I_{max.}$	A	1.800	2.300	1.300	1.080	0.919	0.628

* thermal resistance $R_{th\,2}$ by 40% reduced

Figure A.1: The specifications of the DC Micromotors.

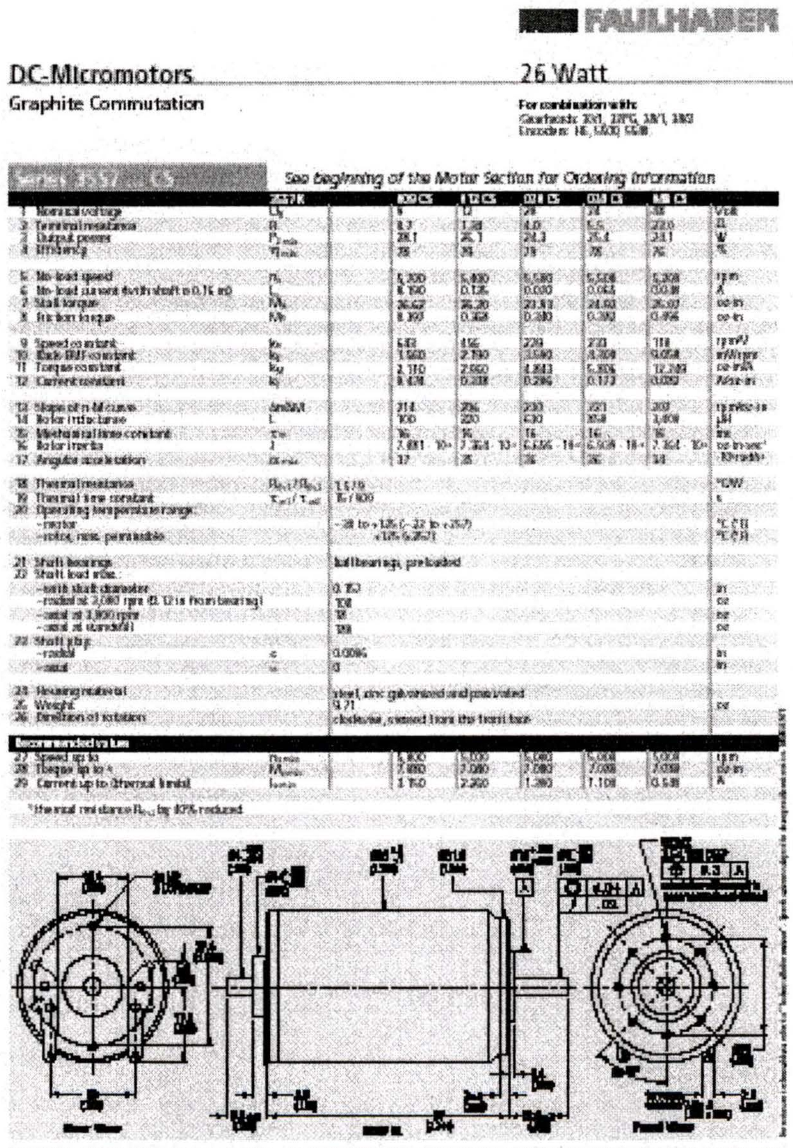

Figure A.2: The specifications of the Supra DC Micromotors.

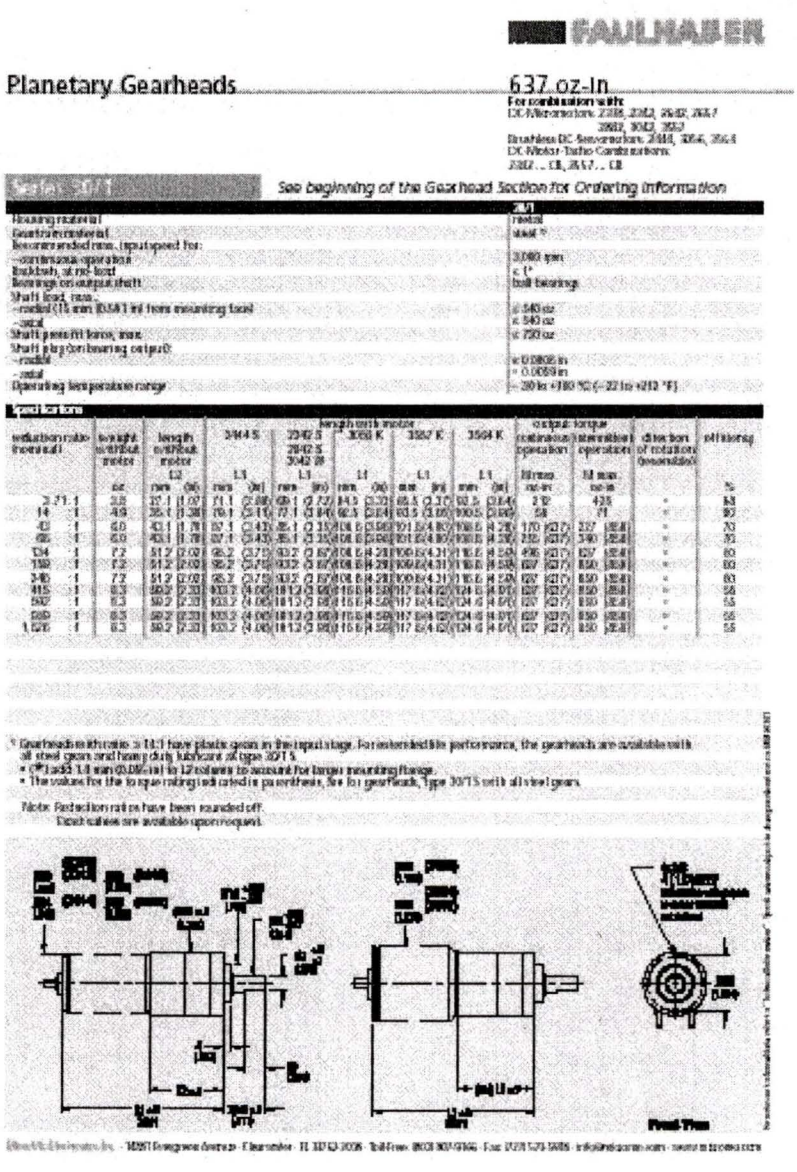

FAULHABER

Planetary Gearheads

637 oz-in

See beginning of the Gearhead Section for Ordering Information

Figure A.3: The specifications of the planetary gearheads used on the Micromotors.

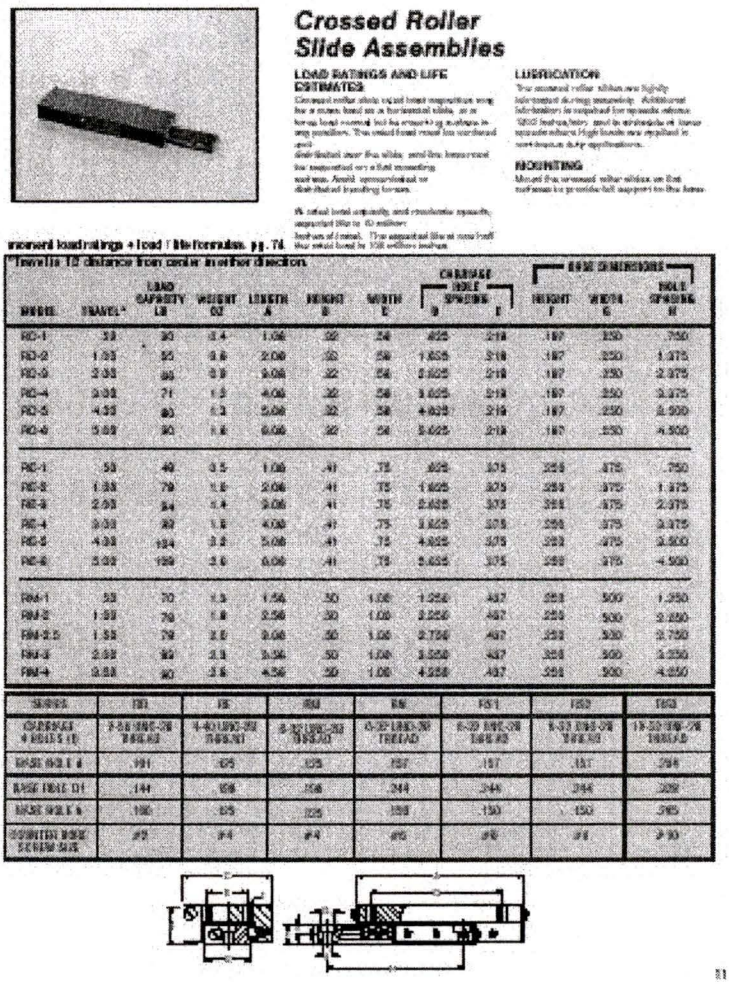

Crossed Roller Slide Assemblies

LOAD RATINGS AND LIFE ESTIMATES

LUBRICATION

MOUNTING

MODEL	TRAVEL*	LOAD CAPACITY LB	WEIGHT OZ	LENGTH A	HEIGHT B	WIDTH E	CARRIAGE HOLE SPACING D	CARRIAGE HOLE SPACING E	BASE DIMENSIONS HEIGHT F	BASE DIMENSIONS WIDTH G	BASE DIMENSIONS HOLE SPACING H
RD-1	.53	30	3.4	1.06	.32	.56	.625	.219	.187	.250	.750
RD-2	1.03	55	5.6	2.06	.32	.56	1.625	.219	.187	.250	1.375
RD-3	2.03	88	8.9	3.06	.32	.56	2.625	.219	.187	.250	2.375
RD-4	3.03	71	11.3	4.06	.32	.56	3.625	.219	.187	.250	3.375
RD-5	4.03	80	13.3	5.06	.32	.56	4.625	.219	.187	.250	4.500
RD-6	5.03	90	15.6	6.06	.32	.56	5.625	.219	.187	.250	4.500
RD-1	.53	40	3.5	1.06	.41	.75	.625	.375	.250	.375	.750
RD-2	1.03	79	7.0	2.06	.41	.75	1.625	.375	.250	.375	1.375
RD-3	2.03	84	11.4	3.06	.41	.75	2.625	.375	.250	.375	2.375
RD-4	3.03	92	15.8	4.06	.41	.75	3.625	.375	.250	.375	3.375
RD-5	4.03	124	20.2	5.06	.41	.75	4.625	.375	.250	.375	3.500
RD-6	5.03	139	24.6	6.06	.41	.75	5.625	.375	.250	.375	4.500
RM-1	.53	70	7.3	1.56	.50	1.00	1.250	.437	.250	.500	1.250
RM-2	1.03	79	11.8	2.56	.50	1.00	2.250	.437	.250	.500	2.250
RM-2.5	1.53	79	14.8	3.06	.50	1.00	2.750	.437	.250	.500	2.750
RM-3	2.03	92	17.3	3.56	.50	1.00	3.250	.437	.250	.500	3.250
RM-4	3.03	90	23.8	4.56	.50	1.00	4.250	.437	.250	.500	4.250

SERIES	RD1	RD2	RD3	RD4	RD5	RD6
CARRIAGE & RAILS (1)	8-36 UNC-2B THREAD	4-40 UNC-2B THREAD	6-32 UNC-2B THREAD	6-32 UNC-2B THREAD	6-32 UNC-2B THREAD	10-32 UNF-2B THREAD
BASE WIDTH A	.191	.125	.125	.187	.187	.281
BASE HOLE D1	.144	.156	.156	.344	.344	.328
BASE HOLE B	.180	.125	.125	.150	.150	.265
MOUNTING HOLE SCREW SIZE	#2	#4	#4	#6	#6	#10

Figure A.4: The specifications of the Deltron linear slides.

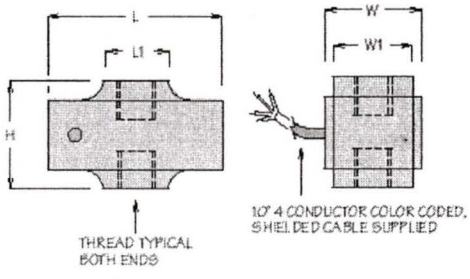

SPECIFICATIONS

Rated Output (R.O.):	2 mV/V nominal
Nonlinearity:	0.1% of R.O.
Hysteresis:	0.1% of R.O.
Nonrepeatability:	0.05% of R.O.
Creep in 20 Min.:	0.05% of R.O.
Zero Balance:	1.0% of R.O.
Compensated Temp. Range:	60° to 160°F
Safe Temp. Range:	-65° to 200°F
Temp. Effect on Output:	0.005% of Load/°F
Temp. Effect on Zero:	0.005% of R.O./°F
Terminal Resistance:	350 ohms nominal
Excitation Voltage:	10 VDC
Safe Overload:	150% of R.O.

		DIMENSIONS (INCHES)							NATURAL RINGING FREQUENCY		
MODEL	CAPACITY LBS.	L	L1	W	W1	H	THREAD	THREAD DEPTH	HZ	DEFLECTION INCHES	WT. OZS.
MLP-10	10	1.504	.600	.54	.375	.75	10-32	.200	2,175	.003	.5
MLP-25	25	1.521	.600	.66	.500	.75	1/4-28	.230	2,200	.003	.7
MLP-50	50	1.584	.625	.66	.500	.75	1/4-28	.230	2,500	.003	.7
MLP-75	75	1.640	.650	.66	.500	.75	1/4-28	.230	2,800	.003	.8
MLP-100	100	1.664	.660	.66	.500	.75	1/4-28	.230	4,500	.003	.8
MLP-150	150	1.642	.575	.93	.750	1.00	3/8-24	.375	4,500	.003	1.3
MLP-200	200	1.688	.580	.93	.750	1.00	3/8-24	.375	5,200	.003	1.4
MLP-300	300	1.748	.600	.93	.750	1.00	3/8-24	.375	5,200	.003	3.0
MLP-500	500	1.658	.580	.93	.750	1.00	3/8-24	.375	5,200	.003	3.0
MLP-750	750	1.734	.585	.93	.750	1.00	3/8-24	.375	5,200	.003	3.0
MLP-1K	1,000	1.784	.615	.93	.750	1.00	3/8-24	.375	5,200	.003	3.0

Figure A.5: The specifications of the Tranducer Techniques load cells.

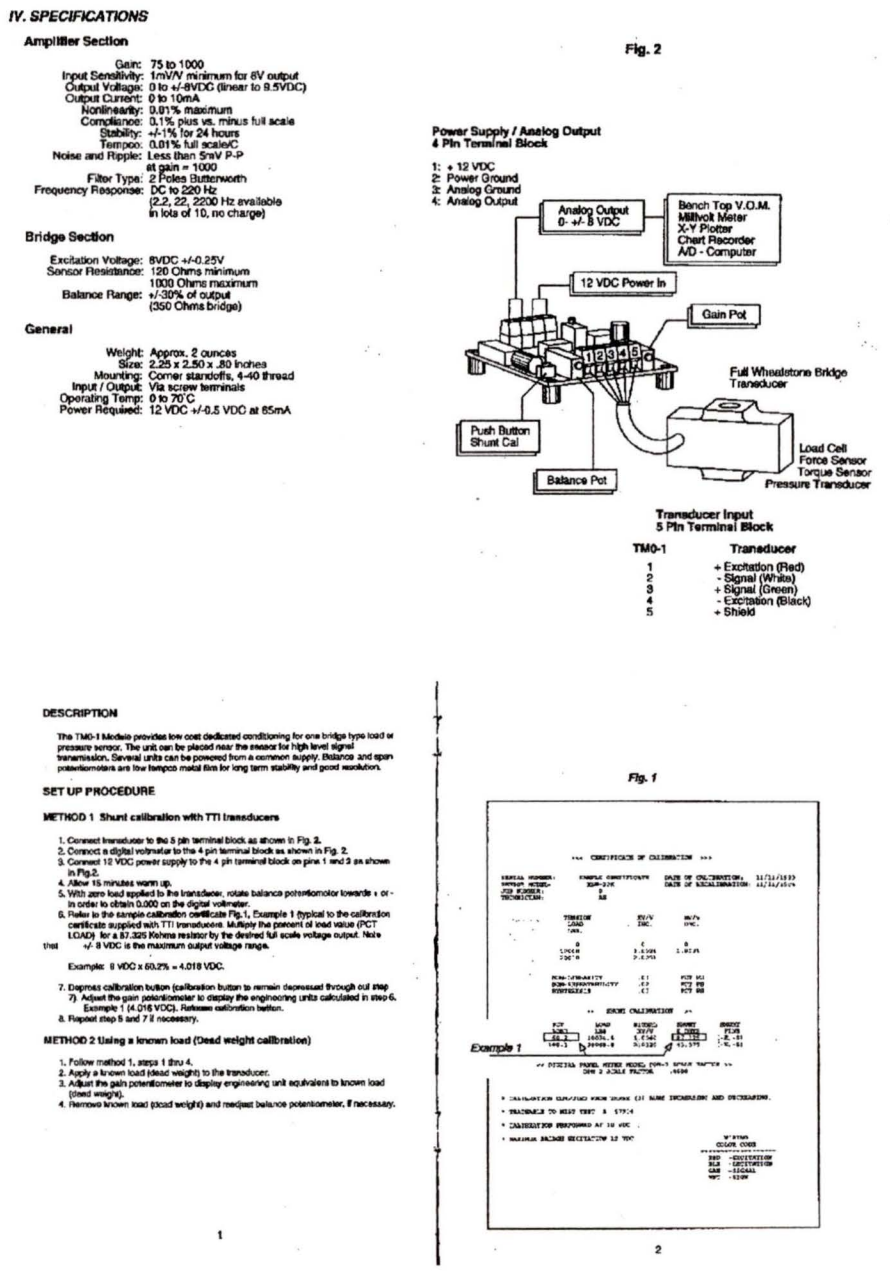

IV. SPECIFICATIONS

Amplifier Section

Gain: 75 to 1000
Input Sensitivity: 1mV/V minimum for 8V output
Output Voltage: 0 to +/-8VDC (linear to 8.5VDC)
Output Current: 0 to 10mA
Nonlinearity: 0.01% maximum
Compliance: 0.1% plus vs. minus full scale
Stability: +/-1% for 24 hours
Tempco: 0.01% full scale/C
Noise and Ripple: Less than 5mV P-P at gain = 1000
Filter Type: 2 Poles Butterworth
Frequency Response: DC to 220 Hz (2.2, 22, 2200 Hz available in lots of 10, no charge)

Bridge Section

Excitation Voltage: 8VDC +/-0.25V
Sensor Resistance: 120 Ohms minimum 1000 Ohms maximum
Balance Range: +/-30% of output (350 Ohms bridge)

General

Weight: Approx. 2 ounces
Size: 2.25 x 2.50 x .80 inches
Mounting: Corner standoffs, 4-40 thread
Input / Output: Via screw terminals
Operating Temp: 0 to 70°C
Power Required: 12 VDC +/-0.5 VDC at 85mA

Fig. 2

Power Supply / Analog Output
4 Pin Terminal Block

1: + 12 VDC
2: Power Ground
3: Analog Ground
4: Analog Output

Analog Output 0- +/- 8 VDC
Bench Top V.O.M.
Millivolt Meter
X-Y Plotter
Chart Recorder
A/D - Computer
12 VDC Power In
Gain Pot
Full Wheatstone Bridge Transducer
Push Button Shunt Cal
Balance Pot
Load Cell
Force Sensor
Torque Sensor
Pressure Transducer

Transducer Input
5 Pin Terminal Block

TM0-1	Transducer
1	+ Excitation (Red)
2	- Signal (White)
3	+ Signal (Green)
4	- Excitation (Black)
5	+ Shield

DESCRIPTION

The TM0-1 Module provides low cost dedicated conditioning for one bridge type load or pressure sensor. The unit can be placed near the sensor for high level signal transmission. Several units can be powered from a common supply. Balance and span potentiometers are low tempco metal film for long term stability and good resolution.

SET UP PROCEDURE

METHOD 1 Shunt calibration with TTI transducers

1. Connect transducer to the 5 pin terminal block as shown in Fig. 2.
2. Connect a digital voltmeter to the 4 pin terminal block as shown in Fig. 2.
3. Connect 12 VDC power supply to the 4 pin terminal block on pins 1 and 3 as shown in Fig.2.
4. Allow 15 minutes warm up.
5. With zero load applied to the transducer, rotate balance potentiomoter towards + or - in order to obtain 0.000 on the digital voltmeter.
6. Refer to the sample calibration certificate Fig.1, Example 1 (typical to the calibration certificate supplied with TTI transducers. Multiply the percent of load value (PCT LOAD) for a 87.325 Kohms resistor by the desired full scale voltage output. Note that +/- 8 VDC is the maximum output voltage range.

   Example: 8 VDC x 60.2% = 4.018 VDC.

7. Depress calibration button (calibration button to remain depressed through out step 7) Adjust the gain potentiometer to display the engineering units calculated in step 6. Example 1 (4.016 VDC). Release calibration button.
8. Repeat step 5 and 7 if necessary.

METHOD 2 Using a known load (Dead weight calibration)

1. Follow method 1, steps 1 thru 4.
2. Apply a known load (dead weight) to the transducer.
3. Adjust the gain potentiometer to display engineering unit equivalent to known load (dead weight).
4. Remove known load (dead weight) and readjust balance potentiometer, if necessary.

1

Fig. 1

Example 1

2

Figure A.6: The specifications of the TMO-1 linear amplifiers/conditioner modules.

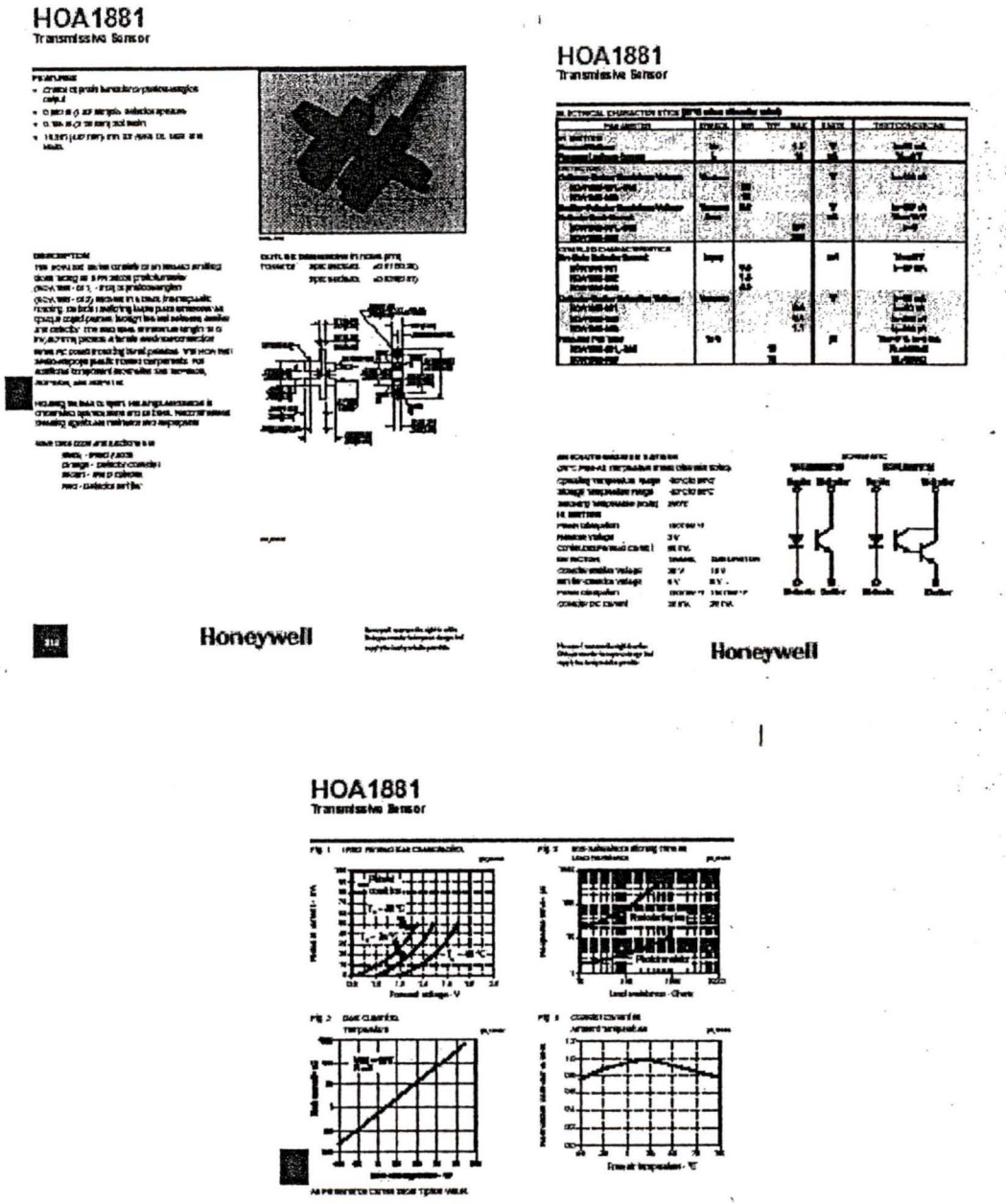

Figure A.7: The specifications of the Hewlett Packard IR homing sensors.

Appendix B

Fabrication Drawings of the RPPM

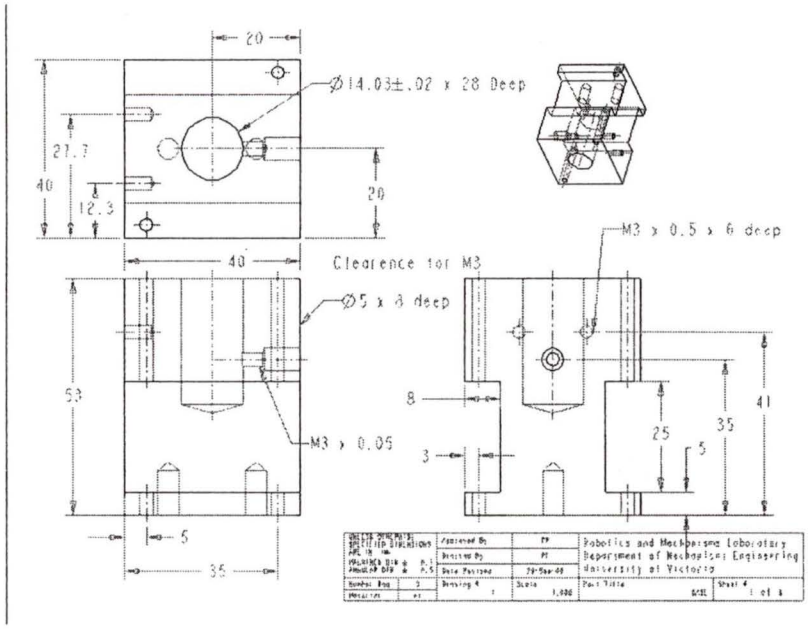

Figure B.1: The RPPM base

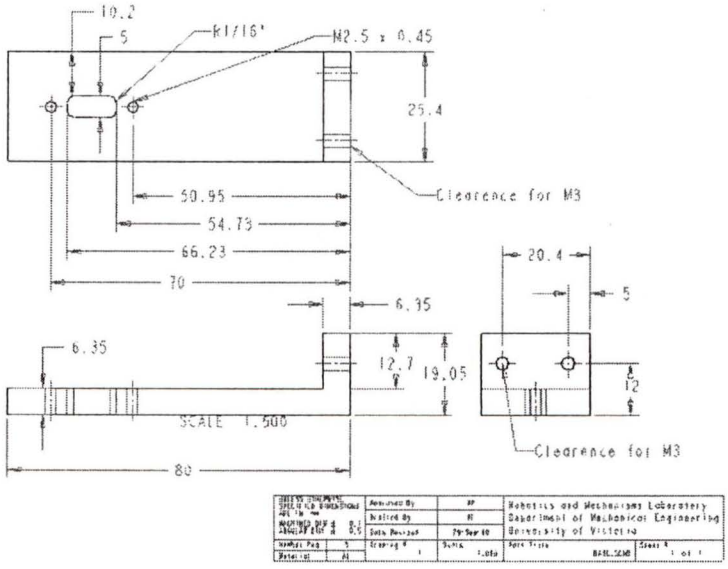

Figure B.2: The cantilever plate for the RPPM base.

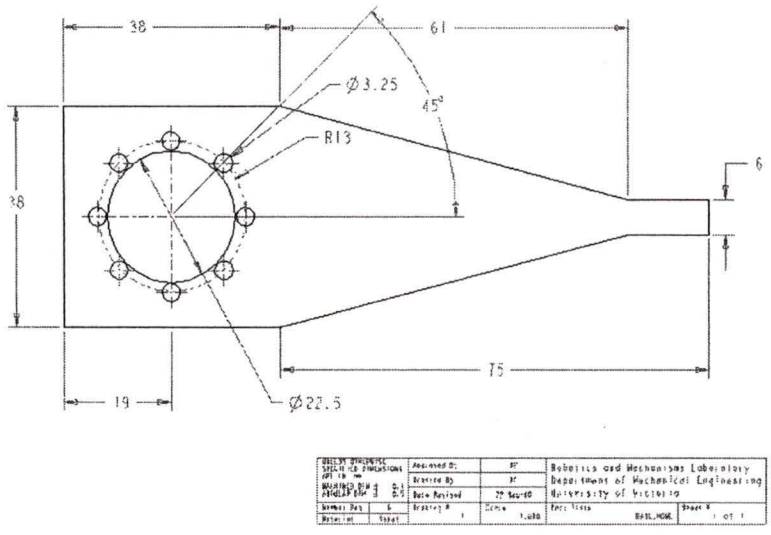

Figure B.3: The homing cutter plate.

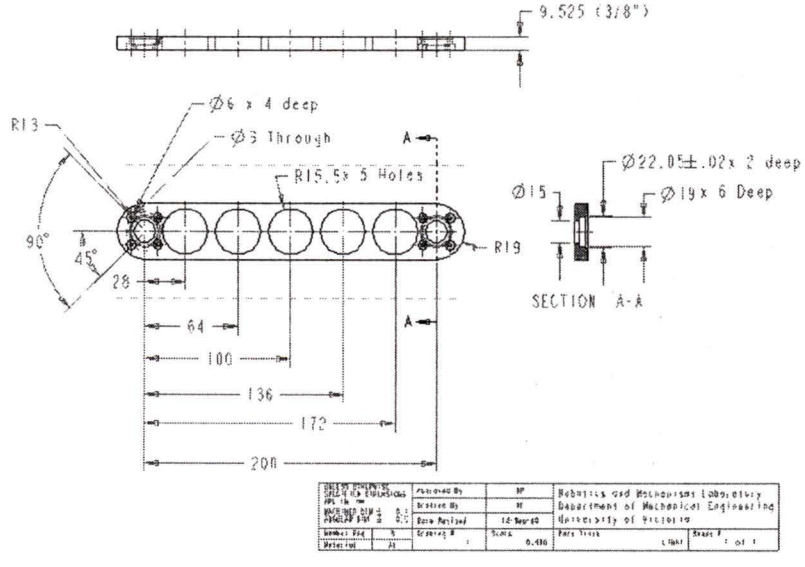

Figure B.4: Link 1 of the RPPM.

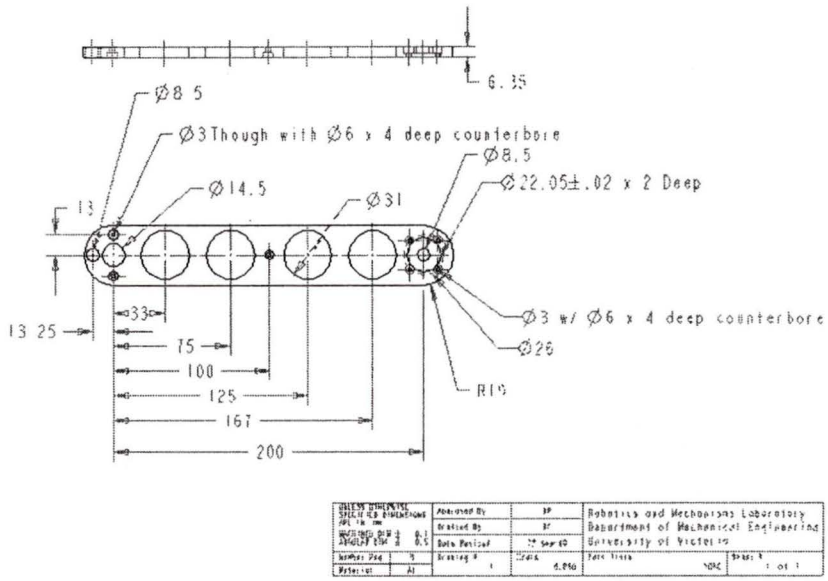

Figure B.5: The lower link of Link2

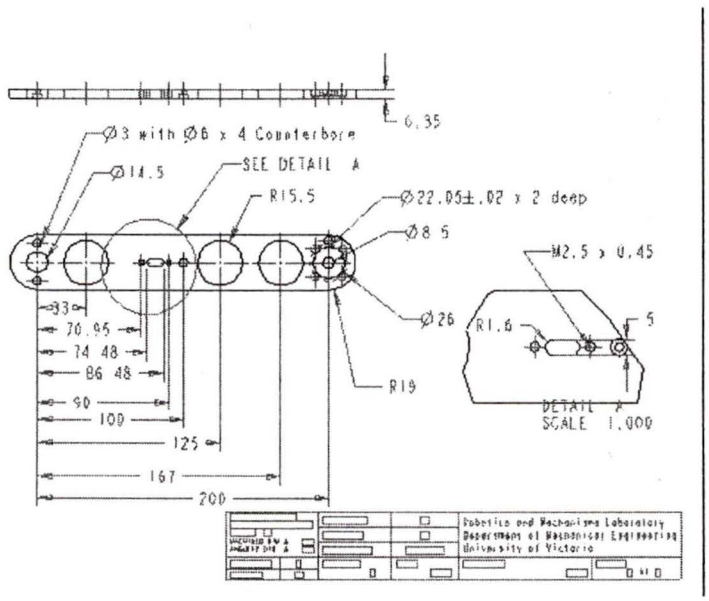

Figure B.6: The upper link of Link 2.

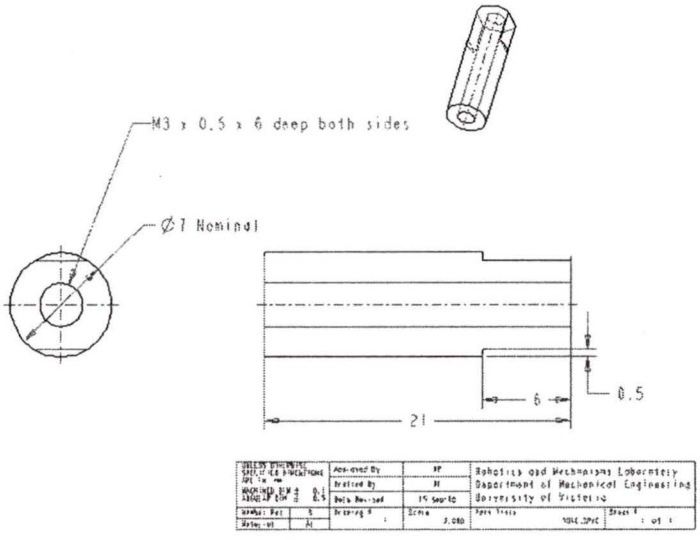

Figure B.7: The seperation peg of Link 2.

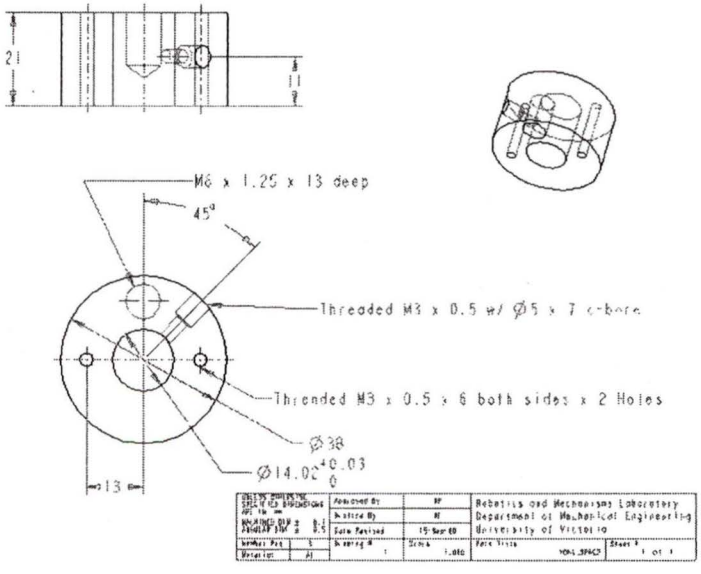

Figure B.8: The joint hub of Link 2.

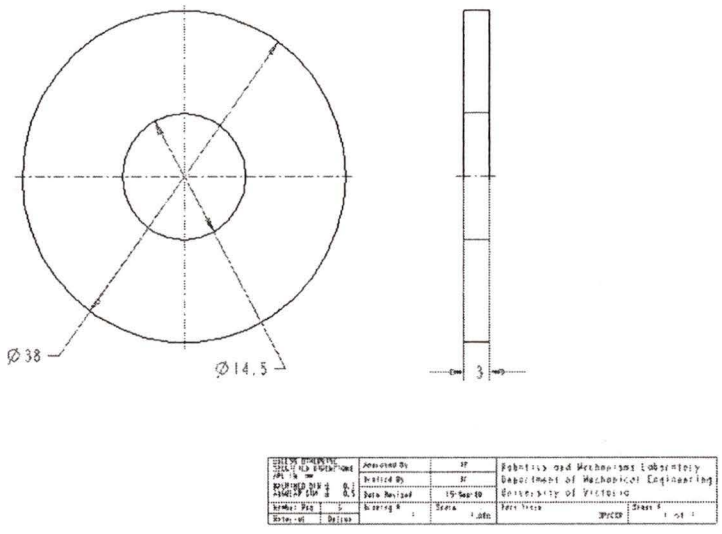

Figure B.9: The delron spacer for the RPPM joints.

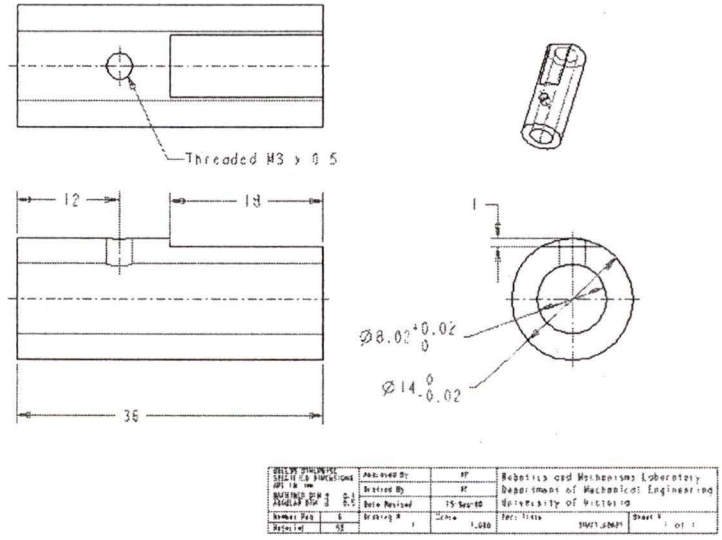

Figure B.10: The adapter shaft for the actuators.

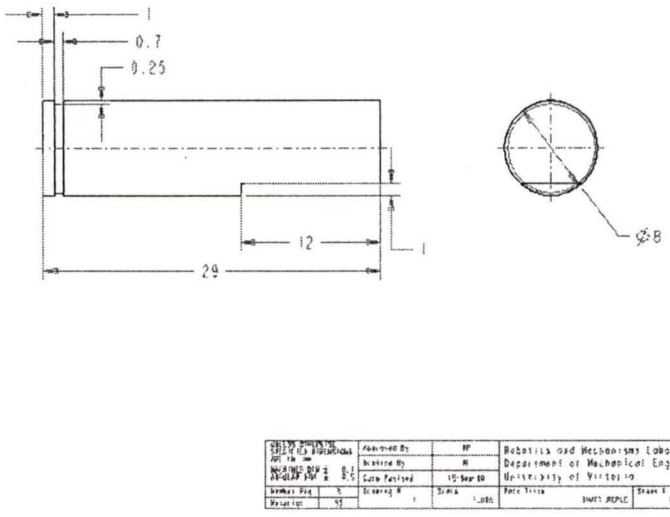

Figure B.11: The replacement shaft for the bearings.

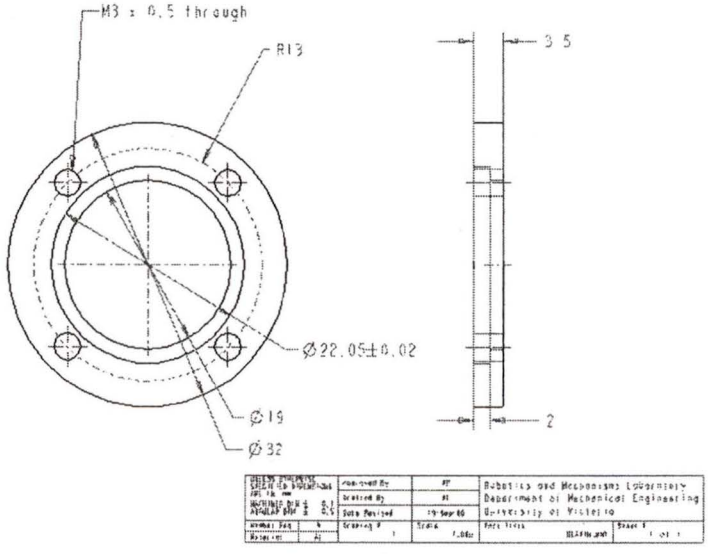

Figure B.12: The bearing mounts.

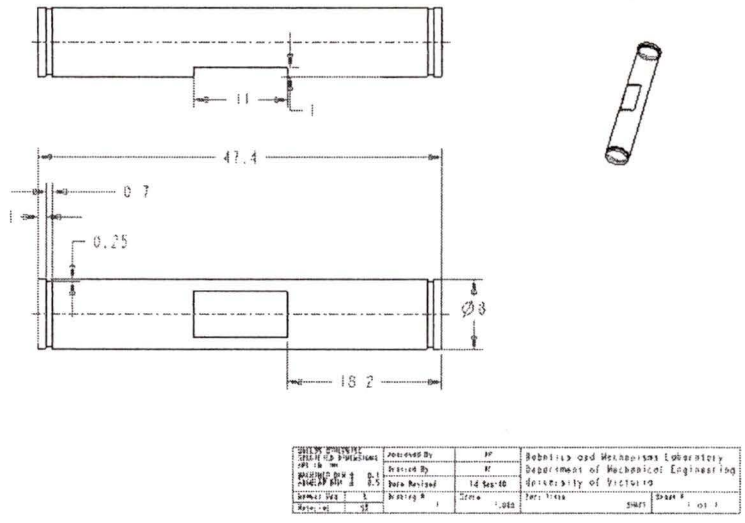

Figure B.13: The wrist shaft.

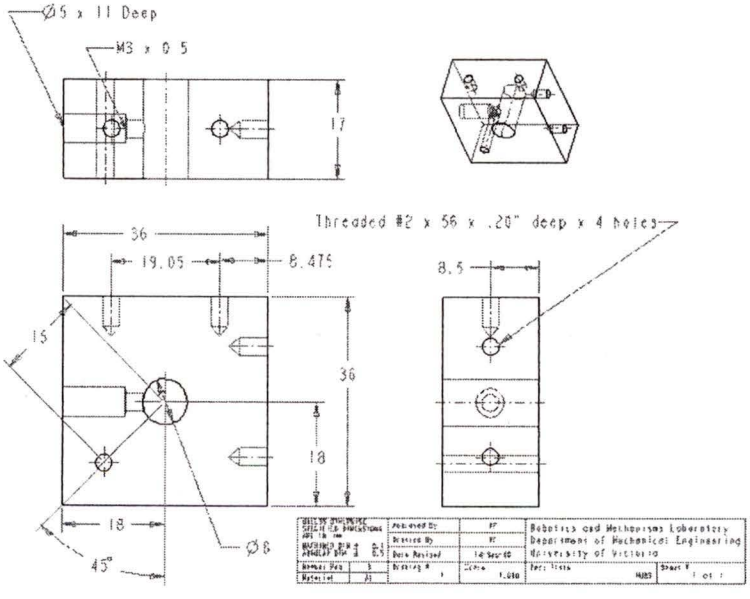

Figure B.14: The wrist of the RPPM.

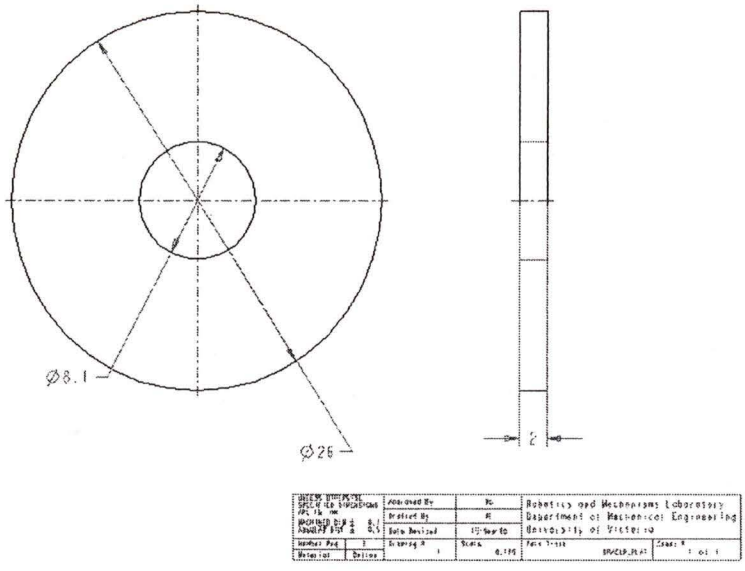

Figure B.15: The delron spacer for the wrists.

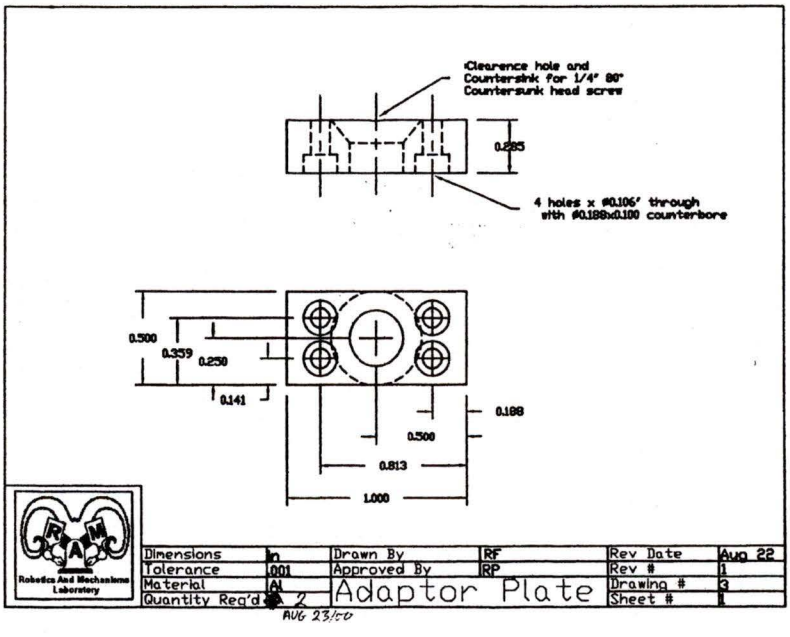

Figure B.16: The adapter plates for the force sensors.

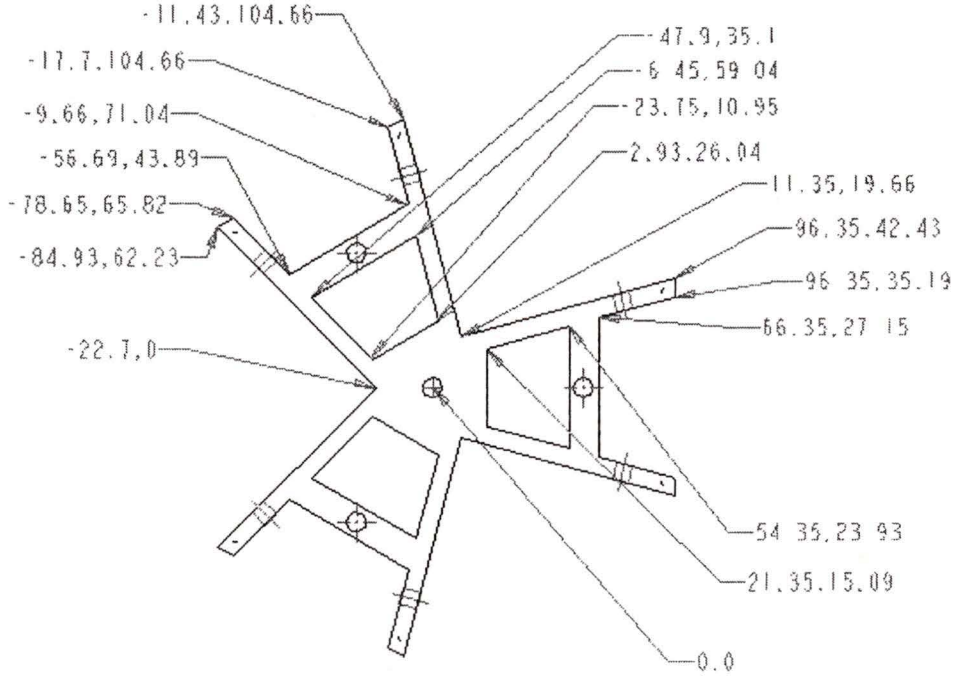

UNLESS OTHERWISE SPECIFIED DIMENSIONS ARE IN UNITS MACHINED DIM ± 0.1 ANGULAR DIM ± 0.5	Approved By	APPROVED_BY	Robotics and Mechanisms Laboratory Department of Mechanical Engineering University of Victoria
	Drafted By	DRAFTED_BY	
	Date Revised	14-Sep-10	
Number Req	SHOW_REQ	Drawing # 2	Scale 0.250
Material	MATERIAL		Part Title PLATFORM
			Sheet # 2 of 7

Figure B.17: The platform of the RPPM.

Appendix C

Interface Board Users Manual by: Darren Erickson

Version 1.0

Written by: Darren Erickson

Date: Dec. 2, 2000

Introduction

This manual describes the interface boards used to integrate the PMD MFIO3A motion control cards with the PMD BTA28V-6A linear amplifiers. Topics covered include all signal and cable connections, jumper settings, digital interface in the host computer, interpretation of status LED's, and the operational procedures.

Signal and Cable Connections

For the following cable connections, please refer to the following diagrams of the interface circuit board. All figures represent the top side, or component layer of the circuit board. Additionally, most signal connections are labeled on the board itself. When pin diagrams are given, they correspond to an orientation of the board in which the printed text is visible and reads from left to right.

Connectors J2A, J2B

There are 2 - 40 pin ribbon cables connecting the interface board with a MFIO3A motion control card. They plug into the receptacles labeled in figure 1 as J2A and J2B. It is important that the connections are made correctly, to prevent damage to either the interface board or the MFIO3A card. The receptacles are also labeled on the board itself.

Amplifier Connectors

There are 3 – 10 pin connectors provided to interface with 3 BTA28V-6A linear amplifiers. They are labeled AMP1, AMP2 and AMP3 in figure 1. The connector shells are polarized to prevent the cables from being connected backwards, but care should be taken to ensure that amplifier #1 is connected to channel #1 on the board, and so on.

Encoder Connectors

There are 3 – 12 pin header connectors provided for making encoder connections. They are labeled ENC1, ENC2 and ENC3 in figure 1. A description of the pin connections is printed on the board next to the header, but is repeated here for clarity.

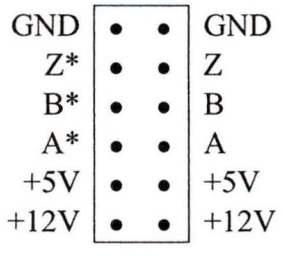

The power connections (+5V, +12V and GND) can be used to power the encoders according to their requirements. The signal connections should be made based on the

type of encoders being used. For single-ended encoders (most common), only the A,B and Z channels will be used. For differential encoders, the additional channels A*, B* and Z* will also be used. Note, not all encoders use an index pulse (Z). If your encoders do not have an index pulse, then this connection will not be used.

These header connectors are not polarized, so it is very important that the shells be properly labeled to prevent incorrect connections. In addition, the supply voltages (+5V and +12V) have not been current limited, so proper resistors should be included in the encoder supply circuitry. Never connect the supply voltage directly to ground.

Limit Switch and Home Sensor Connectors

There is a single 12 pin header connector supplied for making limit switch and home signal connections. It is labeled LIMIT in figure 1. This connector is used to interface all 3 channels of inputs. A description of the pin connections is printed on the board next to the header, but is repeated here for clarity.

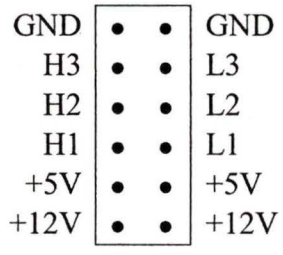

The power connections (+5V, +12V and GND) can be used to power the limit or home sensors according to their requirements. The inputs labeled H1, H2 and H3 are the home sensor inputs. These inputs are tied directly to the digital inputs on port Chi of the MFIO3A card.

The inputs labeled L1, L2 and L3 are the limit switch signals. These signals are intended to be normally pulled to ground expect for when a limit error has occurred. At this time, the limit signal must be pulled high (+5V) by the limit switch hardware. When a high signal is received on these lines, the signal is low-pass filtered in hardware and then latched. The latching occurs on the positive-going edge of the signal, and it maintains the high logic level until cleared.

This header connector is not polarized, so it is very important that the shell be properly labeled to prevent incorrect connections. In addition, the supply voltages (+5V and +12V) have not been current limited, so proper resistors should be included in the limit switch supply circuitry. Never connect the supply voltage directly to ground.

Digital Input Port A

The MFIO3A card supplies 3 – 8 bit ports of digital input. In the design of the interface boards, port A was not required, and is therefore left for future use. There is a 10 pin

header connector supplied for making digital input connections. It is labeled DIO-A in figure 2. A description of the pin connections is not printed on the board due to space constraints, but is shown below.

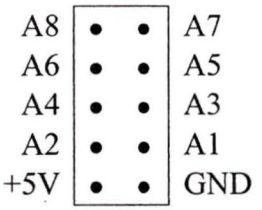

This header connector is not polarized, so it is very important that the shell be properly labeled to prevent incorrect connections.

Current Sensing Connector

The BTA28V-6A linear amplifiers generate an analog signal that is proportional to the current output of the amplifier. Since the MFIO3A board does not include any analog inputs, these signals were not used in the design of the interface boards. The interface board does supply 3 – 2 pin headers to connect these signals to an external analog input board if one is provided. These connectors are labeled CSENSE1, CSENSE2 and CSENSE3 on figure 2.

Fan Connection

A single 2 pin header connector has been provided to power a 12VDC cooling fan. It is labeled FAN on figure 2. A description of the pin connections is printed on the board next to the header, but is repeated here for clarity.

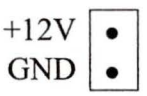

SYNC Signal Connection

The SYNC signal generated by the MFIO3A card was not used in the design of the interface boards, but a single 2 pin header connector is provided for future use. It is labeled SYNC on figure 2. A description of the pin connections is printed on the board next to the header, but is repeated here for clarity.

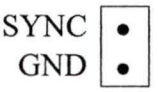

Emergency Stop Button Connection

A single 2-wire screw terminal is provided for connecting an emergency stop button. It is labeled ESTOP on figure 2. The ESTOP button is normally-open, and when pushed it generates an emergency signal by connecting the two pins of the screw terminal. The polarity of the screw terminal connections is arbitrary.

Board to Board Connection

The interface board provides a single 10 pin header to connect several boards in the same system. This is done to share two important signals between all boards. The first is the DISABLE signal. When any interface board receives an error such as a LIMIT or ESTOP signal, the DISABLE signal is generated to disable the amplifiers. This signal is also propagated to all other boards through the board-to-board connector.

The second signal is the RESET signal. When a LIMIT has occurred, this error is latched in the hardware until it is reset. Resetting can be accomplished using either the pushbutton provided on the interface boards, or through a signal sent by the host computer. By sending a RESET signal to any board, the limit switch signal is cleared from all boards connected using the board-to board connector. The pin diagram for this connector is as follows:

1	N/C
2	N/C
3	N/C
4	N/C
5	RESET
6	RESET
7	DISABLE
8	DISABLE
9	+5V
10	GND

Jumper Settings

There are only three jumper settings required on the interface boards. These are found near the limit and home signal connections and are used to enable/disable the limit switch hardware filtering. When filtering is enabled, the limit signals are passed through an RC low pass filter constructed using a 4.7KΩ resistor and a 0.22μF capacitor. When filtering is disabled, these signals bypass the filter and travel directly to the latching circuitry. The jumper settings are made according to the following diagram:

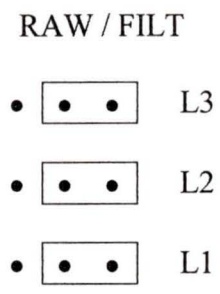

Connecting the jumper across the rightmost two pins enables hardware filtering (as shown), while connecting across the leftmost two pins disables filtering and passes the raw limit signal to the rest of the circuit.

Digital Interface to the Host Computer

The interface to the host computer is accomplished through the MFIO3A motion control cards. A complete description of the input and output signals is given in the MFIO3A user manual. The interface boards utilize digital I/O ports B and C for communication with the motion control cards. A list of the digital I/O signals is given in the following tables:

Port A

A7	A6	A5	A4	A3	A2	A1	A0
rfu	rfu	rfu	rfu	rfu	rfu	rfu	rfu

*rfu = reserved for future use

Port B

B7	B6	B5	B4	B3	B2	B1	B0
LIMIT3	LIMIT2	LIMIT1	FLT3	FLT2	FLT1	WDOG	ESTOP

Port C (Chi | Clo)

C7	C6	C5	C4	C3	C2	C1	C0
rfu	HOME3	HOME2	HOME1	RESET	AMP3	AMP2	AMP1

Ports B and Chi are used for input to the computer, while port Clo is used for output to the interface board. Port B contains all sources of error that are capable of generating an emergency stop condition. Therefore, the port B interrupt capability should be enabled on the MFIO3A card. Port Chi includes the home signal input which can also be set to generate an interrupt, but is not required for safe operation of the hardware.

The port Clo output contains 4 signals. The three AMP signals are used to enable the linear amplifiers when a high logic level is sent. Setting the AMP signals to a low logic level disables the amplifiers. The RESET signal is set to high to clear the limit signals from the hardware latch. It is VERY IMPORTANT to set the RESET signal back to low after a short interval. Failure to do this will result in the RESET signal being held high, which effectively disables all of the LIMIT signals.

Interpretation of Status LED's

A 10 position LED block is provided on the board to display the status of all error signals. When an error is encountered, the LED will glow red until that error is cleared. A diagram of the LED block and the procedure for clearing errors is as follows:

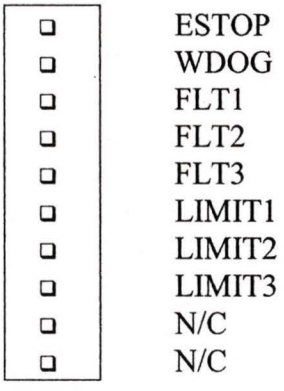

ESTOP:	Pull up or disconnect the emergency stop button
WDOG:	Send a WDOGReset signal to the MFIO3A cards
FLT:	Power-cycle the amplifiers
LIMIT:	Press the pushbutton or send a RESET signal from the computer

Operational Procedures

The following procedures should be used when operating the interface boards:

1) Ensure that all cable connections are correct and secure with the power off to all equipment.
2) Turn on the power to the computer and amplifiers.
3) When powered on, the error signals may be set to an indeterminate state. Clear all error signals by resetting the WDOG, LIMIT and FLT signals. Finally, ensure that the emergency stop button is released.
4) Configure the digital I/O ports to the correct state:
   Port A = unused
   Port B = input
   Port Clo = output
   Port Chi = input
5) Configure Port B to generate interrupts.
6) When finished, power down all equipment.

7)

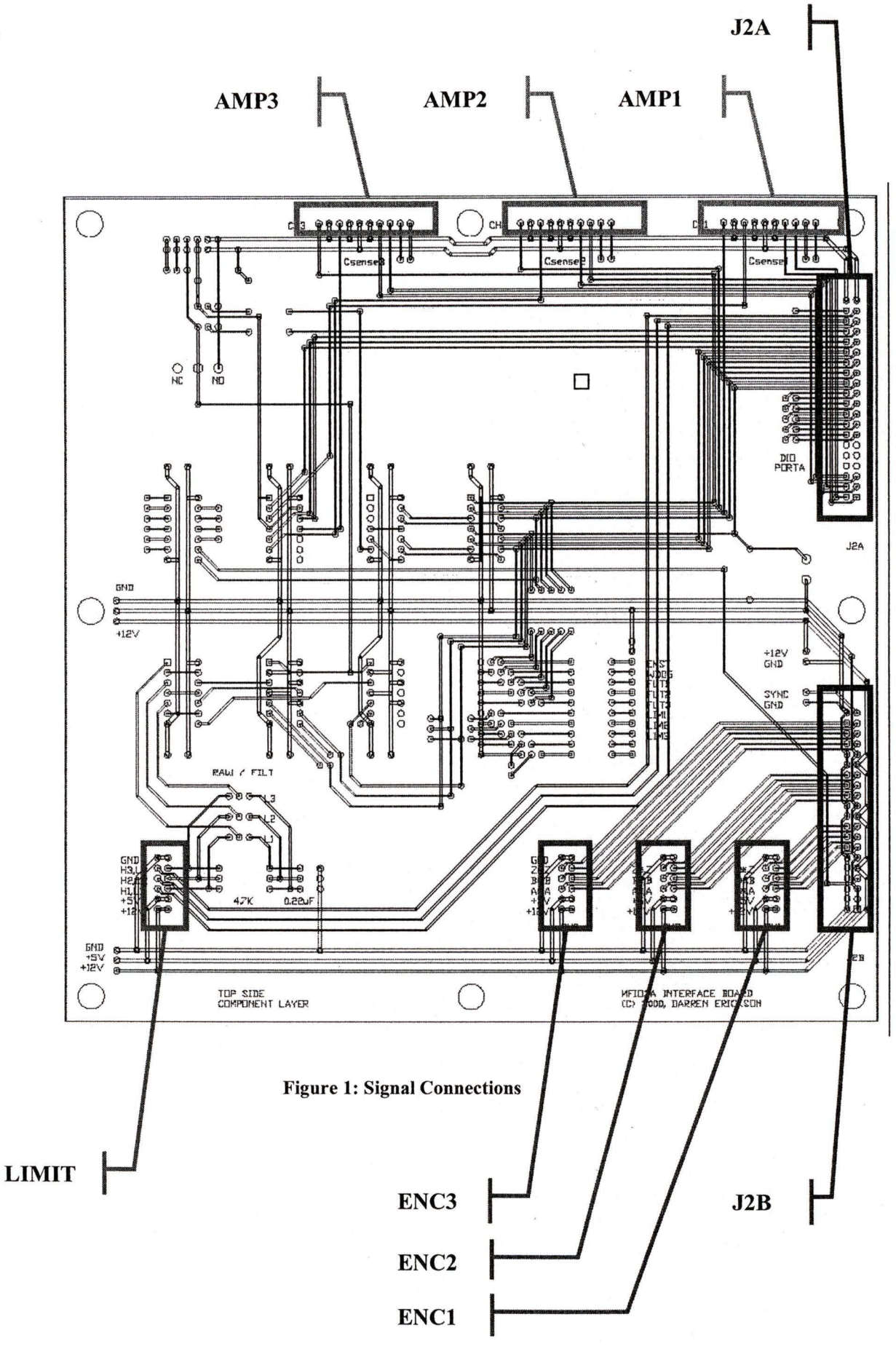

Figure 1: Signal Connections

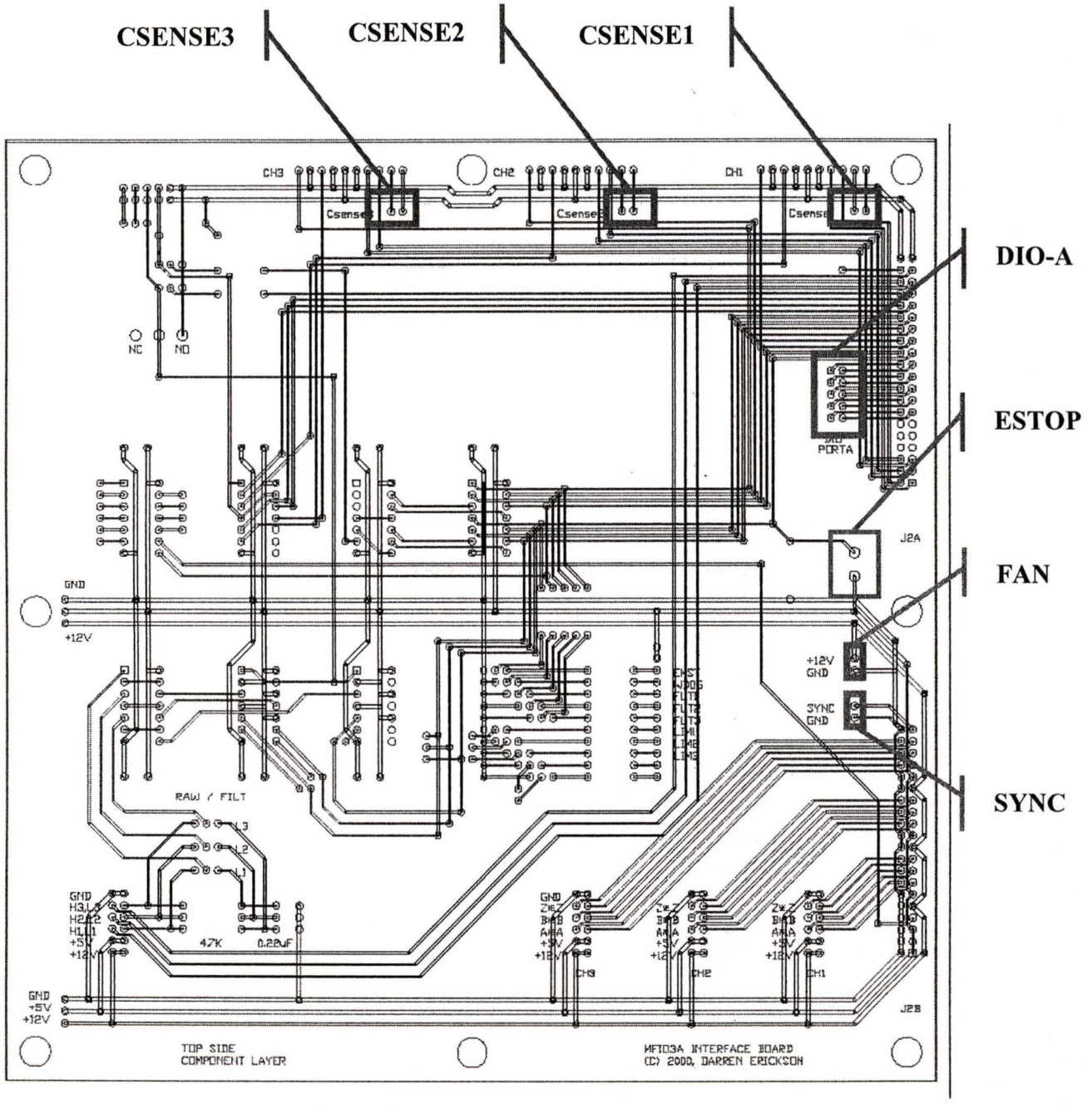

Figure 2: Additional Connections

Vita

Surname: Fisher **Given Names:** Ryan

Place of Birth: Fernie, B.C, Canada
Date of Birth: August 11, 1977

Educational Institutions Attended:

University of Victoria 1995 to 2003

Degrees Awarded:

B. Eng. (Mechanical) University of Victoria 2000

Honours and Awards:

Publications:

R. Fisher, R.P. Podhorodeski and S.B. Nokleby "A Reconfigurable Planar Parallel Manipulator (RPPM), Proceedings of the 2001 CCToMM Symposium on Mechanisms, Machines, and Mechatronics, June 1, 2001, Saint-Hubert, Canada, 2 pages.

Partial Copyright License

I hereby grant the right to lend my thesis to users of the University of Victoria Library, and to make single copies only for such users or in response to a request from the Library of any other university, or similar institution, on its behalf or for one of its users. I further agree that permission for extensive copying of this thesis for scholarly purposes may be granted by me or a member of the University designated by me. It is understood that copying or publication of this thesis for financial gain shall not be allowed without my written permission.

Title of Thesis:

Design and Implementation of a Redundantly Actuated Reconfigurable Planar Parallel Manipulator

Author [redacted]

Ryan Fisher

April 7, 2003